 © 2004 Russian Academy of Sciences and Turpion Ltd

DOI 10.1070/RC2004v073n06ABEH000821

The structure of X-ray photoelectron spectra of light actinide compounds †

Yu A Teterin, A Yu Teterin

Contents

I. Introduction 541
II. Thorium compounds 542
III. Uranium compounds 547
IV. Neptunium compounds 560
V. Plutonium compounds 564
VI. General rules of the formation of fine structure in the XPS spectra of actinide compounds 568
VII. Conclusion 575

Abstract. The results of X-ray photoelectron spectroscopy (XPS) studies of the structures of the outer and inner electron shells of compounds of light actinides (Th, U, Np, Pu, Am, Cm, Bk, Cf) in the binding energy (E_b) range of 0 – 1250 eV are generalised. The regularities of formation of the fine structure in the X-ray photoelectron (XPS) spectra of these compounds are considered. The mechanisms of appearance of such structure are analysed, and the correlations between the fine structure parameters and actinide oxidation states and local environment, the magnetic properties of compounds, the nature of the chemical bond and secondary electronic processes that accompany photoemission of electrons are discussed. Experimental evidence for effective formation of the outer (E_b = 0 – 15 eV) and inner valence (E_b = 15 – 50 eV) molecular orbitals, in particular, from the fully occupied An6p and L*n*s orbitals of the neighbouring actinide (An) and ligand (L) atoms in the compounds in question is presented. The use of fine spectral structure parameters, together with the electron binding energies and line intensities extends significantly the scope of application of the XPS method in structural studies.
The bibliography includes 276 references.

I. Introduction

Actinides (An) are the An5f transition elements located after actinium in the Periodic Table with atomic numbers (Z) in the range $90 \leqslant Z \leqslant 103$. These elements can be conventionally subdivided into two groups, namely, light actinides (Th, Pa, U, Np, Pu, Am, Cm), which are readily accessible for X-ray spectral studies, and heavy actinides (Bk, Cf, Es, Fm, Md, No, Lr), less accessible for such studies, which is mainly due to the relatively short half lives of the longest-lived actinide isotopes (Table 1). The electronic configuration of actinide atoms can be expressed as $\{Rn\}5f^n6d^m7s^2$, where $\{Rn\}$ is the electronic configuration of radon, $0 \leqslant n \leqslant 14$, $m = 0, 1$. In the ground state, actinides, except for thorium, protactinium, uranium, neptunium, curium and, possibly, lawrencium have no An6d electrons ($m = 0$); however, transition of one or two An5f electrons to the An6d shell does not require much energy. In compounds, actinides can occur in various oxidation states.[1–4]

Currently, nuclear energy is widely used in science and engineering. The permanent growth of the demand for the raw materials stimulates the design of economical nuclear-chemical processes used in all stages of nuclear energy production ranging from ore mining to transmutation of the spent nuclear fuel [1–7] and for the solution of the concomitant environmental problems using X-ray spectral methods.[8–16] Despite the fact that a number of industrially important actinide (Th, U, Pu) compounds have been widely studied in the last decades, many aspects concerning the physicochemical properties of these compounds still remain unknown.[1–4] Therefore, study of the electronic structures of actinide compounds and elucidation of the relationship between

Table 1. Electronic configurations and half lives ($T_{1/2}$) of the longest-lived isotopes of actinides.[1–3]

Isotope	Electronic configuration	Z	$T_{1/2}$ (see [a])
^{227}Ac	$6d7s^2$	89	21.8
^{232}Th	$6d^27s^2$	90	1.41×10^{10}
^{231}Pa	$5f^26d7s^2$	91	3.28×10^4
^{238}U	$5f^36d7s^2$	92	4.47×10^9
^{237}Np	$5f^46d7s^2$	93	2.14×10^6
^{244}Pu	$5f^67s^2$	94	8.1×10^7
^{243}Am	$5f^77s^2$	95	7380
^{247}Cm	$5f^76d7s^2$	96	1.64×10^7
^{247}Bk	$5f^97s^2$	97	1380
^{249}Cf	$5f^{10}7s^2$	98	350
^{254}Es	$5f^{11}7s^2$	99	277 days
^{257}Fm	$5f^{12}7s^2$	100	100 days
^{258}Md	$(5f^{13}7s^2)$ [b]	101	54 days
^{259}No	$(5f^{14}7s^2)$ [b]	102	~1.5 h
^{260}Lr	$(5f^{14}6d7s^2$ or $5f^{14}7s^27p)$ [b]	103	~3 min

[a] When no units are given, the half lives are expressed in years. [b] Putative electronic configurations.

Yu A Teterin, A Yu Teterin Institute of General and Nuclear Physics, Russian Research Centre 'Kurchatov Institute', pl. Kurchatova 1, 123182 Moscow, Russian Federation. Fax (7-095) 196 05 31.
Tel. (7-095) 196 92 52. E-mail: teterin@ignph.kiae.ru (Yu A Teterin),
Tel. (7-095) 196 90 28. E-mail: ateterin@tochka.ru (A Yu Tetererin)

Received 10 February 2003
Uspekhi Khimii **73** (6) 588 – 631 (2004); translated by Z P Bobkova

† Dedicated to Academician Anatolii Petrovich Aleksandrov on the occasion of the 100th anniversary of his birthday.

its parameters and their properties is a fairly topical task. In addition, investigation routes for the electronic structures and properties of transactinide compounds with atomic numbers in the range of $104 \leqslant Z \leqslant 118$ have taken shape in recent years.[17,18]

In the last decades, the design of high-precision X-ray photoelectron spectrometers[19–23] and development of quick methods for the calculation of electronic structures such as X_α-methods[24–28] and spectral structure parameters[29–35] enabled X-ray photoelectron spectroscopy studies into the electronic structures of actinide compounds to be carried out at a qualitatively new level. The results show that not only the spectra of core electronic shells[29,36,37] or outer valence molecular orbitals (OVMO),[38–44] but also spectra of the inner valence molecular orbitals (IVMO)[38,45–48] provide information about the physical and chemical properties of these compounds. Not only the chemical shifts of electronic levels and line intensities can be used for analysis. Useful information concerning the physicochemical properties of compounds and secondary processes that accompany photoemission can also be drawn from fine structure parameters of the spectra of both the core and outer electrons.[20–23,49–56] This is especially important in those cases where reliable determination of electron binding energies and line intensities of some electronic levels is difficult. In the spectra of actinide compounds, a complex fine structure is observed for almost all electron shells in the binding energy (E_b) range of $\sim 0 \leqslant E_b \leqslant 1250$ eV. This energy range is normally used for XPS measurements. The fine structure provides information on the actinide oxidation states in compounds (Th,[23,57–64] U,[39,40,60–78] Np,[79–81] Pu,[29,64,79,81–86] Am,[29,79,87,88] Cm, Bk, Cf[79,81,87,88]), on the magnetic properties (Th,[44,58,89] U,[43,44,55,89–91] Np[44,55,89,90]), on the structures of compounds (Th,[55,58] U,[26,38,45,47,48,55,66,92–97] Np,[55,80] Pu,[29,55,82] Am,[29,79] Cm, Bk, Cf[79]), on the nature of the chemical bond (Th,[37,52,53,55,58,98–100] U,[26,40,47,48,52,53,55,66,92–94,98,101–112] Np,[41,51–53,55,80,81,87–90,113–115] Pu,[29,37,41,52,53,55,82,87–91,115,116] Am,[29,37,79,81,87–89,91] Cm, Bk, Cf[79,81,87,88]), on the secondary electronic processes that accompany the emission of photoelectrons (Th,[55,58,117–120] U,[47,55,56,103–105,117] Np,[55,56,79,80] Pu,[29,55,79,82,121] Am,[29,79] Cm, Bk, Cf[79]), and so on. Therefore, analysis of the reasons for the appearance of the fine spectral structure and identification of the correlation between its characteristics and the properties of the considered compounds, which represent key goals of this review, are fairly topical.

The XPS spectra of light actinide compounds clearly show the bands for the outer valence MO (Th,[39,58] U,[38,40,65,66,70,111,122] Np,[41,80,89] Pu,[41,82,83,89] Am,[79,88,89] Cm, Bk, Cf[79,88]); inner valence MO (Th,[53,58] U,[47,53,66,93,94,102,104,109,110,123] Np,[36,53,80,113] Pu,[36,53,82] Am,[29] Cm, Bk, Cf[53]); the multiplet line splitting due to the presence of unpaired An5f electrons in actinide ions (Th,[55,58] U,[55] Np,[80] Pu,[82] Am,[29] Cm, Bk, Cf[79]); a dynamic effect due to the giant Coster–Kronig transitions within the core and valence levels during the core electron photoemission (Th,[56,62,119,120,124] U,[47,56,66] Np,[55,56,80] Pu,[29,82] Am,[29] Cm, Bk, Cf[54,55]); many-body perturbation caused by simultaneous excitation of valence electrons during photoemission, which gives rise to satellites on the higher binding energy side from the basic XPS lines (so-called shake up satellites) (Th,[117,118,125] U,[52,66,105] Np,[79,80] Pu,[29,82,85,126] Am,[29,127,128] Cm, Bk, Cf[79]), and other effects.

Despite the fact that different mechanisms of the appearance of fine spectral structure occur simultaneously, for electrons of a particular shell, the probability of a particular mechanism is usually much higher than that of other mechanisms.[52,54,55] Therefore, to study particular mechanisms of the formation of fine spectral structure in actinide compounds, it is expedient to use compounds of those elements in the spectra of whose electronic shells this mechanism shows itself with the highest probability.

Most often, the fine structure of the XPS spectra of actinide compounds is interpreted based on the results of theoretical calculations (U,[24–26,31,32,42,55,93,129–137] Th,[124,125,129] Np,[33,36,136] Pu,[33,36,138] Am,[33,35,138] Cm, Bk, Cf[35,137,138]). However, such calculations are usually labour-consuming and are performed after the experimental spectra have already been measured. Therefore, in practice, spectra that have been thoroughly studied both theoretically and experimentally are often used as references to analyse the XPS spectra of new compounds.

X-Ray photoelectron spectroscopy is the most appropriate technique for the study of the physicochemical states of actinides. It is used to estimate the oxidation states of actinides, their electronic configurations, and the degree of participation of electrons in the chemical bond on the surface of solids (Th,[79] U,[139,140] Pu[141,142]), in alloys and other materials (Th,[143] U,[144–147] Pu,[82,146] Am, Cm, Bk, Cf[79]) and to determine radionuclides in the environment. This method is used in the quantitative elemental analysis of actinide materials;[148] in particular, it has been successfully used to determine the elemental and ionic composition of the reactor fuel melts from the Chernobyl nuclear power plant,[9,91,149,150] to study the nature and the structure of 'new-formed' materials grown on these melts,[10,150,151] to study the mechanisms of interaction of the uranyl group (UO_2^{2+}) with calcite and diabase,[12,152–157] humic acids,[11,157–160] apatite[161,162] and biosorbents,[91] to study the microbial reduction of the U^{6+} ions to U^{4+} (Refs 163, 164) and the effect of visible light on the decomposition of the uranyl citrate complex;[165] and to study the elemental and ionic composition of highly hazardous 'hot' particles[8] containing U, Cs,[15,166–169] Sr[15,170–172] and Ru,[13,14,173–175] which have been formed during the simulation of a nuclear power plant accident under laboratory conditions. Together with other X-ray spectral methods,[16] X-ray photoelectron spectroscopy[11,152,158,161] is efficiently used to solve problems related to radionuclide transfer in the environment.

For interpretation of XPS spectra, in particular, of actinide compounds, as has been shown previously for lanthanide compounds,[54] the binding energy range of the electrons (0–1250 eV) can be divided conventionally into three regions. The first one is from 0 to ~15 eV; this exhibits the spectral structure mainly caused by the An5f and OVMO electrons. The second region (~15 to ~50 eV) shows a structure that is largely related to the IVMO electrons and whose parameters correlate with the degree of participation of the An6p and L*n*s atomic orbitals (AO) in the chemical bond and with the structure of the local environment of the actinide ion. The third region (~50 to 1250 eV) reflects the fine spectral structure of the core electron levels; the mechanisms of its formation may be different.

This review mainly deals with the fine structure of the X-ray photoelectron spectra of compounds of light actinides (Th, U, Np, Pu, Am, Cm, Bk, Cf) observed in the binding energy range of 0–1250 eV, the mechanisms of formation of this structure and the dependence of its characteristics on the physicochemical properties of compounds and the nature of the chemical bond in them. We are going to answer the following questions.

1. What are the mechanisms and general regularities of the formation of fine XPS structure for actinide compounds?

2. How do the parameters of the fine structure in question correlate with the properties of actinide compounds and the nature of the chemical bond in them?

3. What new quantitative and qualitative information on the physicochemical properties of actinide compounds can be gained from the parameters of the fine XPS structure?

To simplify the discussion of the fine structure of XPS spectra in the region of valence electrons, we use atomic designations in addition to molecular ones.

II. Thorium compounds

Since the electronic configuration of thorium is $\{Rn\}6d^27s^2$ (see Table 1), the simplest structure of the XPS spectra should be expected of compounds formed by tetravalent thorium. This is due to the fact that Th^{4+} does not contain unpaired electrons (the electronic configuration is $\{Rn\}5f^0$). Filling of the An5f shell with

an increase in the atomic number of the actinide complicates the spectral structure due to the multiplet splitting, which is caused, as noted above, by the presence of unpaired valence electrons in the actinide ion; this results in a complex structure of the final state of this ion upon photoemission of an outer or an inner electron.

This Section presents the results of analysis of the XPS spectra of thorium [57, 120, 176, 177] and its compounds,[52, 55, 59–62, 64, 118, 119, 125, 177] in particular, ThO_2,[53, 58, 61, 98, 99, 117] ThF_4,[53, 58, 98, 99] $Th(NO_3)_4 \cdot 4H_2O$,[53, 58] $Th(SO_4)_2 \cdot nH_2O$, $Th(OH)_4$, $Th(CO_3)_2 \cdot nH_2O$,[55] $ThSiO_4 \cdot nH_2O$,[61, 63] mainly dealing with their fine structure and dependence of its characteristics on the oxidation state of thorium, the structure of compounds, and the nature of the chemical bond in them. This information is also necessary for interpretation of the XPS structure of heavier actinide compounds containing unpaired An5f electrons.

1. Spectral range of valence electrons

In the low binding energy range (around the Fermi level for metals), the XPS spectra of thorium compounds (Figs 1, 2) exhibit a poorly resolved band due to electrons of the OVMO. This band largely reflects the participation of the $Th6d^27s^2$ and L*n*p electrons of thorium and the surrounding ligands L in chemical bonds. The full widths at half maximum (FWHM) of these bands for ThO_2, $Th(NO_3)_4 \cdot 4H_2O$ and ThF_4 are 3.3, 2.5 and 3.7 eV, respectively [55, 58] (see Fig. 2).

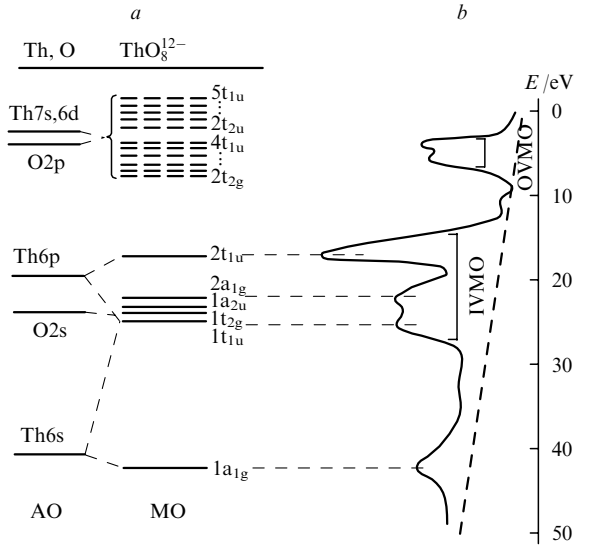


Figure 1. Scheme of MO formation in the ThO_8^{12-} cluster (O_h group of symmetry) (*a*) and X-ray photoelectron spectrum of the oxide ThO_2 (*b*).[58, 62] The dashed line in Fig. 1 *b* is the background.

In a binding energy range of ~10–50 eV, the spectra show a structure due to the Th6s, Th6p and L*n*s electrons. This structure is more complicated than that expected for the sum of the atomic spectra of the elements contained in the given compounds. Thus, the experimental spin–orbit splittings (ΔE_{sl}) for the Th6p electrons differ markedly for the oxide (9.0 eV), fluoride (7.2 eV), thorium metal (7.9 eV) and atomic thorium (9.2 eV) (Tables 2, 3).[55, 57, 58, 62, 178, 179] For ThO_2 and ThF_4, this binding energy difference between the $Th6p_{3/2}$ and $Th6p_{1/2}$ electrons cannot be attributed to the superposition of the Th6p line onto the neighbouring lines related to the ligands. In this case, the components of the thorium doublet would shift in the opposite direction, and apparent splitting of this level for ThO_2 would be lower than for ThF_4. It is known from numerous experimental data that in the low-energy range, the spin–orbit splitting of the core levels depends only slightly on the chemical environment.[21, 23]

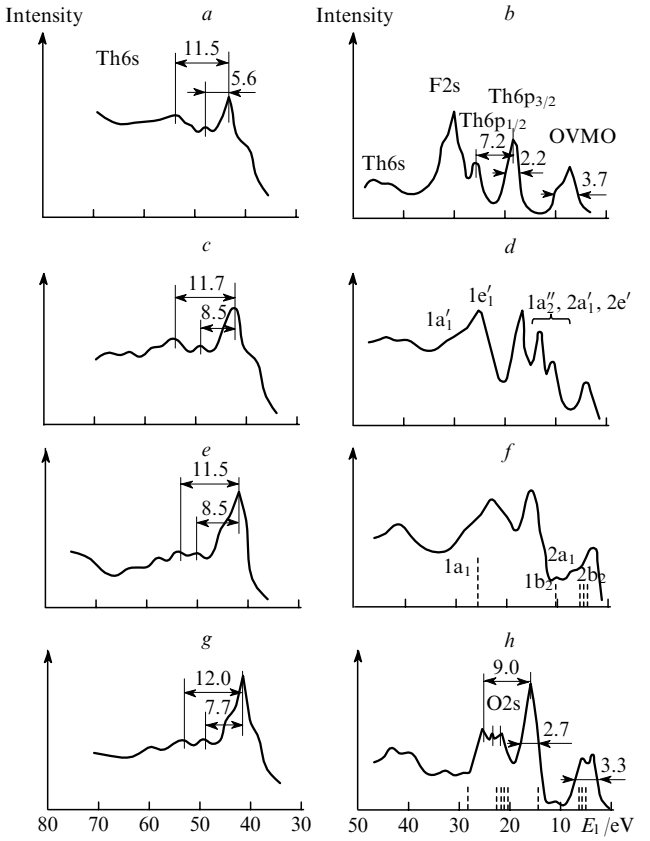


Figure 2. XPS spectra of thorium compounds in the range of weakly bound electrons
(*a*, *b*) ThF_4; (*c*, *d*) $Th(NO_3)_4 \cdot nH_2O$; (*e*, *f*) $Th(OH)_4$; (*g*, *h*) ThO_2. The Th6s spectra (*a*, *c*, *e*, *g*) show the dynamic effect with the formation of final states of the type $Th6s^16p^66d^0 \rightleftharpoons Th6s^26p^46d^1$; the vertical lines below the spectrum *h* show the MO energies for the ThO_8^{12-} cluster (O_h symmetry);[180] the vertical strokes below spectrum *f* show the experimental spectrum of H_2O;[19] the designations for the MO of the NO_3^- ligand (D_{3h} symmetry) are presented above spectrum *d*.

The extra structure present in the O2s and F2s binding energy range cannot be explained by the presence of ligand atoms in different oxidation states in ThO_2 and ThF_4. In this case, the corresponding structure would also be observed in the O1s and F1s spectra. This is due to the fact that the chemical shift does not depend significantly on the core electron binding energy in the E_b range up to ~1000 eV.[21, 23] The O1s and F1s spectra of ThO_2 and ThF_4 consist of single lines with FWHM of 1.4 and 1.7 eV, respectively.[58]

The most complicated fine structure is observed in the low-energy XPS range for thorium compounds containing organic ligands. In this case, the thorium spectrum is superimposed by a spectrum of the IVMO electrons of the ligands. (For some compounds, these MO are also shown in Fig. 2.)

On the basis of the XPS data, taking into account the results of theoretical calculations,[129, 137, 180, 181] it has been suggested [51, 55, 58, 59, 101, 102] that an important reason for the formation of the fine structure in the spectra of these thorium compounds is efficient (experimentally observed) formation of IVMO from the Th6p and L2s atomic shells.

The foregoing can be illustrated in relation to the spectrum of the low binding energy electrons of ThO_2. The local environment of thorium in this compound can be simulated by the ThO_8^{12-} cluster (O_h group of symmetry) in which the Th–O bond length (R_{Th-O}) equals 0.241 nm (Fig. 3, see Fig. 1).[54] The results of theoretical calculations performed for the ground state of this cluster in the non-relativistic spin-limited SCF X_α-DV approx-

Table 2. Binding energies (E_b) and photoionisation cross-sections (σ) for thorium and its compounds.[62]

Orbital Th, L (nl_j)	E_b /eV								σ(Th, L) [a]
	ThF_4	$Th(SO_4)_2 \cdot n H_2O$	$Th(NO_3)_4 \cdot n H_2O$	$Th(OH)_4$	$Th(CO_3)_2 \cdot n H_2O$	ThO_2	Th_{metal} (see [57])	Th_{theor} (see [178])	
OVMO	8.3	7.3	5.6	5.6	5.2	5.8			–
Th6$p_{3/2}$	18.4	18.8	18.4	17.5	17.2	16.5	16.6	24.8	0.37
Th6$p_{1/2}$	25.6	–	–	–	–	25.5	24.5	34.0	0.13
Th6s (see [b])	44.5	44.6, 50.8	43.7	42.6	41.9, 50.1	41.9	41.4	53.5	0.16
Th5$d_{5/2}$	88.5	88.2	87.8	86.8	86.7	86.3	85.4	95.6	3.15
Th5$d_{3/2}$	95.5	95.2	94.8	93.8	93.6	93.3	92.5	102.7	2.15
Th5$p_{3/2}$ (see [b])	177.8, 181.0, 197.9	177.3, 181.1, 198.6	176.7, 180.0, 198.9	– 179.2, 197.0	– 179.0, 198.8	175.1, 178.6 194.1	– 177.2	– 197.6	– 2.05
Th5$p_{1/2}$	236.7	–	237.0	234.8	236.6	233.4	233.8	244.1	0.66
Th5s	288.7	289.1	289.0	289.7	289.0	288.7	–	307.4	0.70
Th4$f_{7/2}$	336.6	336.3	335.8	335.0	334.8	334.3	333.1	343.6	23.94
Th4$f_{5/2}$	345.9	345.7	345.2	344.2	344.0	343.6	342.4	352.8	18.81
Th4$d_{5/2}$	678.4	677.9	677.1	676.4	676.1	675.6	675.2	678.0	16.31
Th4$d_{3/2}$	715.5	715.0	714.8	713.9	713.6	712.7	712.4	715.0	10.82
Th4$p_{3/2}$ (see [b])	967.5, 969.5	969.2	–	969.2	966.6	966.7	966.4	969.8	7.46
O2s		25.4	26.7	22.5	24.9	22.0			0.14
O1s		532.5	533.3	532.0	531.8	530.2			2.93
F2s	29.8								0.21
F1s	685.5								4.43
N1s			407.7						1.80
S2$p_{3/2}$		169.7							1.68
S2s		233.4							1.43
C1s					289.0				1.00

[a] The σ values are expressed in the units used in Ref. 62: 13.6 barn (b) per atom. [b] The E_b values corresponding to the line maxima in the corresponding binding energy ranges are given.

Table 3. Binding energy differences (ΔE_i) for various electron shells of thorium and ligands.[55]

Compound	$\Delta E_i = E_k - E_l$ /eV					
	6$p_{3/2}$ – 6$p_{1/2}$	6$p_{3/2}$ – 6$s_{1/2}$ (see [a])	6$p_{3/2}$ – 4$f_{7/2}$	6$s_{1/2}$ – 4$f_{7/2}$ (see [a])	5$d_{5/2}$ – 4$f_{7/2}$	L2s – L1s (see [b])
ThO_2	9.0	25.4	317.8	292.4	248.0	508.2, 506.2
$Th(CO_3)_2 \cdot \cdot n H_2O$	–	24.7	317.6	292.9	248.1	506.9
$Th(OH)_4$	–	25.1	317.5	292.4	248.2	509.5
$Th(NO_3)_4 \cdot \cdot n H_2O$	–	25.3	317.4	292.1	248.0	506.6
$Th(SO_4)_2 \cdot \cdot n H_2O$	–	25.8	317.5	291.7	248.1	507.1
ThF_4	7.2	26.1	318.2	292.1	248.1	655.7
Th_{metal} (see [57])	7.9	24.8	316.5	291.7	247.7	–
Th_{theor} (see [178])	9.2	28.7	318.8	290.1	248.0	–

[a] The binding energies corresponding to the most intense peaks in the Th6s spectra are used. [b] The ΔE_i differences for oxygen and fluorine are given.

imation[180] are presented in Fig. 3 for convenient qualitative comparison with the experimental data. It follows from Fig. 3 that the MO system can be conditionally subdivided into two groups, inner valence and outer valence MO.

The outer valence MO (OVMO) group consists of vacant $2t_{2u}-6t_{1u}$ orbitals and filled $2t_{2g}-4t_{1u}$ orbitals, which contain occupied Th5f states, whereas free thorium atoms contain no Th5f electrons. It has been shown experimentally [99, 100] that relatively high line intensity in the XPS spectra of ThO_2 and ThF_4 in the OVMO energy range is largely related to the presence of filled Th5f states in these compounds. This is consistent with the results of studies of $L_{\alpha 1,\beta 2,4}$(Th)-emission of thorium oxide and halides.[182]

The other group of molecular orbitals includes the $1a_{1g}$, $1t_{1u}$, $1t_{2g}$, $1a_{2u}$, $2a_{1g}$ and $2t_{1u}$ IVMO. Analysis shows that, whereas OVMO mainly consist of vacant valence Th5f, Th7s, Th6d, Th7p and O2p atomic orbitals, the IVMO are mainly composed of fully occupied inner valence Th6s, Th6p and O2s AO. For example, orbitals of the $1t_{1u}$ and $2t_{1u}$ IVMO pair, one of which can be considered as a bonding orbital ($1t_{1u}$) and the other, as an antibonding one ($2t_{1u}$), consist of 18% of Th6p plus 68% of O2s and 55% of Th6p plus 27% of O2s, respectively (see Fig. 3). Significant mixing of the Th6s and O2s AO takes place during formation of the $1a_{1g}$ and $2a_{1g}$ IVMO pair. However, for uranium oxides, it has been shown [123, 180] that inclusion of relativistic effects in the calculation leads to a lower degree of mixing. This is mainly due to splitting off of the Th6$p_{1/2}$ component from the Th6$p_{3/2}$ level (ΔE_{sl} = 7.9 eV), which allows the use of non-relativistic calculation results in interpretation of the low binding energy spectra of actinide compounds.

The energies of occupied OVMO electronic levels do not differ much (−11.21 to −9.39 eV) and fall within a range of 1.82 eV. The energies of the inner valence MO vary over a broader range and form an energy structure typical of this cluster. This makes it possible to construct qualitative structural schemes for the IVMO of various model clusters (see Figs 1, 3).

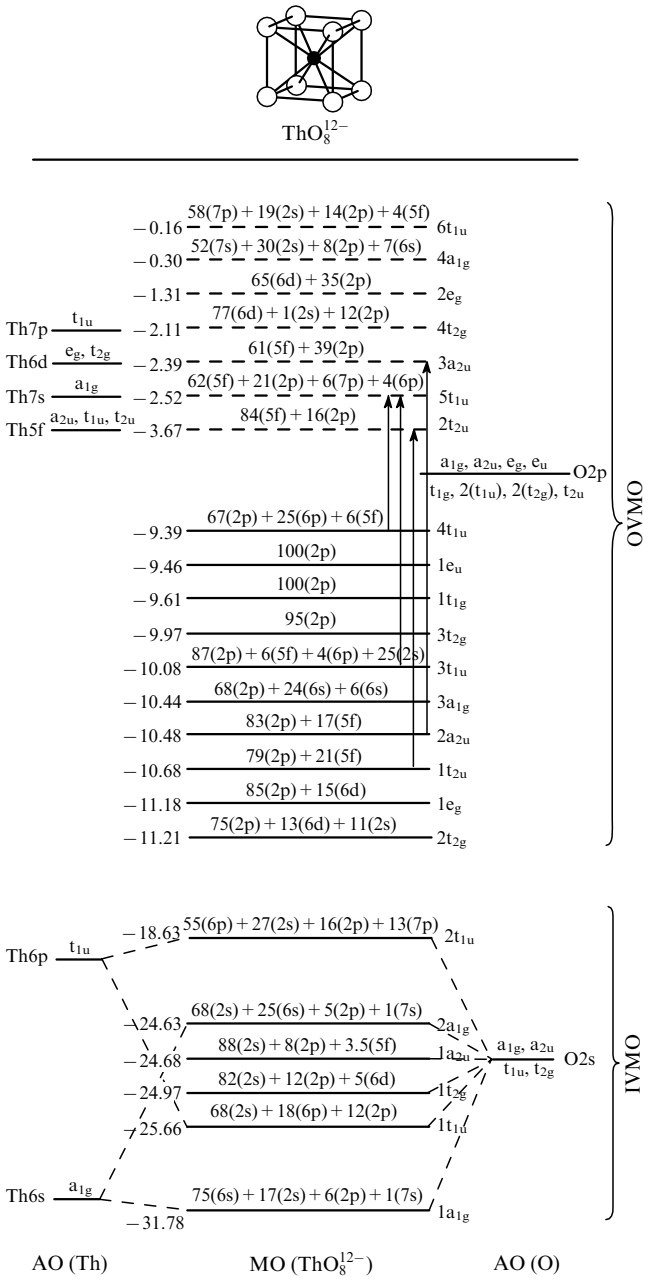


Figure 3. Composition (%) and the structure of MO of the ThO_8^{12-} cluster (O_h symmetry) for $R_{Th-O} = 0.241$ nm (X_α-DVM calculations).[180] The vacant MO are shown by horizontal dashed lines; here and below, AO and related IVMO are connected by dashed lines. The arrows show the most probable electronic shake up transitions which accompany the photoemission of a core electron (the energy scale is not maintained).

Experimental data for ThO_2 are presented in Fig. 4, which provides their qualitative comparison with the results of theoretical calculations and shows the binding energy differences between the valence and core electrons for separate atoms and the ThO_8^{12-} cluster, which can be determined experimentally.

It can be seen from Fig. 4 that the formation of molecular orbitals from the Th6p and O2s AO can induce a relative shift of the $2t_{1u}$ level toward lower binding energies compared to that of the Th6p electrons by a Δ_1' value. The formation of IVMO from the Th6s and O2s AO can entail a relative shift of the $1a_{1g}$ level toward higher binding energies compared to that of the Th6s electrons of the Th metal by a Δ_2 value. Note that MO formation can induce some other significant effects that influence the line shifts, for example, a change in the effective charge of the nucleus.

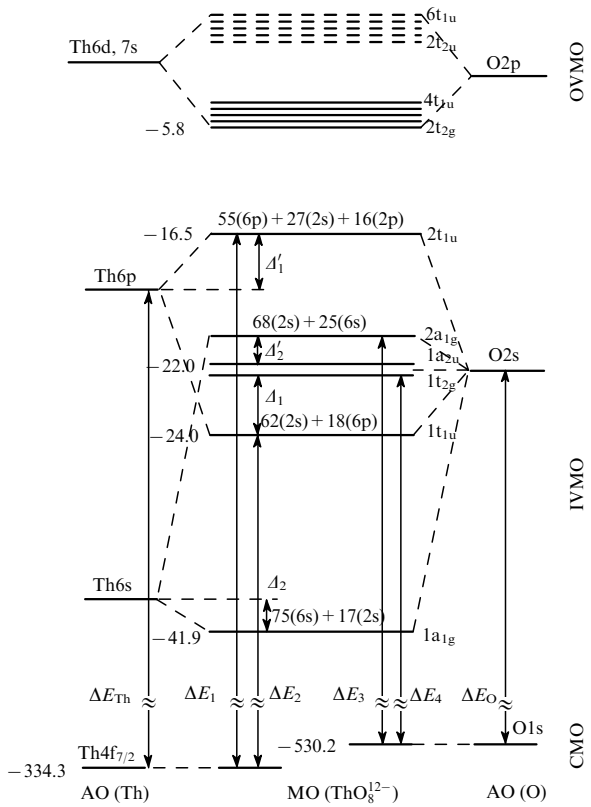


Figure 4. Diagram of MO of the ThO_8^{12-} cluster (O_h symmetry) reflect the structure of the nearest environment of the thorium atom in ThO_2. Chemical shifts induced by MO formation from AO are not reflected. The diagram is based on the XPS spectrum and calculation results.[180]

These shifts of the levels related to MO formation can be determined rather reliably by comparing the energy differences between various valence and core levels ΔE_i ($i = 1-4$), ΔE_{Th} and ΔE_O (see Fig. 4) found from the XPS spectra of thorium compounds (see Table 3).

It follows from the data of Table 3 that on passing from thorium metal to thorium compounds, the binding energy differences (ΔE_i) between the core $Th4f_{7/2}$ and $Th5d_{5/2}$ electrons change to the least extent. Substantial deviations in the ΔE_i energies are found for the formal $\Delta E_{sl}(Th6p_{3/2} - Th6p_{1/2})$ and $\Delta E_1(Th6p_{3/2} - Th4f_{7/2})$ values, which describe the energy shifts of valence electrons. These results are consistent with the assumption that at least the $Th6p_{3/2}$ and O2s atomic shells are involved in the $2t_{1u}$ IVMO, which is formally antibonding.

The formation of IVMO in the oxide ThO_2 and the fluoride ThF_4 is confirmed by X-ray $O_{4,5}$(Th) emission spectroscopy.[99,100,183–186] Additional information on the valence electron states of thorium dioxide and tetrafluoride can be gained from X-ray $O_{4,5}$(Th) [187–190] and $M_{3,4,5}$(Th) absorption spectra.[191]

2. Electronic structure of ligands

The low binding energy spectra of $Th(SO_4)_2 \cdot n\,H_2O$, $Th(NO_3)_4 \cdot n\,H_2O$, $Th(CO_3)_2 \cdot n\,H_2O$ and $Th(OH)_4$ [55] can be represented approximately as the summary spectra of clusters with a Th central atom surrounded by the ligands NO_3^-, SO_4^{2-}, CO_3^{2-}, OH^- and H_2O (see Fig. 2).

To estimate qualitatively the contribution of ligands to complication of the structure of the general low binding energy spectrum of thorium compounds, let us consider the spectral structure of the ligands taking the NO_3^- group as an example.

The low binding energy spectral range of $Th(NO_3)_4 \cdot n\,H_2O$ can be approximately regarded as a superposition of the spectra from thorium involved in the chemical binding with oxygen, the

NO_3^- ligand and H_2O (see Fig. 2 *c*,*d*). The experimental XPS spectrum of water (C_{2v} group of symmetry)[19,55] reflecting the system of its MO is shown in Fig. 2 *f* by vertical dashed lines. The spectral structure of the NO_3^- ligand (D_{3h} group of symmetry) with $R_{N-O} = 0.121$ nm is conveniently illustrated by the MO diagram (Fig. 5) constructed on the basis of results of semiempirical CNDO/2 calculations. These results are in satisfactory agreement with the data for $Ni(NO_3)_2 \cdot 6\,H_2O$ whose XPS spectrum exhibits, in the low binding energy range, only an OVMO band for nickel at low E_b values.[55] Except for the thorium line in the valence band, the spectral structures for nickel and thorium nitrates have much in common. The molecular orbitals of the NO_3^- ligand are shown in Fig. 2 *d* above the spectra of thorium nitrate. The contributions of the electrons from various MO to the covalent bonding in the NO_3^- ligand [58] were estimated based on the resonance energy value E^{α}_{N-O} (measured in au),[52,53] which characterises the fraction of covalent bonding in the chemical bond; the corresponding energy values are indicated in parentheses in Fig. 5.

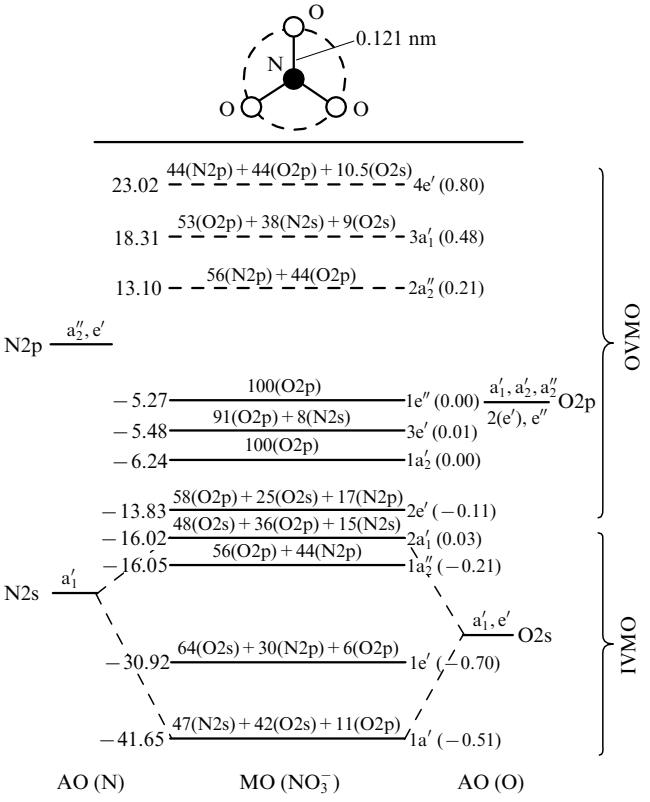


Figure 5. Composition (%) and structure of the MO of the NO_3^- ligand (D_{3h} symmetry) (CNDO/2 calculation).[58]
The values in parentheses are resonance energies (E^{α}_{N-O}, au; see Refs 52, 53). The vacant MO are shown by horizontal dashed lines (the energy scale is not maintained).

As can be seen from Fig. 5, the energies of occupied MO of the NO_3^- ligand are located within a 36.38 eV range, which almost overlaps the range of MO of the ThO_8^{12-} cluster; taking them into account provides a satisfactory description of the additional structure observed in the experimental XPS spectrum of thorium nitrate (see Fig. 2 *d*). This IVMO structure is expected to arise also in the spectra of compounds containing CO_3^{2-} and SO_4^{2-} groups (D_{3h} and T_d symmetry, respectively).[52]

The results indicate that the spectra of complex ligands of the thorium compounds studied have a characteristic structure caused by OVMO and IVMO electrons extended in a binding energy range of ~35 eV. This structure can be used to identify these substances. In addition, the low energy range of the spectra may display an additional structure caused by secondary electrons and other processes. Since these processes are also reflected in the core electron spectral structures, they can be studied more conveniently in the spectra of core levels.

3. Core electron spectra of thorium compounds

When performing quantitative elemental and ionic analysis using XPS spectra, the stoichiometric compositions of compounds and the oxidation states of ions are determined using the most intense single sharp lines for the core levels. The most suitable line for these studies of thorium compounds is a component of the doublet (caused by the spin–orbit splitting) of the $Th4f_{7/2}$ electrons.[58,60,117,121,125]

The core electron fine structure (shake up satellites) related to many-body perturbation reflects the composition and energy distribution of molecular orbitals. The many-body perturbation is due to the extra final states of thorium ion which arise upon the transition (excitation) of a valence electron to a vacant outer MO simultaneously with the photoemission of a core electron (shake up process[21–23,49]). This gives rise to shake up satellites on the higher binding energy side from the basic lines. Such satellites are observed in the spectra of all core and valence levels; however, as the electron binding energy decreases, their intensity diminishes (see, for example, the study[192] dealing with $LnNbO_4$). These satellites are more specific in the Th4f and Th5d spectra (Fig. 6). Since the excitation of ligand-related electrons from filled MO to vacant, mainly metallic AO can take place during the electron photoemission from a core metallic level (see Fig. 3), the corresponding satellites can be attributed to the charge transfer from the ligand L to the metal M: $Lnl \rightarrow Mn'l'$, where n (n') and l (l') are the principal and orbital quantum numbers, respectively.[23] These excitations, which satisfy the monopolistic selection rules, $\Delta l = \Delta s = 0$ (s is the spin quantum number) are shown for ThO_8^{12-} in Fig. 3 by arrows. A simple two-level theoretical model[22,23,118,193] makes it possible to calculate the satellite intensity, which is related to the change in the partial electron density on a filled AO of the metal caused by electron photoemission from a core level. On the basis of this model, it was shown that the satellite intensity diminishes as the metal electron density on a certain filled MO increases and the magnitude of its change upon the photoemission of the core electron decreases. The energy distance from a satellite to the basic line depends on the ionic–covalent nature of the chemical bond in the compound. In the case of 3d-metal compounds, this distance increases and the satellite intensity decreases with an increase in the ionic contribution to the bond.[193] The spectra containing shake up satellites are typical of a particular thorium compound and reflect the actinide oxidation

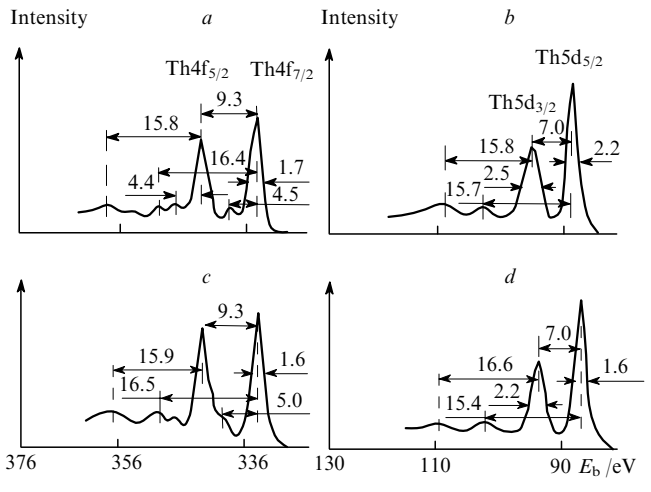


Figure 6. XPS spectra of thorium compounds in the Th4f (*a*, *c*) and Th5d (*b*, *d*) binding energy ranges.[55] (*a*, *b*) ThF_4; (*c*, *d*) ThO_2.

state and the stoichiometric composition. A similar satellite structure can also be followed in the Th5d spectra (see Fig. 6).

It is also noteworthy that, despite the complication of the Th4f and Th5d spectral structures due to many-body perturbation, the observed basic lines are relatively sharp. The intensity ratios of individual components of doublets are close to the theoretical values, while the spin–orbit splittings (ΔE_{sl}) are constant for different compounds, being equal to 9.3 and 7.0 eV for the Th4f and Th5d electrons, respectively. A similar spectral pattern for some shells of transition elements is usually observed when the multiplet splitting and dynamic effect are feebly manifested in the spectra of these electrons.[22, 23, 193]

The Th6s binding energies reported in several papers [20, 57, 58] are different. This discrepancy can be explained by the errors of measurements resulting from the relatively small Th6s photoionisation cross-section and unexpectedly wide energetic interval ($\sim$40 eV) in which the complex fine spectral structure arises. The most intense maximum in the Th6s spectrum from ThO_2 is observed at $E_b \approx 42$ eV (see Fig. 2 *g*).

On the basis of theoretical calculations, [129, 137, 180] it was suggested that the Th6s shell can markedly participate in the MO formation in thorium compounds. Therefore, for a number of thorium compounds, the low binding energy XPS spectra of Th6s electrons were recorded and analysed [55, 58] (see Fig. 2). In a range of $\sim$40 eV, the Th6s spectra show structure that cannot be attributed to the participation of Th6s in the chemical bond alone. This participation could result in the shift of the Th6s line or appearance of a fine structure with a width of several electron-volt. Since the compounds in question are diamagnetic and do not contain unpaired electrons, their XPS spectra are not expected to display multiplet splitting. The maxima observed at the same relative energies as the Th4f and Th5d spectra can probably be attributed to the shake up satellites in those cases where the corresponding line intensities do not exceed $\sim$10% of the basic lines.

Similar considerations are also valid for spectral structure of the Th5p electrons (Fig. 7). Instead of the expected doublet caused by the spin–orbit splitting, this spectrum exhibits a much more complicated fine structure. The spin–orbit splitting is given by ΔE_{sl}(Th5p) = 47 eV, while the binding energies (see Table 2) are as follows: $E_b(Th5p_{3/2}) = 182$ eV and $E_b(Th5p_{1/2}) = 229$ eV.[20] However, the spectra of thorium compounds exhibit a clear-cut additional line at $\sim$200 eV and the $Th5p_{1/2}$ lines are broadened (see Fig. 7). These structural changes in the spectra of relatively deep electron shells cannot be attributed to the crystal field splitting. Moreover, splittings of about several electron-volt are also observed in the $Th4p_{3/2}$ spectra.[55] These spectra are complicated due to the appearance of additional broad OKLL Auger bands. The most individual fine structure in the $Th4p_{3/2}$ spectra is found in the spectrum of thorium tetrafluoride containing no O atoms.[55]

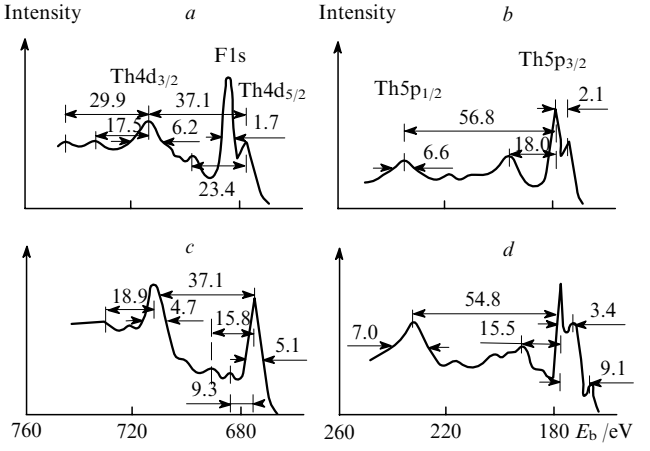


Figure 7. XPS spectra of thorium compounds in the Th4d (*a*, *c*) and Th5p (*b*, *d*) binding energy ranges.[58] (*a*, *b*) ThF_4; (*c*, *d*) ThO_2. The Th5p spectra for both compounds show the dynamic effect, resulting in the formation of final states of the type $Th5p^5 5d^{10}(6s^2 6p^6)5f^0 \rightleftharpoons Th5p^6 5d^8(6s^2 6p^6)5f^1$.

The XPS spectra of thorium and its compounds may clearly manifest the dynamic effect due to the giant Coster–Kronig transitions within the core and outer shells during the electron photoemission from an atom or an ion. This results in several final states of an ion and, as a consequence, a complicated fine structure is observed in the spectra instead of sharp single lines. For thorium compounds, the ratios of the binding energies of core and outer electronic levels are favourable for this effect to appear during the photoemission of core electrons from the Th atom. Indeed, since the binding energies of thorium levels obey the ratios $E_b(Th6s) \approx 2E_b(Th6p)$; $E_b(Th5d) \approx 2E_b(Th6s)$; $E_b(Th5p) \approx 2E_b(Th5d)$; $E_b(Th4f) \approx 2E_b(Th5p)$; $E_b(Th4d) \approx 2E_b(Th4f)$; $E_b(Th4p) \approx E_b(Th4d) + E_b(Th5s)$, and the dynamic effect has a resonance nature,[55] the probability of this effect for thorium compounds is rather high (see Table 2). The dynamic effect gives rise to an additional two-hole final state (apart from the ground one-hole state), due to the electron transition from an intermediate fully occupied level to a level with a hole that has appeared upon electron photoemission from the atom and to the nearest low-energy vacant level in the molecule under consideration. This two-hole state should have the same orbital quantum number L as the ground one-hole final state and a similar energy.[119, 120, 194] According to estimates,[119, 124] the following one-hole and two-hole final states are expected to appear with the highest probability for Th^{4+} compounds after photoemission of the core electron: $Th6s^1 6p^6 6d^0 \rightleftharpoons Th6s^2 6p^4 6d^1$ (see Fig. 2); $Th5p^5 5d^{10}(6s^2 6p^6)5f^0 \rightleftharpoons Th5p^6 5d^8(6s^2 6p^6)5f^1$ (see Fig. 7, Table 2); $Th5s^1 5p^6 5d^{10}(6s^2 6p^6) \rightleftharpoons Th5s^2 5p^5 5d^9(6s^2 6p^6)5f^1$. It is assumed [55, 58] that the dynamic effect can also be observed in the $Th4p_{3/2}$ spectra. This can be attributed, for example, to the formation of final states of the type $Th4p^5 4d^{10} 5s^2 . (5p^6 5d^{10} 6s^2 6p^6) \rightleftharpoons Th4p^6 4d^9 5s^1 (5p^6 5d^{10} 6s^2 6p^6) 7p^1$.

The structure of the Th5s spectra caused by the dynamic effect is difficult to observe, as it is superimposed by the C1s spectrum;[55, 58] however, it has been shown theoretically that this structure should occur in this binding energy range.[124, 194]

It follows from the above examples that, on the one hand, the fine spectral structure complicates gaining the traditional information concerning the binding energies and line intensities for the core electrons, but, on the other hand, this structure provides significant additional information on the electron structure, the nature of chemical bonds and the secondary electronic processes that accompany the electron photoemission from ions.

A number of industrially important thorium compounds have now been studied by XPS. Although thorium is formally tetravalent in each of the compounds studied, the binding energies imply that the thorium oxidation state increases in the following sequence: ThO_2, $Th(CO_3)_2 \cdot n H_2O$, $Th(OH)_4$, $Th(NO_3)_4 \cdot 4 H_2O$, $Th(SO_4)_2 \cdot n H_2O$, ThF_4.[55, 58] This results in an increase in the $Th4f_{7/2}$ binding energy by $\Delta E_b = 1.8$ eV. Thus, in the series of thorium compounds, the ionic nature of the chemical bond increases.

To conclude this Section, we would like to note that the understanding of the mechanism of fine structure formation in the XPS spectra of thorium compounds is highly favourable for gaining the most detailed and reliable information on the properties of these compounds and the nature of the chemical bond in them.

III. Uranium compounds

Solid-state uranium compounds have been studied by XPS in most detail.[45, 47, 53, 55, 57, 65, 66, 75, 78, 93, 94, 177, 195–198] The gaseous UF_6, $U(BH_4)_4$, $U(BH_3Me)_4$ and $U(C_8H_8)_2$ molecules have been

studied.[199–201] Photoelectron spectroscopy data for the UF_4, UCl_4 and ThF_4, $ThCl_4$ molecules in the gas phase have also been reported.[179, 202] Theoretical analysis of the electronic structures of these compounds has received much attention.[53, 55, 123, 129–132, 203–206] X-Ray photoelectron spectroscopy has proved to be the most adequate method for determining the oxidation states and ionic compositions of uranium in oxides and other compounds, in particular, in ores.[66] Knowledge of the uranium oxidation state in ores is especially important for underground leaching.[207, 208] In a number of studies,[47, 65, 66, 92–94] uranium compounds have been studied by XPS in order to develop a non-destructive method for determining the uranium oxidation states in compounds and minerals and the stoichiometric compositions of minerals on the basis of XPS fine structure parameters.

1. Uranium oxides

a. The U5f spectra

X-Ray photoelectron studies of uranium oxides have shown[38–40, 45, 53, 65–68, 76, 77, 93, 111, 190, 209, 210] that the fine structures of the low binding energy spectra ($E_b = 0-50$ eV) of UO_2 and UO_3 are substantially different (Fig. 8). Since the U^{6+} ion in the trioxide γ-UO_3 has the electronic configuration $\{Rn\}5f^0$, while the electronic configuration of U^{4+} in the dioxide UO_2 is $\{Rn\}5f^2$, the XPS spectrum of the latter,[40, 45, 65–68, 93, 209] unlike the spectrum of γ-UO_3, exhibits a rather narrow intense line at $E_b = 1.9$ eV, which belongs to the U5f electrons participating only slightly in the chemical bond. In addition, some differences in the structures of OVMO and IVMO bands for uranium dioxide and trioxide are also observed (see Fig. 8).

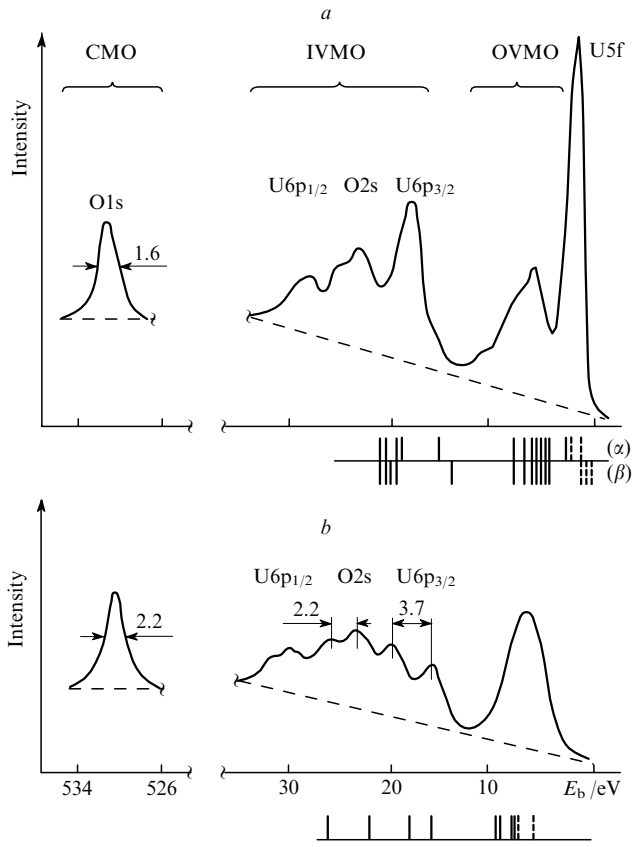


Figure 8. XPS spectra of uranium oxides UO_2 and γ-UO_3 in the low binding energy range and in the O1s range.[53, 93]
(*a*) UO_2, (*b*) γ-UO_3. The intensities of electrons from different shells are not normalised. The dashed lines show the background. The vertical lines under the spectra show the energy levels found by non-relativistic spin-unrestricted (*a*) and spin-restricted (*b*) SCF X_α-SW calculations.[93]

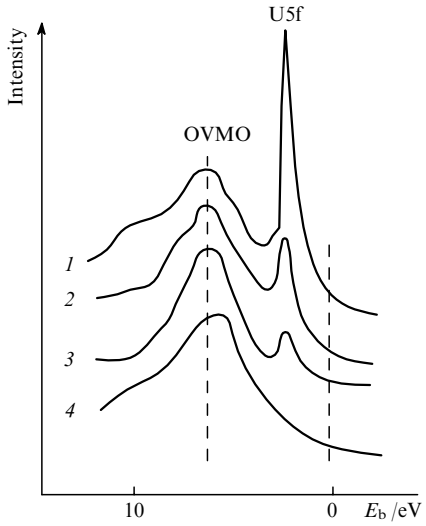


Figure 9. XPS spectra of synthetic uranium oxides in the U5f and OVMO binding energy ranges.[65]
(*1*) $UO_{2.06}$; (*2*) U_2O_5; (*3*) U_3O_8; (*4*) γ-UO_3.

X-Ray photoelectron spectra of low binding energy electrons (0 to $\sim$50 eV) which participate in the MO formation reflect the band structure and represent lines with a width of several electron-volt. The line around a zero binding energy observed in the spectrum of uranium dioxide containing unpaired U5f electrons has the FWHM $\Gamma \approx 1.4$ eV, which is typical of core electrons (see Fig. 8). In the spectra of the U_4O_9, U_2O_5 and U_3O_8 oxides, the intensity of the U5f line decreases (Fig. 9).

Since the ratio of photoionisation cross-sections $\sigma(U6d)/\sigma(U5f)$ is appreciably lower than unity,[203] the U6d line in the XPS spectra should be much less intense than the line for the unbound U5f electrons. For the U^{4+} ion with the electron configuration $\{Rn\}5f^2$, $\sigma(U5f_{5/2})/[3\sigma(U4f_{7/2})] = 0.0213$,[35] which is almost half the corresponding experimental relative intensity[65] $I = I(U5f)/I(U4f_{7/2})$ for UO_2, equal to 0.0383 (Fig. 10).

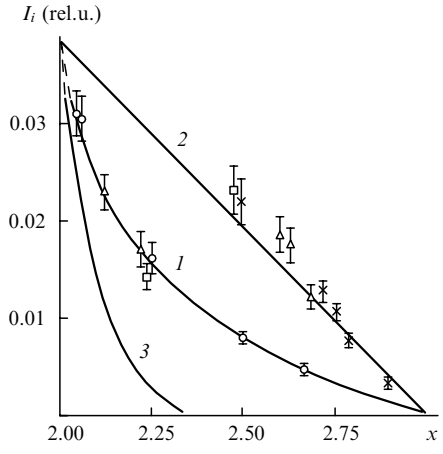


Figure 10. Relative intensity (I_i) of the U5f line in the XPS spectra of synthetic and natural uranium oxides UO_x *vs.* the oxygen coefficient x.[65, 66]
(*1*) I_1 calculated from Eqn (1); (*2*) I_2 calculated from Eqn (2), (*3*) I_3 calculated from Eqn (6); the dots correspond to experimental data: the circles show the data for synthetic oxides; triangles and squares, natural oxides; crosses, UO_2 and γ-UO_3 mixtures.

The energy difference between the U5f and OVMO lines is ~4.2 eV, which permits reliable determination of the intensity of the former. For elucidating the dependence of the intensity (I_1) of the U5f line on the number of oxygen atoms (oxygen coefficient x) in the UO_x oxides, found as the intensity ratio of the U5f lines to the $U4f_{7/2}$ lines without inclusion of the shake up satellites, a number of synthetic uranium oxides have been studied.[65,66] The dependence of the relative intensity I_1 of the line observed in the XPS spectra of the UO_x oxides around zero binding energy, which is caused presumably by the unbound U5f electrons, on the oxygen coefficient x for synthetic oxides can be described as follows (see Fig. 10):

$$I_1 = 5.4x^{-7.2}. \quad (1)$$

Extrapolation of the curve for the dependence of I_1 on x gave the relative intensity $I_1 = 0.0383$ for UO_2. This allows one to construct a similar dependence for mixtures of UO_2 and UO_3 obtained upon homogenisation. This dependence is given by[66]

$$I_2 = -0.0383x + 0.1148. \quad (2)$$

The values of the relative intensity I_2 of the U5f line for mechanical mixtures of the UO_2 and γ-UO_3 oxides fit satisfactorily into this straight line (see Fig. 10).

Since unpaired electrons are responsible for paramagnetism of molecules, it appeared pertinent to compare the dependences of the U5f line intensity in the XPS spectra and the magnetic susceptibility (χ) of the UO_x oxides on the oxygen coefficient x. An increase in x in the range $2 < x \leqslant 3$, entails a decrease in the magnetic susceptibility,[55,90,211] the corresponding dependence being described by the following relation (Fig. 11)

$$\chi = (55.8x^{-0.95} - 19.6) \times 10^{-6}\ g^{-1}. \quad (3)$$

Similar results as regards the magnetic properties have been obtained in another study.[212] It was concluded that $\{Rn\}5f^2$ or $\{Rn\}5f^16d^1$ is the most probable electronic configuration of uranium in the dioxide UO_2 ($\mu_{ef} = 3.2\ \mu_B$), while the trioxide UO_3 possesses a weak temperature-independent paramagnetism, which can be neglected.[212]

For synthetic oxides, the specific magnetic susceptibility χ correlates with the relative intensity I_1 in the following way[91] (Fig. 12):

$$\chi = 62.3 \times 10^{-6} I_1^{0.579}\ g^{-1}. \quad (4)$$

In this case, the I_1 grows faster than the magnetic susceptibility following a decrease in x (see Fig. 10–12).

It has been noted[212] that on a further decrease in the oxygen coefficient x from 2 to 1.835, the magnetic susceptibility of UO_x drops from 8.74×10^{-6} to $8.38 \times 10^{-6}\ g^{-1}$. Unfortunately, the change in the U5f line intensity upon the removal of an oxygen atom from the UO_2 surface, for example, by means of an argon gun, has not been studied quantitatively.

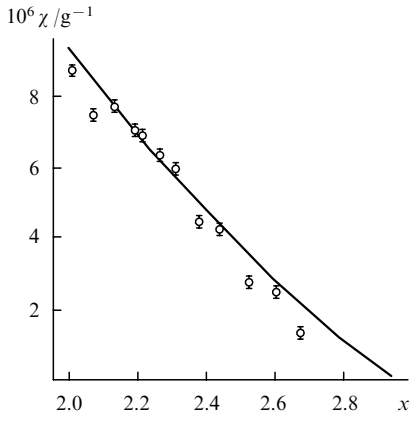


Figure 11. Specific magnetic susceptibility (χ) of synthetic oxides UO_x *vs.* the oxygen coefficient x [see Eqn (3)] plotted using the data of Ref. 211.

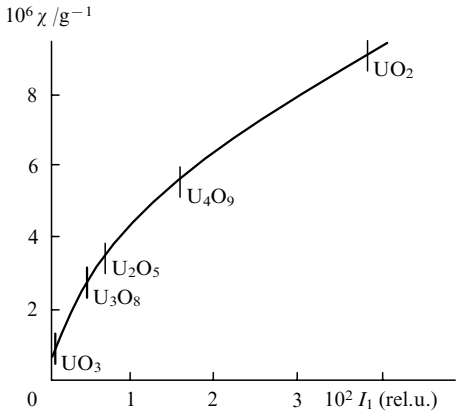


Figure 12. Specific magnetic susceptibility (χ) of synthetic oxides UO_x *vs.* relative intensity I_1 of the U5f line in the XPS spectrum [see Eqn (4)].[65,211] No correction for diamagnetism was done.

For oxide mixtures, the dependence of χ on the intensity I_2 is nearly linear[44,55] (Fig. 13):

$$\chi = 730 \times 10^{-6} I_2^{1.35}\ g^{-1}. \quad (5)$$

It is natural to expect that the magnetic susceptibility would grow proportionally to the intensity I_2 following an increase in the UO_2 concentration in the mixture provided that the intensity of the line under consideration is due to the unpaired unbound U5f electrons.

It follows from the above correlations that the line around the zero binding energy in the XPS spectra of UO_x can be assigned to the unpaired U5f electrons and the configuration of the U^{4+} ion in the dioxide UO_2 is given by $\{Rn\}5f^2$ (see Ref. 55). The relationship between the χ and I values is not as simple as would be expected if the magnetic properties of uranium oxides were governed only by the full spin of the U5f electrons. In addition, the results imply that synthetic oxides are not mere mixtures of UO_2 and UO_3. For example, the dependence of the intensity I_1 on the x value cannot be interpreted under the assumption that the oxides UO_x contain only U^{4+} and U^{6+} ions (see Fig. 10), but it can be explained with the assumption that these oxides contain also U^{5+} ions.[65,66] The presence of U^{5+} ions in complex oxides is consistent with the results of XPS studies[74] and the data of X-ray $L_{III}(U)$ near-edge absorption spectroscopy of the UO_{2+x} oxides.[182] In this case, the difference $\Delta I = I_2 - I_1$ describes the decrease in the content of U^{4+} ions and the formation of U^{5+} ions in UO_x following an increase in x. The approximate relation for the decrease in the

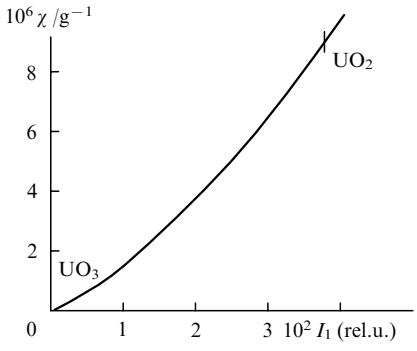


Figure 13. Specific magnetic susceptibility (χ) of synthetic oxides UO_x ($2 \leqslant x \leqslant 3$) *vs.* relative intensity I_2 of the U5f line in the XPS spectrum of oxide mixtures [see Eqn (5)].[55] No correction for diamagnetism was done.

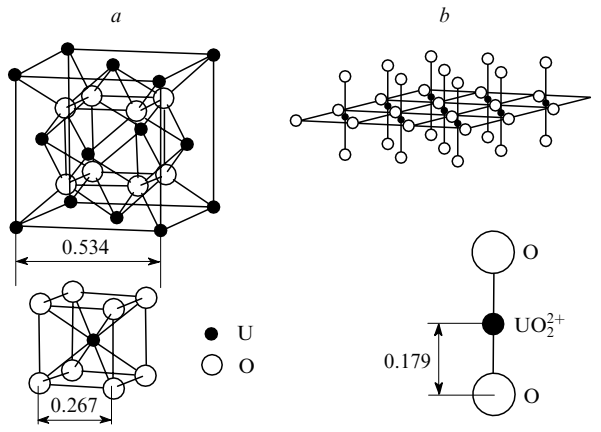


Figure 14. Crystal structure and the local environment of uranium ions in oxides.[5,7]
(*a*) UO_2, (*b*) γ-UO_3. The bond lengths are in nm.

relative intensity I_3 depending on the content of U^{4+} ions has the form

$$I_3 = I_2 - 2(I_2 - I_1) = 2I_1 - I_2. \quad (6)$$

It follows from Fig. 10 that upon an increase in x from 2 to 2.35, the U^{4+} ions disappear from UO_x. This is consistent with X-ray diffraction data indicating that synthetic uranium oxides with $x \to 2.38$, virtually do not contain a structure with the lattice parameters of UO_2 containing eight-coordinate uranium (Fig. 14).[213]

The above dependences (see Fig. 10) can be used to determine the relative contents of different uranium ions in oxides (Table 4). For example, it follows from the data of Table 4 that the oxides U_2O_5 and U_3O_8 mainly contain ions with spectral characteristics close to those of U^{5+} and U^{6+} in 1 : 1 and 1 : 2 ratios, respectively. This does not attest to any violation of the stoichiometric compositions of these oxides, as we are dealing with the formal ionic oxidation states determined from the spectral parameters that reflect the formal number of unbound U5f electrons. More information on the energy distribution of the uranium U5f electrons in oxides can be gained from $O_{4,5}(U)$,[187,189] $M_{III,IV,V}(U)$[191] and $L_{III}(U)$[214] near-edge X-ray absorption spectra. The U, UO and UO_2 species have been studied by high-temperature photoelectron spectroscopy in the gas phase;[215] the results of relativistic Hartree–Fock–Slater theoretical calculations of the electronic structures of these molecules were used to assign the spectral lines to the electrons of some shells.

Table 4. Binding energies (E_b / eV), binding energy differences (ΔE_i / eV) and relative contents of uranium [k (%)] in synthetic uranium oxides.[65,66]

Parameter	UO_2	U_4O_9	U_2O_5	U_3O_8	γ-UO_3
E_b(U5f)	1.9	2.1	2.0	2.1	–
E_b(OVMO)	6.1	6.2	6.0	6.0	6.2
E_b(U6p$_{3/2}$)	–	–	14.4,[b]	–	–
	–	15.7,	15.8,	16.0,	15.7,
	18.0	17.8,	18.0,	18.2,	–
		19.3	19.6	19.4	19.4
ΔE_i(U6p$_{3/2}$)[a]	–	3.6	3.8	3.4	3.7
E_b(U6p$_{1/2}$)	28.5	28.4,	28.9,	29.2,	28.9,
		31.1	31.2	31.1	30.4
E_b(O2s)	23.3,	23.5,	23.5,	23.2,	23.3,
	24.8	25.6	25.7	26.0	25.5
ΔE_i(O2s)	–	2.1	2.2	2.8	2.2
E_b(O1s)	530.5	530.8,	530.5,	530.5,	–
		532.0	531.5	531.5	531.4
ΔE_i(O1s)	–	1.2	1.0	1.0	–
k(U^{4+})	65	9	–	–	–
k(U^{5+})	29	66	50	33	–
k(U^{6+})	6	25	50	67	100

[a] Difference ΔE_i (U6p$_{3/2}$) for the U^{6+} state. [b] Energy corresponding to the additional peak.

b. Structure of the U6p–O2s spectra

In the U6p–O2s binding energy ranges (E_b = ~12–35 eV), a complex fine spectral structure is observed instead of the expected summary atomic spectrum due to the U6p doublet with the spin–orbit splitting ΔE_{sl}(U6p) = 10.0 eV and the O2s lines (see Fig. 8). This structure is more pronounced in the spectrum of γ-UO_3 than in the spectrum of uranium dioxide.[38,45,51,53,65,66,93] Unlike the spectrum of UO_2, the spectrum of γ-UO_3 in the U6p$_{3/2}$ binding energy range (~12–21 eV) displays two clear-cut components. In the U6p$_{1/2}$ spectral range (~27–~35 eV), two components are also observed for these oxides. For oxygen-containing U^{6+} compounds, the presence of two components in the U6p$_{3/2}$ spectrum was explained[45] by splitting of the U6p$_{3/2}$ level of the U^{6+} ion in the asymmetric electric crystal field of ligand ions present in the local environment, which arises on passing from the symmetric structure of the UO_2 dioxide to the asymmetric planar structure of γ-UO_3 (see Fig. 14 *b*).

A structure containing at least two peaks is also observed in the binding energy range of O2s electrons (~21–~27 eV). In the XPS spectrum of γ-UO_3, these peaks are separated by 2.2 eV. These have been attributed[45] to different oxygen ions located in the axial and equatorial positions with respect to the central atom in the uranyl compounds containing a U^{6+} ion. However, it has been noted[66,92,93,103,104] that this explanation does not work for the two peaks observed in this range in the case of UO_2 (see Table 4), because all the oxygen ions in this oxide are chemically equivalent (see Fig. 14 *a*). It should be expected[21,23] that the shifts of the O2s and O1s lines should be commensurable in magnitude. However, the spectrum of UO_2 exhibits a single relatively sharp O1s line, while in the spectrum of γ-UO_3, this line is broadened by 0.6 eV, due to the non-equivalence of two oxygen atoms (see Fig. 8). This single line is also present in the spectra of some uranium complexes.[216] This has led to the conclusion[66,92,93,103,104] that the two peaks observed in the spectrum of γ-UO_3 in the O2s binding energy range cannot be attributed to different types of oxygen ions present in this oxide, as was believed earlier.[45]

Comparison of the binding energy differences between the low-energy ($E_b \approx 12-35$ eV) and core electrons in uranium metal (which has a virtually atomic spectrum in this energy range) and uranium oxides shows that the formation of chemical bonds between uranium and oxygen atoms brings about significant differences between the XPS spectra of the metal and oxides (Table 5). Thus the energy level characteristic of the U6p$_{3/2}$ electrons in the UO_2 spectrum is shifted with respect to the U4f$_{7/2}$ level of uranium metal to lower binding energies by ΔE = 2.3 eV. In the case of γ-UO_3, the corresponding shift of the higher binding energy component equals 2.4 eV and that for the lower binding energy component is 6.1 eV. It is noteworthy that this allows one to observe the shifts of the low binding energy peaks not only for γ-UO_3 but also for UO_2 in which the environment of the uranium ion is symmetric.

Using the data on the causes and mechanisms of formation of the fine structure in the XPS spectra of actinides and other elements[38–40,45,52,65,79] and taking into account the results of theoretical calculations,[24,25,92,93,129–131,137,180,217] Teterin and coworkers[66,92,93,103,104,112] have suggested that the fine structure in the binding energy range $E_b \approx 12-35$ eV of the spectra of uranium oxides is due to IVMO electrons supplied mainly from the filled U6p and O2s AO of neighbouring atoms. This is consistent with the conversion electron spectroscopy data for uranium oxides in this energy range,[218–221] the

Table 5. Binding energy differences (ΔE_i) for various shells of uranium and ligands.[55]

Compound, element	$\Delta E_i = E_k - E_l$ /eV					
	$6p_{3/2} - 6p_{1/2}$	$6p_{3/2} - 6s_{1/2}$ (see [a])	$6p_{3/2} - 4f_{7/2}$	$6s_{1/2} - 4f_{7/2}$ (see [a])	$5d_{5/2} - 4f_{7/2}$	$L2s_{1/2} - L1s_{1/2}$ (see [b])
UO_2	10.5	27.6, 29.4	362.9	335.3, 333.5	283.6	507.2, 505.7
UO_2 (see [57])	10.6	27.8	362.5	334.7	283.8	507.9
UF_4	–	28.2	362.6	334.4	283.6	655.6
UF_4 (see [70])	11.7	–	362.8	–	–	655.4
γ-UO_3	–	–	363.0, 366.7	–	284.0	505.9, 508.1
U_{metal}	10.0	–	360.6	–	283.0	–
U (see [57])	10.0	27.1	360.6	333.5	283.2	–
U_{theor} (see [178])	10.4	31.0	360.9	329.9	283.0	–

[a] The E_i values corresponding to the most intense peaks in the U6s spectra were used. [b] The ΔE_i differences for oxygen and fluorine are given.

structure of the XPS spectra of uranium halides [26, 43, 44, 47, 53, 55, 69, 70, 82, 98, 101, 102, 105, 109, 200, 201] and the results of theoretical calculations.[31, 122, 123, 132–134, 202, 222–233] The formation of IVMO in uranium oxides is confirmed by the X-ray $O_{4,5}$(U) emission [185, 234] and $OL_IL_{II,III}L_{II,III}$-Auger spectroscopy data.[235, 236]

The energetic spectral structure in the U6s, U6p and O2s binding energy range can be illustrated by a diagram reflecting the formation of IVMO in γ-UO_3 in the non-relativistic approximation (Fig. 15). This Figure shows the changes that take place in the IVMO system on passing from the UO_2^{2+} cluster ($D_{\infty h}$ group of symmetry) to the $[UO_2O_4]^{6-}$ cluster (D_{4h} group of symmetry). The spectrum of γ-UO_3 in the same binding energy range is given for comparison. It follows from this diagram that the XPS spectra in this binding energy range reflect the electron distribution in oxides over quasi-atomic and molecular orbitals. The partial contributions of the U6p AO and the O2s AO into each MO characterise the substantial overlap of these uranium and oxygen AO. Although these results were obtained in the non-relativistic approximation, they allow one to identify the spectral lines in the U6$p_{3/2}$ and O2s binding energy ranges. However, complete description of the electronic structure of γ-UO_3 requires performing relativistic calculations (see Section VI).

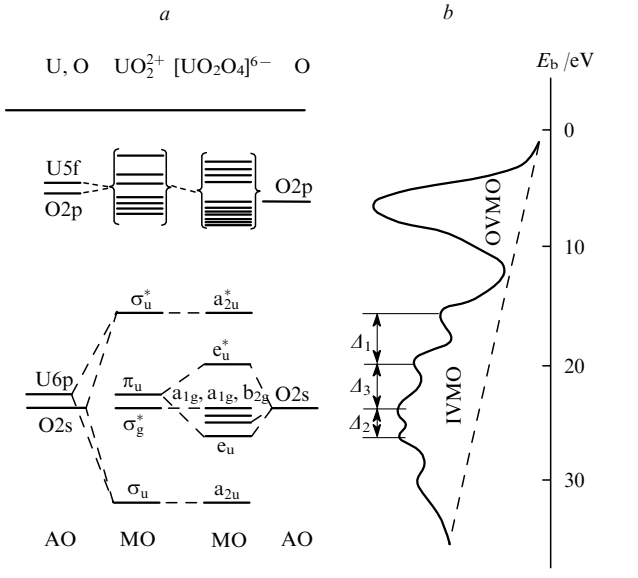


Figure 15. Diagram of MO formation in the UO_2^{2+} and $[UO_2O_4]^{6-}$ clusters ($D_{\infty h}$ and D_{4h} groups of symmetry, respectively) from the studies [25, 26, 102] (*a*) and X-ray photoelectron spectrum of the oxide γ-UO_3 (*b*).
The dashed line in Fig. 15 *b* corresponds to the background.

Analysis of the spectral structures of UO_2 and γ-UO_3 caused by MO electrons in the $\sim 0-35$ eV binding energy range suggests that the fine structure in the spectra of the U_4O_9, U_2O_5 and U_3O_8 oxides in this energy range can be considered to be a superposition of the spectra of simple oxides. It was shown [66] that the spectral structure in the U6$p_{3/2}$ energy range due to the UO_2^{2+} uranyl group becomes more pronounced as the oxygen coefficient x increases. Simultaneously, an additional line appears in the O2s energy range and the intensity of the U5f line diminishes.

c. XPS spectra of synthetic uranium oxides in the core electron binding energy range

The XPS spectra of UO_x oxides in the binding energy range of the core levels ($E_b \approx 40-1250$ eV), which exhibits the lines for U4p, U4d, U4f, U5s, U5p, U5d and U6s electrons, have been extensively studied.[47, 55, 66, 103, 105, 108, 109, 210, 215, 229]

The results are presented in Table 6 and in Figs 16–18. As the oxygen coefficient x for the synthetic oxides UO_x increases in the $2 < x \leqslant 3$ range, the core level binding energy grows by $\sim 0-1.5$ eV (see Table 6). This is due to the increase of uranium oxidation state on going from UO_2 to γ-UO_3. All of the spectra in this energy range show a complex fine structure; in some cases, this precludes precise determination of the binding energies and line intensities for some levels. Nevertheless, as has been mentioned above, the structure itself is characteristic of particular oxides and can be used for identification and for study of their properties.

Table 6. Binding energies (E_b /eV), line widths at half maximum (Γ /eV), spin–orbit splittings (ΔE_{sl} /eV), distances from the basic lines to satellites (ΔE_{Sat} /eV) and their relative intensities [I_{Sat}/I_0 (%)] for synthetic uranium oxides.[66]

Parameter	UO_2 (see [a])	U_4O_9	U_2O_5	U_3O_8	γ-UO_3
$E_b(U4f_{7/2})$	380.9	381.4	381.6	381.9	382.4
$\Gamma(U4f_{7/2})$	2.1	2.8	2.6	2.1	1.5
$E_b(U4f_{5/2})$	391.8	392.3	392.5	392.6	393.1
ΔE_{sl}(U4f)	10.9	10.9	10.9	10.7	10.7
ΔE_{Sat}	– 6.9	4.2, 6.7	– 7.8	3.8, 7.3	3.9, 9.5
I_{Sat}/I_0 (see [b])	25	10	10	10	29
$E_b(U4d_{5/2})$	739.3	740.4	740.6	740.4	741.0
$\Gamma(U4d_{5/2})$	5.9	9.8	5.9	5.1	5.1
$E_b(U4d_{3/2})$	781.6	782.2	782.7	782.4	783.3
ΔE_{sl}(U4d)	42.3	41.8	42.1	42.0	42.3
$E_b(U5d_{5/2})$	97.3	97.7	97.9	98.0	98.4
$\Gamma(U5d_{5/2})$	2.5	2.7	2.9	2.0	1.8
$E_bU5d_{3/2}$	105.5	106.4	105.9	106.6	107.1
ΔE_{sl}(U5d)	8.2	8.7	8.0	8.6	8.7
ΔE_{Sat}	– 7.1	4.6	3.0, 5.4	4.2	3.8, 7.8
$E_b(U5p_{3/2})$ (see [c])	197.4	–	197.5	198.2	199.1
$\Gamma(U5p_{3/2})$	7.8	–	7.0	6.8	7.4
$E_b(U4p_{3/2})$ (see [c])	1046.7	–	–	–	1048.0
$\Gamma(U4p_{3/2})$	7.4	–	–	–	6.6
E_b(U6s) (see [d])	46.5, – 75.0	–	–	–	47.5, 50.4, 74.4

[a] The binding energies are given for $UO_{2.06}$. [b] The ratio of the satellite intensity I_{Sat} to the basic line intensity I_0. [c] The binding energies were measured as the weight average of the complex line. [d] Binding energies for the most intense components.

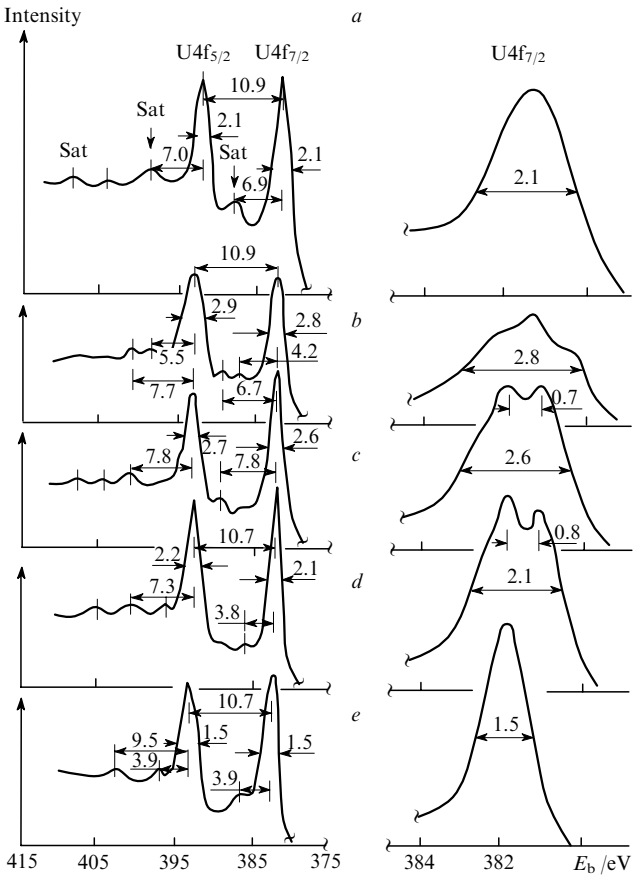


Figure 16. XPS spectra of synthetic uranium oxides in the U4f binding energy range.[66]
(*a*) UO_2, (*b*) U_4O_9, (*c*) U_2O_5, (*d*) U_3O_8, (*e*) γ-UO_3; Sat is satellite. The $U4f_{7/2}$ lines are shown separately for clarity.

d. The spectra of U4f electrons

The U4f XPS spectra of uranium oxides exhibit shake up satellites.[66, 105, 151, 237, 238] These spectra, like the spectra of U5f electrons, show that the U_2O_5 and U_3O_8 oxides contain two types of uranium ions.[66] However, these oxides are not mere mechanical mixtures of the simple oxides UO_2 and UO_3, they are complex phases whose lattices contain interrelated uranium and oxygen ions of two types.[55]

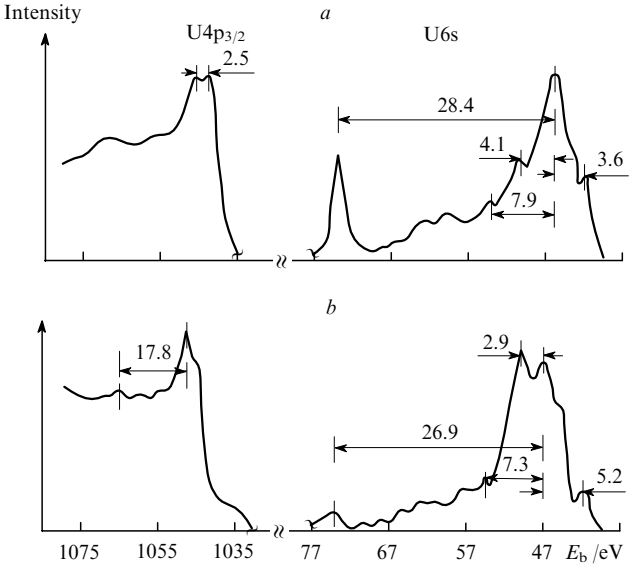


Figure 17. XPS spectra of uranium oxides in the U6s and U4p binding energy ranges.[56]
(*a*) UO_2, (*b*) γ-UO_3.

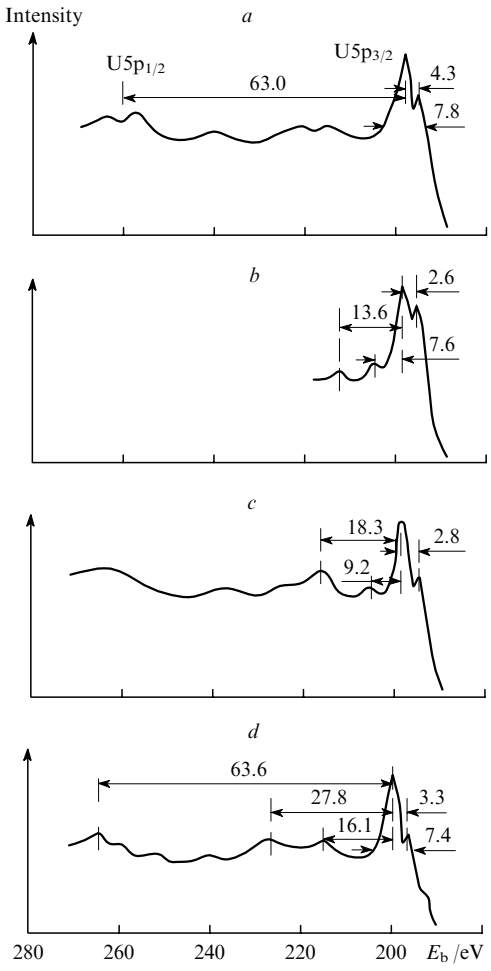


Figure 18. XPS spectra of uranium oxides in the U5p binding energy range.[56, 66]
(*a*) UO_2, (*b*) U_2O_5, (*c*) U_3O_8, (*d*) γ-UO_3; $\Delta E_{sl}(U5p) = 65$ eV.[20]

The spectral characteristics suggest that these complex oxides contain U^{5+} and U^{6+} ions. In this approximation, the $U4f_{7/2}$ lines of the given oxides were decomposed into two components (Fig. 16) and the contribution of each of the ions was quantitatively estimated.[55, 66] It was found that U_2O_5 and U_3O_8 contain U^{5+} and U^{6+} ions in 1 : 1 and 1 : 2 ratios, respectively, which agrees with the XPS spectra of the U5f electrons in these oxides. In addition, these conclusions are confirmed by the intensity ratio of the components of the $U4f_{7/2}$ lines and the corresponding $U4f_{7/2}$ binding energies found from decomposition of these lines (for U_2O_5, 381.5 and 382.3 eV; for U_3O_8, 381.5 and 382.4 eV).

The data on the contents of the two types of uranium ion in these oxides[55, 66] are in line with XPS data,[38, 60, 105] magnetic measurements,[211] and, in the case of U_3O_8, also with X-ray diffraction data.[5] The UO_2 and γ-UO_3 oxides contain U^{4+} and U^{6+} ions, respectively,[55, 66] which is also consistent with X-ray diffraction data.[5]

The binding energy distances between the satellites and the basic U4f lines in the XPS spectra reflect the MO structure and are characteristic of particular oxides (see Fig. 16). Thus in the spectrum of UO_2, the distance from the low energy satellite to the basic $U4f_{7/2}$ line is 6.9 eV, while the spectrum of γ-UO_3 exhibits two satellites spaced by 3.9 eV and 9.5 eV from the basic

$U4f_{5/2}$ component of the doublet. The spectra of other oxides exhibit more complicated satellite structures, which can be correlated to a certain approximation with the satellite structures in the spectra of UO_2 and γ-UO_3.

e. The spectra of the U5d and U4d electrons

The U5d binding energy range of the spectra of the oxides under study [55, 66, 103, 104] exhibits, instead of the expected doublet caused by the spin – orbit splitting, a more complicated fine structure. The $U5d_{3/2}$ component is broadened compared to the $U5d_{5/2}$ line, the binding energy difference between these electrons increasing on passing from UO_2 to UO_3. This is not related to the change in the spin – orbit splitting [(ΔE_{sl}(U5d) = 8.6 eV for U metal [57]] following the increase in the uranium oxidation number, but is due, first of all, to the multiplet splitting. Since the U^{6+} ion in γ-UO_3 does not contain unpaired electrons, this splitting should not be manifested in the XPS spectrum in the U5d binding energy range. Therefore, the value ΔE_{sl}(U5d) = 8.7 eV is closer to the true value of the spin – orbit splitting (see Table 6). Other reasons for broadening of the U5d doublet may include the superimposition of the shake up satellites onto the $U5d_{3/2}$ component and the dynamic effect.

In the spectra of deeper U4d electrons, the spin doublet lines are much broader than the U4f lines,[55, 238] which complicates decomposition of the U4d line of complex oxides into separate components. Nevertheless, the measured spin – orbit splittings for the U4d level for uranium dioxide and trioxide are equal and amount to 42.3 eV [ΔE_{sl}(U4d) = 42.3 eV for U metal [57]]. The observed change in the ΔE_{sl} value for complex oxides is attributable to the structure caused by the presence of uranium in different oxidation states.

f. The spectra of the U6s, U5p and U4p electrons

The XPS spectra of uranium and its compounds exhibit a complex structure in the U6s binding energy range.[55, 56, 106] Indeed, instead of the expected single relatively sharp line, the spectra of UO_2 and γ-UO_3 contain a complex fine structure in an energy range covering up to $\sim$40 eV (see Fig. 17).[56]

The spectral structure observed in the U6s range has much in common with the XPS structure observed for the Th6s electrons (see Fig. 2). Therefore, this structure has been suggested [55, 56] to be mostly due to the dynamic effect giving rise to the final states of the type $U6s^1 6p^6 5f^n 6d^m \rightleftharpoons U6s^2 6p^4 5f^n 6d^{m+1}$, because E_b(U6s) $\approx$ 2 E_b(U6p). This is in qualitative agreement with the results of calculation [32] of the U6s spectrum performed with the assumption that uranium occurs in the U^{6+} state.

A similar analysis of the reasons of formation of the fine spectral structure has also been carried out [56, 66] for the U5p and $U4p_{3/2}$ electrons (see Figs 17, 18). This structure in the spectra of uranium oxides in the U5p binding energy range induces splitting of the $U5p_{3/2}$ line and substantial smearing of the $U5p_{1/2}$ component of the doublet [(ΔE_{sl}(U5p) = 65 eV [20]. A similar situation is observed in the $U4p_{3/2}$ energy range [56] (see Fig. 17). Comparison of the magnitudes of splitting of the main components in the U6s, U5p and $U4p_{3/2}$ spectra has shown that these values change insignificantly as the electron binding energy increases from $\sim$50 to $\sim$1000 eV and, hence, the fine structure cannot be mainly due to the effect of the crystal field, as has been suggested [79] for the electrons of some shells.

Since the fine structure observed in the range of core levels for thorium dioxide containing no unpaired Th5f electrons has much in common with the corresponding spectral structure of UO_2, it has been suggested [56, 66] that this structure in the spectra of U5p and U4p electrons of UO_x cannot be related, to a large extent, to the multiplet splitting or many-body perturbation, but is mainly due to the dynamic effect, resulting in the final states of the types $U5p^5 5d^{10}(6s^2 6p^6)5f^n \rightleftharpoons U5p^6 5d^8(6s^2 6p^6)5f^{n+1}$ and $U4p^5 4d^{10}(4f^{14}).5s^2(5p^6 5d^{10} 6s^2 6p^6)5f^n np^0 \rightleftharpoons U4p^6 4d^9(4f^{14})5s^1(5p^6 5d^{10} 6s^2 6p^6).5f^n np^1$, respectively.[55, 56] This structure is superimposed by the satellites corresponding to many-body perturbation. This further complicates the spectral structure.

2. Uranyl compounds

Uranyl compounds contain the UO_2^{2+} group coordinated by four, five or six atoms of the ligand L (L = O, F, Cl, Br, *etc.*) in the equatorial plane.[239–241] The U – O bond length (R_{U-O}) in the UO_2^{2+} group of these compounds is usually smaller than the distances from the uranium atoms to the neighbouring ligand atoms located in the equatorial plane.[7, 53, 71–73, 240–243] In recent years, researchers' attention has been focused on the calculation of the electronic structures of uranyl derivatives (Refs 24, 26–28, 36, 42, 93, 102, 123, 130, 204, 233) which has been stimulated by the appearance of numerous publications devoted to X-ray photoelectron spectra of these compounds (Refs 26, 42–48, 55, 82, 94–97, 102, 109, 216, 244). It should be noted that only the actinyl group AnO_2^{n+} (An = U, Np, Pu, Am, *etc.*) has an almost linear structure, whereas a molecule of gaseous ThO_2 is bent at an angle of 122 $\pm$ 2° (see Ref. 245).

A number of uranyl compounds have been studied by XPS (Table 7) in order to establish the relationship of fine spectral structure parameters with the structure of these compounds and the nature of the chemical bond in them.[47, 55] To confirm the stoichiometric compositions and the structures of these compounds, the spectra of all elements contained in their molecules were analysed. For identification of XPS lines of uranyl compounds in the low binding energy range, the spectra of ligands based on $Ni(NO_3)_2$, NaOAc, Na_2CO_3 and CsCl have also been studied.

a. The spectra of uranyl compounds in the low binding energy range

As noted above, the XPS spectra of highly symmetric U^{4+} compounds (see Fig. 14), for example, UO_2 (see Fig. 8) and UF_4 (Fig. 19), containing U5f electrons not involved in the chemical bond, exhibit a sharp line at around a zero binding energy.

The spectra of uranyl compounds containing U^{6+}, for example, γ-UO_3 (see Fig. 8) and UO_2F_2 (see Fig. 19), do not exhibit this line. The absence of the U5f line in the XPS spectra of uranyl compounds directly confirms that the uranium oxidation state is

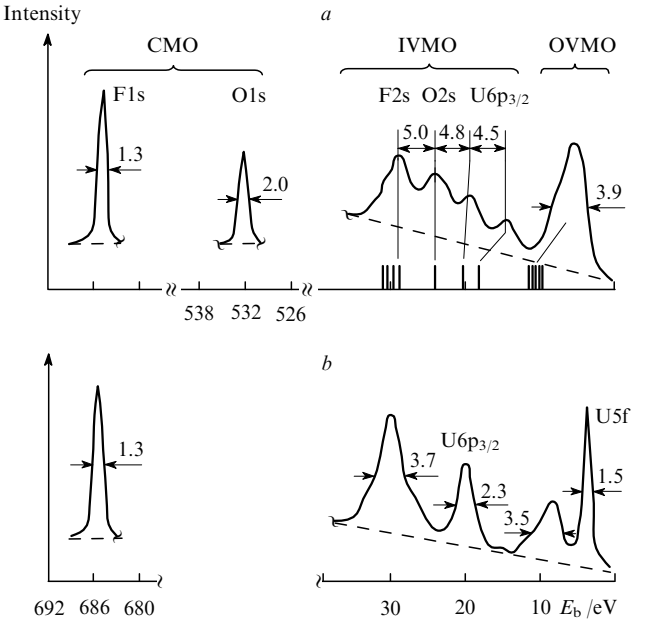


Figure 19. XPS spectra of uranium compounds.[98]
(*a*) UO_2F_2, (*b*) UF_4. Vertical lines below the spectrum: (*a*) results of non-relativistic calculation (X_α-DV [102]) of the electronic structure of the $[UO_2F_6]^{4-}$ cluster (D_{6h} group of symmetry) for R_{U-O} = 0.174 nm, R_{U-F} = 0.243 nm. The dashed lines show the background.

Table 7. Binding energies (E_b/ eV), binding energy differences (ΔE_i/ eV), bond lengths in the UO_2^{2+} groups (R_{U-O}/ nm), distances from the basic lines to the satellites (ΔE_{Sat}/ eV) and their relative intensities [I/I_0 (%)].[47]

Compound	E_b(OVMO) (see [a])	E_b(U6p$_{3/2}$)	ΔE_i(U6p$_{3/2}$)	R_{U-O} (see [b])	E_b(O2s)	ΔE_i(O2s)	E_b(U6p$_{1/2}$) (see [c])	E_b(U6s) (see [a])	E_b(O1s)	E_b(U5d$_{5/2}$)	E_b(U5d$_{3/2}$)	ΔE_{Sat} (see [d])	I/I_0	E_b(U5p$_{3/2}$) (see [c])
UF_4	9.0	20.1						48.3		99.1	107.1	7.0	10	195.9, 199.8, 203.0
UO_2F_2	6.7	15.6, 20.1	4.5	0.174	22.3, 24.9	2.6		49.3	532.4	99.2	107.9	4.1	5	200.2
$K_4UO_2(CO_3)_3$	5.1	14.6, 19.8	5.2	0.172	22.7, 24.4	1.7	28.8, 31.2	47.1	531.4	98.1	106.5	3.4	20	195.0, 198.5, 200.6
$UO_2(OAc)_2 \cdot 2H_2O$	6.0	15.6, 19.8	4.2	0.174	23.3, 25.3	2.0	28.4, 31.4	49.0	532.3	98.8	107.4	3.6	8	199.8, 205.4
$NaUO_2(OAc)_3$	5.8	15.1, 20.0	4.9	0.173	22.3, 25.1	3.0	28.6	48.2	532.2	98.5	107.3	3.8	19	199.5
$CsUO_2(OAc)_3$	5.6	15.2, 20.1	4.9	0.173				49.5	532.1	98.4	106.9	3.4	20	193.8, 199.8, 204.0
$UO_2(NO_3)_2 \cdot 2H_2O$	6.4	19.9	4.0	($\leqslant$0.175)	26.0, 27.5	1.5	29.0, 31.4	48.0	533.6	99.2	107.7	3.2	20	202.2, 204.1
$CsUO_2(NO_3)_3$	6.9	20.1	3.5	($\leqslant$0.176)	24.6, 27.2	2.6	29.9, 32.2	49.0	533.9	99.5	108.1	3.5	20	200.2, 203.0
$RbUO_2(NO_3)_3$	6.5	20.3	3.5	($\leqslant$0.176)	25.8, 27.3	1.5	29.7, 32.5	50.3	533.6	99.9	107.9			200.4
$UO_2(DMSO)_5(ClO_4)_2$	6.0	17.1, 20.9	3.8	0.176	25.6, 27.4	1.8	30.2, 32.5	46.7	532.4	98.8	107.6	2.5	20	190.8, 199.8, 204.9
$K_4UO_2(OO)_3 \cdot 5H_2O$	4.9	14.5, 19.5	5.0	0.172	24.9, 26.7	1.8	30.7		531.5	97.2	106.1	3.4	20	190.7, 198.4
$CaUO_2O_2$	5.2	15.7, 17.2	1.5	0.191	21.6		29.2, 30.0		530.2	97.6	106.3	4.0	10	195.3, 199.0
$K_3UO_2F_5$	6.7	15.5, 19.5	4.0	0.175	22.6, 24.5	1.9	30.0, 33.0	47.6	531.9	99.2	107.8	2.4	8	197.4, 200.3
$Cs_3UO_2F_5$	5.9	15.3, 19.3	4.0	0.175				50.7	531.6	98.9	107.4	2.8	5	191.8, 198.4
$Cs_2UO_2Cl_4$	5.6	15.4, 19.8	4.4	0.174	24.5, 26.5	2.0	30.9, 32.8	48.2	531.6	98.1	106.9	3.3	20	
$Cs_2UO_2Br_4$	4.6	15.2, 19.8	4.6	0.173			30.8, 32.9	49.9	532.4	97.8	106.9	3.7	20	199.4, 203.7

Compound	E_b(U5p$_{1/2}$) (see [a])	E_b(U4f$_{7/2}$)	ΔE_{Sat} (see [d])	E_b(U4f$_{5/2}$)	ΔE_{Sat} (see [d])	I/I_0	E_b(U4d$_{5/2}$)	E_b(U4d$_{3/2}$)	E_b(U4p$_{3/2}$) (see [c])	L (nl_j)	E_b[L (nl_j)]	L (nl_j)	E_b[L (nl_j)]
UF_4	264.5	382.7	7.3	393.5	6.9	20	741.2	783.6	1048.1				
UO_2F_2	264.1	383.4	3.5	394.1	3.5	10	741.5	784.0	1048.2			F2s,1s	29.9, 685.3
$K_4UO_2(CO_3)_3$	263.8	382.1	3.7	392.9	3.7	18	740.6	782.7	1047.1	K3p$_{3/2}$,3s,2s	16.9, 32.8, 377.4		
$UO_2(OAc)_2 \cdot 2H_2O$	261.4	382.7	3.7	393.6	3.8	12	741.3	783.9	1047.5				
$NaUO_2(OAc)_3$	264.6	382.6	3.6	393.5	3.5	20	740.1	783.1	1047.1	Na2p$_{3/2}$,2s,1s	30.5, 63.5, 1071.6		
$CsUO_2(OAc)_3$		382.4	3.5	393.3	3.5	18		782.8	1048.3	Cs5p$_{3/2}$,5s,4s	11.0, 23.9, 230.2		
$UO_2(NO_3)_2 \cdot 2H_2O$		383.1	3.3	394.0	3.3	18	741.9	784.8	1048.7			N1s	407.8
$CsUO_2(NO_3)_3$	264.7	383.3	3.5	394.1	3.6	16		783.6	1048.1	Cs5p$_{3/2}$,5s	10.8, 24.1	N1s	407.9
$RbUO_2(NO_3)_3$		383.0	3.4	393.8	3.4	18	742.0	784.0	1049.0	Rb4p$_{3/2}$,4s	14.2, 29.7	N1s	407.8
$UO_2(DMSO)_5(ClO_4)_2$		382.9	2.8	393.6	2.8	17	741.4	783.5	1051.8	S3p,2s	12.0, 230.8	Cl3s,2p$_{3/2}$	15.0, 208.1
$K_4UO_2(OO)_3 \cdot 5H_2O$	266.9	381.3	4.2	392.2	4.0	17	739.6	781.8	1055.7	K3p$_{3/2}$,3s,2s	17.2, 33.1, 377.5		
$CaUO_2O_2$	261.0	381.6	3.7	392.4	3.8	8	740.4	782.8	1047.3	Ca3p$_{3/2}$,3s	25.0, 44.2		
$K_3UO_2F_5$	262.8	383.2	2.4	394.1	2.4	7	741.8	784.0	1049.2	K3p$_{3/2}$,3s	17.1, 33.1	F2s,1s	28.5, 684.2
$Cs_3UO_2F_5$		382.8	2.8	393.6	2.8	5		783.1	1046.5	Cs5p$_{3/2}$,5s	10.3, 23.3	F2s,1s	28.1, 683.8
$Cs_2UO_2Cl_4$		382.1	3.7	393.0	3.8	15		783.1	1044.9	Cs5p$_{3/2}$,5s	10.2, 23.6	Cl3s,2p$_{3/2}$	15.8, 198.8
$Cs_2UO_2Br_4$		381.7	3.7	392.5	3.9	25		783.3	1047.6	Cs5p$_{3/2}$,5s	10.3, 23.7	Br4s,3d$_{5/2}$	26.4, 69.1

[a] Weight average binding energies. [b] Determined upon estimation of the bond lengths in the UO_2^{2+} groups on the basis of relation (8). The values in parentheses are given with an accuracy of $\pm$0.002 nm. [c] The E_b values for the peaks in the corresponding binding energy ranges. [d] ΔE_{Sat} for the most intense satellites.

Table 8. Symmetry of the environment of UO_2^{2+} in compounds, binding energy differences (ΔE_i, Δ_i /eV) for various electronic levels, $U-O_{ax}$ bond lengths (R_{U-O} /nm) in UO_2^{2+} and distances from uranium atoms to equatorial atoms of the ligands (R_{U-L} /nm).[94]

Compound	Cluster	Group of symmetry	n_O/n_L (see [a])	ΔE_1	ΔE_2	Δ'_1	Δ_1	Δ'_2	Δ_2	R_{U-O} (see [b,c])	R_{U-L} (see [b,c])	Symmetry of the environment of UO_2^{2+} (see [b,d])
γ-U (**1**)	UO_8^{12-}	O_h		360.6	–	–	–	–	–		0.297 [e]	
UO_2 (**2**)	$[UO_2O_6]^{10-}$	D_{6h}	2:6	362.9 [f]	–	2.3	2.9	–	–	0.237		
$Ca(UO_2)O_2$ (**3**)	$[UO_2O_6]^{10-}$	D_{6h}	2:6	365.9	364.4	5.3	6.1	3.8	–	0.191	0.229	S_6
$CsUO_2(NO_3)_3$ (**4**)	$[UO_2O_6]^{10-}$	D_{6h}	2:6	(367.0) [g]	363.2	(6.4)	7.4	2.6	4.1	0.180	0.250	D_{3h} (C_3)
$RbUO_2(NO_3)_3$ (**5**)	$[UO_2O_6]^{10-}$	D_{6h}	2:6	(367.2)	362.7	(6.6)	8.0	2.1		0.178(2)	0.248(1)	D_{3h} (C_3)
$UO_2(NO_3)_2(H_2O)_2$ (**6**)	$[UO_2O_6]^{10-}$	D_{6h}	2:6	(367.4)	363.2	(6.8)	7.4	2.6	3.5	0.176(7) [h]	0.248(5)	C_{2v}
$K_4UO_2(CO_3)_3$ (**7**)	$[UO_2O_6]^{10-}$	D_{6h}	2:6	367.5	362.3	6.9	7.6	1.7	3.0	(0.175)	(0.260)	
$UO_2(OAc)_2(H_2O)_2$ (**8**)	$[UO_2O_6]^{10-}$	D_{6h}	2:6	367.1	362.9	6.5	7.2	2.3	3.1	0.172	0.250	C_{2v} (C_2)
$NaUO_2(OAc)_3$ (**9**)	$[UO_2O_6]^{10-}$	D_{6h}	2:6	367.5	362.6	6.9	–	2.0	3.5	0.171	0.249	D_{3h} (C_3)
$CsUO_2(OAc)_3$ (**10**)	$[UO_2O_6]^{10-}$	D_{6h}	2:6	367.2	362.3	6.6	8.0	1.7	3.5	(0.178)	(0.261)	
$K_4UO_2(CO)_3 \cdot 5H_2O$ (**11**)	$[UO_2O_6]^{10-}$	D_{6h}	2:6	366.8	361.8	6.2	7.9	1.2	3.3	(0.182)	(0.270)	
$UO_2(DMSO)_5(ClO_4)_2$ (**12**)	$[UO_2O_5]^{8-}$	D_{5h}		365.8	362.0	5.2	5.9	1.4	3.1	(0.192)	(0.266)	
UO_2F_2 (**13**)	$[UO_2F_6]^{4-}$	D_{6h}	2:6	367.8	363.3	7.2	–	2.7	3.2	0.174(2)	0.243(2)	S_6
UF_4 (**14**)	UF_8^{4-}	D_{4d}		362.6 [f]	–	2.0	2.5	–	–		0.229(3)	
$K_3UO_2F_5$ (**15**)	$[UO_2F_5]^{3-}$	D_{5h}	2:5	367.7	363.7	7.1	–	3.1	3.5	0.176(3)	0.224(3)	D_{5h}
$Cs_3UO_2F_5$ (**16**)	$[UO_2F_5]^{3-}$	D_{5h}	2:5	367.5	363.5	6.9	–	2.9	3.5	(0.175)	(0.239)	D_{5h}
γ-UO_3 (**17**)	$[UO_2O_4]^{6-}$	D_{4h}	2:4	366.7	363.0	6.1	7.1	2.4	3.2	0.179(6)	0.230(5)	
$Cs_2UO_2Cl_4$ (**18**)	$[UO_2Cl_4]^{2-}$	D_{4h}	2:4	366.7	362.3	6.1	7.4	–	–	0.181	0.262	D_{4h} (D_{2h})
$Cs_2UO_2Br_4$ (**19**)	$[UO_2Br_4]^{2-}$	D_{4h}	2:4	366.5	361.9	5.9	7.6	–	–	0.169	0.281	D_{4h}

Note. The ΔE_1, ΔE_2, Δ'_1, Δ_1, Δ'_2, Δ_2 parameters are shown in Fig. 23. They have been found using the values ΔE_U [$\Delta E(U6p_{3/2}) = 360.6$ eV, $\Delta E(U6p_{1/2}) = 350.6$ eV], $\Delta E_O = 508.1$ eV, $\Delta E_F = 655.3$ eV, $\Delta E(U6p_{3/2} - O2s) = 2.1$ eV. The ΔE_1 and ΔE_2 values were measured to an accuracy of ±0.2 eV; the Δ'_1, Δ_1, Δ'_2, Δ_2 values, to an accuracy of ±0.3 eV. [a] Ratio of the number of oxygen atoms located in the axial position (O_{ax}) to the number of ligand atoms located in the equatorial plane. [b] Data of the studies [240–242] [c] The R_{U-O} values given in parentheses were measured to an accuracy of ±0.002 nm, the R_{U-L} values, to an accuracy of ±0.004 nm. [d] Experimental results. [e] Bond length between the closest uranium atoms in metallic γ-U.[243] [f] For UO_2 and UF_4, the ΔE_i and Δ_i differences are shown in Fig. 24. [g] The values in parentheses are ΔE_1 determined using relations (9) and (10). [h] The average R_{U-O} and R_{U-L} values are underlined.

six.[96,98] The presence of the UO_2^{2+} group may be indicated, in particular, by the structure of the XPS spectrum in the U6p and O2s ranges. Thus in the fluoride UF_4, the uranium ion occurs in a relatively symmetric environment formed by fluorine atoms (D_{4d} group of symmetry). In this case, as for UO_2, the XPS spectrum of the $U6p_{3/2}$ electrons exhibits a single line (see Fig. 19). The uranium environment in the UO_2F_2 molecule is less symmetric (D_{6h} group of symmetry), and the spectrum shows two components of the $U6p_{3/2}$ line. The spectra of UO_2F_2 and UF_4 exhibit fine structure over the whole U6p and O2s-, F2s binding energy ranges (see Fig. 19 [246–248]). The O2s and F2s lines in the XPS spectra of these compounds are much broader than the corresponding O1s and F1s lines and exhibit a fine structure. The binding energy difference $\Delta E_i(6p_{3/2} - 4f_{7/2}) = 362.6$ eV for UF_4 is much greater than the similar value $\Delta E_i = 360.6$ eV for uranium metal (Table 8, see also Table 5). This is consistent with the assumption that the $U6p_{3/2}$ line in the spectrum of UF_4 is not atomic, but is due to electrons of an antibonding MO. Therefore, it has been suggested [47,55,246–248] that the structure of low energy spectra of UF_4 and UO_2F_2 is mainly due to the effective formation of IVMO largely composed of U6p, O2s and F2s AO. In the case of UO_2F_2, this is in qualitative agreement with the results of calculation of the electronic structure of the $[UO_2F_6]^{4-}$ cluster (D_{6h} group of symmetry).[246–248]

The low binding energy region of the XPS spectrum of $Cs_2UO_2Cl_4$ shows a more complicated structure than the spectrum of UO_2F_2, due to the Cs5p and Cs5s lines present in this energy range (Fig. 20). The line for the Cl3s electrons that belong to chlorine atoms arranged in the equatorial plane occurs in the binding energy range of the U6p electrons, which implies a more essential involvement of the Cl3s AO, together with the $U6p_{3/2}$ AO, in the formation of IVMO than in the case of the F2s and $U6p_{3/2}$ fluorine and uranium AO.[26,47]

The results of non-relativistic SCF X_α-SW calculation [26] for the electronic structure of the $[UO_2Cl_4]^{2-}$ cluster (D_{4h} group of symmetry), which mimics the local environment of uranium in $Cs_2UO_2Cl_4$ molecules, provide a qualitative interpretation of the low binding energy spectrum of the compound under consideration (see Fig. 20). The energy range of OVMO, mainly consisting of the U5f, U6d, O2p and Cl3p AO, covers 3.9 eV, which is

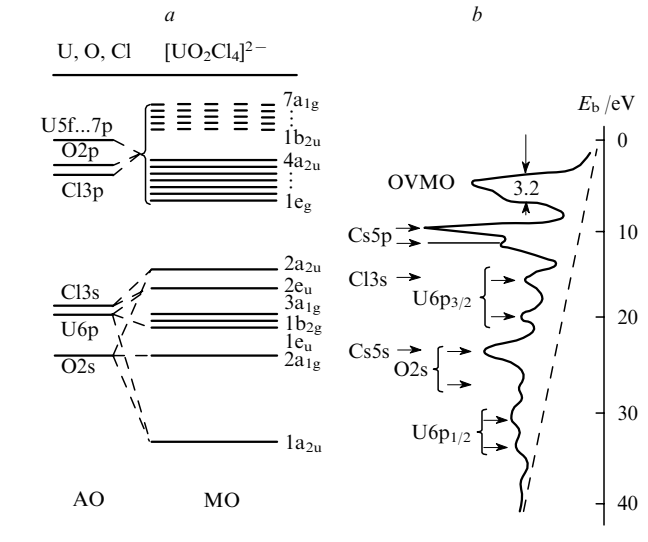


Figure 20. Diagram of MO in the $[UO_2Cl_4]^{2-}$ cluster (D_{4h} symmetry) based on the data of X_α-SW calculations (*a*) and XPS spectrum of $Cs_2UO_2Cl_4$ (*b*).[26,47] The dashed line in Fig. 20 *b* shows the background.

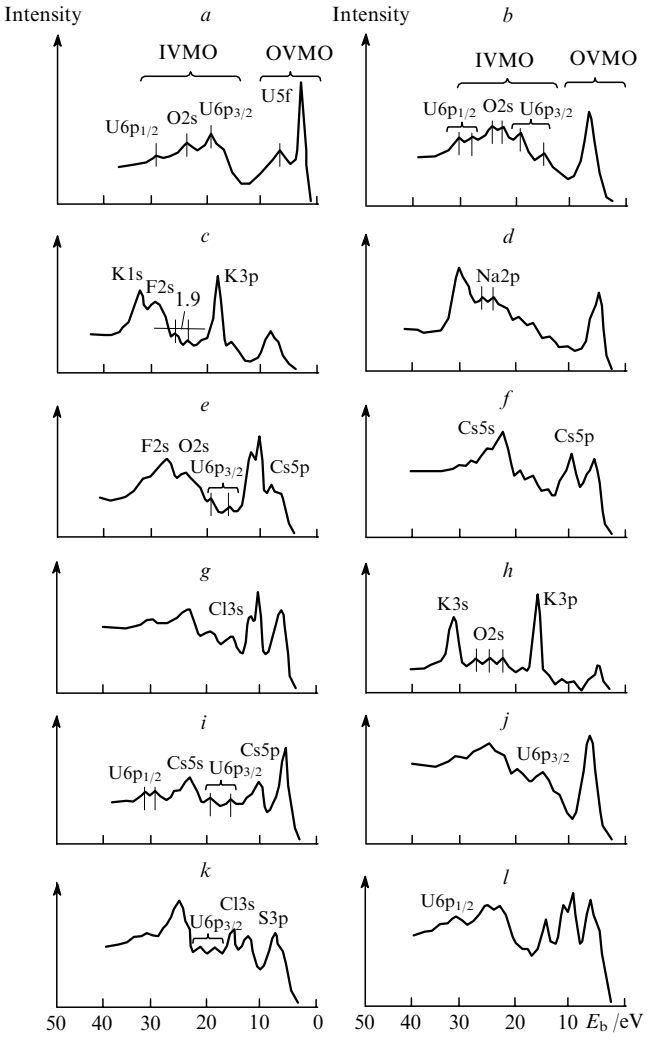


Figure 21. Low-energy range of the XPS spectrum of oxygen-containing uranium compounds.[26,47]
(*a*) UO_2, (*b*) $UO_2(OAc)_2 \cdot 2H_2O$, (*c*) $K_3UO_2F_5$, (*d*) $NaUO_2(OAc)_3$, (*e*) $Cs_3UO_2F_5$, (*f*) $CsUO_2(OAc)_3$, (*g*) $Cs_2UO_2Cl_4$, (*h*) $K_4UO_2(CO_3)_3$, (*i*) $Cs_2UO_2Br_4$, (*j*) $UO_2(NO_3)_2 \cdot 2H_2O$, (*k*) $UO_2(DMSO)_5(ClO_4)_2$, (*l*) $CsUO_2(NO_3)_3$.

comparable with the experimental width of these lines in the spectrum, which equals 3.2 eV. In this compound, IVMO are formed efficiently from U6p, O2s and Cl3s AO.

The fine structure caused by the IVMO electrons is observed also in the XPS spectra of other uranyl compounds (Fig. 21).[47] The line near the binding energy zero also corresponding to U5f electrons not involved in chemical bonds is not detected for these compounds. This is in qualitative agreement with the known fact that the oxidation number of uranium in these compounds is six.

The OVMO-related bands in the spectra of uranyl compounds are characterised by FWHM of $\sim 3-4$ eV and by poorly resolved structures (see Fig. 21). The binding energies of these electrons in oxygen-containing uranium compounds measured as weight average values of the components lie in the range of $\sim 5-6$ eV (see Table 7). If fluorine or the NO_3 group are present as ligands, these values are somewhat greater (~ 7 eV).

The XPS spectra of the compounds in question in the IVMO region may become more complicated due to the overlap with the lines due to alkali metal ions. However, these lines can be interpreted rather easily

b. The IVMO spectral structure and the structure of uranyl compounds

In an early stage of the XPS studies of uranyl compounds, it was found[45,47,55,65,66,92,93,104] that the line splitting in the $U6p_{3/2}$ binding energy range [$\Delta E(U6p_{3/2})$] depends on the bond length R_{U-O} in the UO_2 group (Fig. 22). It has been suggested[45] that this splitting is due to the crystal field.

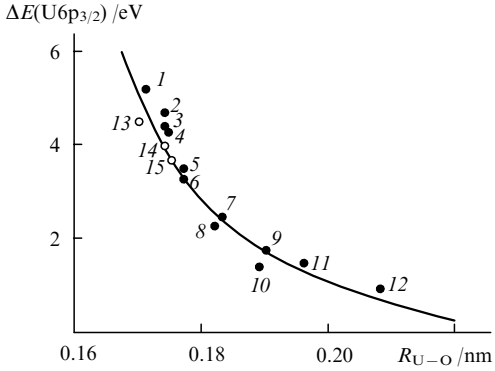


Figure 22. Dependence of splitting $\Delta E_b(U6p_{3/2})$ on the R_{U-O} bond length in the UO_2^{2+} group [see Eqn (7)] for a number of uranium compounds.
(*1*) UO_2CO_3, (*2*) $LiUO_2F_3 \cdot 2H_2O$, (*3*) $NaUO_2F_3 \cdot 2H_2O$, (*4*) $UO_2C_2O_4 \cdot 3H_2O$, (*5*) β-$UO_2(OH)_2$, (*6*) γ-$UO_2(OH)_2$, (*7*) $Li_2U_2O_7$, (*8*) LiU_3O_{10}, (*9*) Li_2UO_4, (*10*) α-Na_2UO_4, (*11*) $CaUO_4$, (*12*) Cr_2UO_6, (*13*) UO_2F_2, (*14*) $UO_2(NO_3)_2 \cdot 2H_2O$, (*15*) γ-UO_3; the light circles show the data from the study;[55] dark circles, from the study.[45]

The dependence of the $\Delta E(U6p_{3/2})$ value on R_{U-O} shown in Fig. 22 can be expressed as follows:

$$\Delta E(U6p_{3/2}) = -1.59 + 0.138(R_{U-O} - 0.149)^{-1}. \quad (7)$$

Hence, the expression for R_{U-O} has the form

$$R_{U-O} = 0.149 + 0.138[\Delta E(U6p_{3/2}) + 1.59]^{-1}. \quad (8)$$

Equation (8) can be used to estimate the R_{U-O} bond lengths in the UO_2^{2+} groups in these compounds (see Table 7).

A more profound understanding of the nature of the fine spectral structure in the low binding energy range of uranium compounds can be gained from theoretical and experimental results which allow one to consider the data on fine XPS spectral structure from a different standpoint.[94,96,97,107–109,245] Comparison of the E_b values for the outer electrons for various uranium compounds does not provide a vivid representation of the dependence of spectral characteristics on the properties and structures of these compounds. Indeed, the $U6p_{3/2}$ binding energies usually change little on passing from one compound to another (see Table 7). Therefore, for elucidating the regular features of the formation of IVMO structure, the binding energy differences between the valence and core electrons (ΔE_i) in these compounds have been considered (see Table 8). The data of Table 8 are illustrated by the MO diagram for the $[UO_2O_6]^{10-}$ cluster (D_{6h} group of symmetry), which reflect the local environment for a large number of oxygen-containing uranyl compounds (Fig. 23). The diagram shows the binding energy differences ΔE_U, $\Delta E_1 - \Delta E_6$, ΔE_O and ΔE_L. The ΔE_i values for uranium metal and its compounds can be measured experimentally. This provides the values Δ_1, Δ_2, Δ_3 and Δ'_1, Δ'_2, Δ'_3, which characterise quantitatively the type of MO (bonding, antibonding, non-bonding) and the degree of participation of the corresponding AO of the neighbouring atoms in the MO formation (see Fig. 23). Thus, the MO structure for uranium compounds can be determined experimentally.

The above results imply that, to a certain approximation, ligand atoms located in the axial positions and in the equatorial

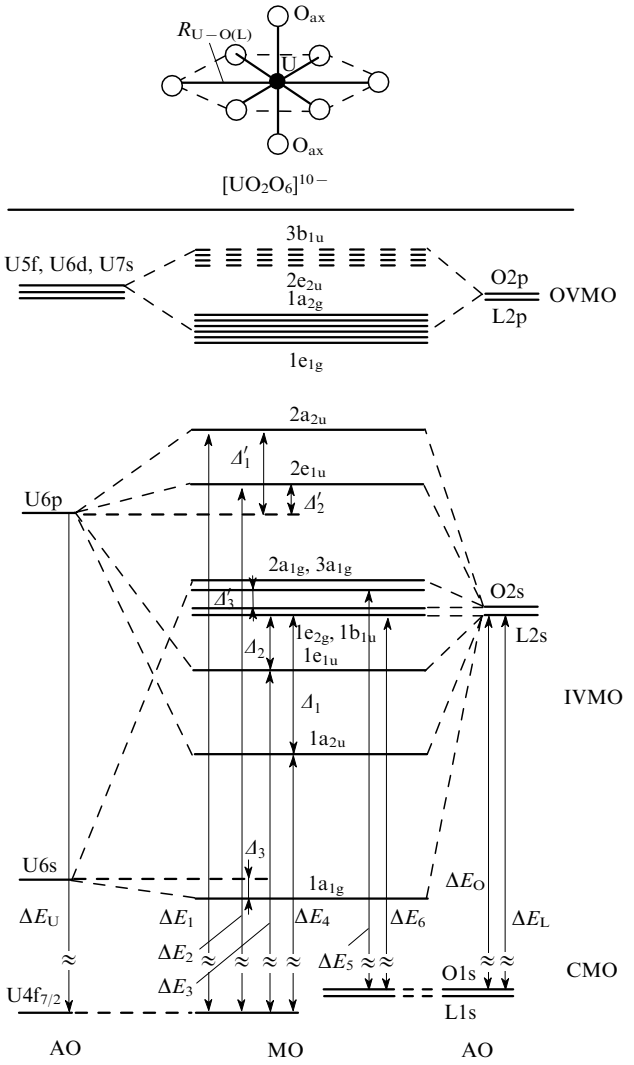


Figure 23. Diagram of MO energy levels in $[UO_2O_6]^{10-}$ (D_{6h} symmetry) constructed using experimental data and results of calculations.[26, 48]
The chemical shifts of the energy levels upon the formation of the cluster from single atoms are not shown. The arrows show the energy differences that can be derived from experimental spectra.

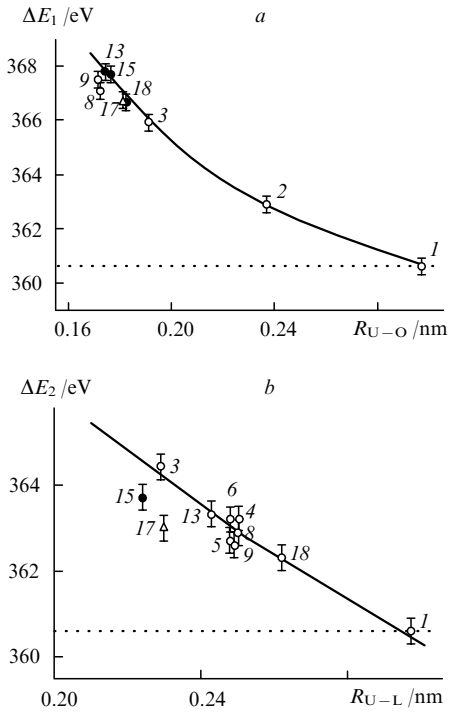


Figure 24. Dependences [see Eqns (9), (11)] of the relative binding energies ΔE_i ($U6p_{3/2} - U4f_{7/2}$) on the $R_{U-O_{ax}}$ bond lengths (*a*) and distances from the uranium atom to the ligand atom in the equatorial plane R_{U-L} (*b*) in the uranyl compounds (the dots are experimental data, the curves correspond to the calculation).[48, 94]
The theoretical curve in Fig. 24 *b* corresponds to oxygen-containing compounds (L = O) with D_{6h} symmetry. Here and in Fig. 25, the numbers of dots correspond to the numbers of compounds in Table 8; the light circles are oxygen-containing ligands; dark circles, F, Cl; triangle, γ-UO_3.

plane around a uranium ion influence in different ways the XPS spectral structure in the low binding energy range. Thus, it is possible to obtain experimental dependences of the spectral structure parameters in the given range on both the R_{U-O} bond length in the UO_2^{2+} group and the R_{U-L} distance between the uranium atom and the ligands L located in the equatorial plane (Fig. 24).

As an illustration of the efficiency of IVMO formation in uranium compounds, Fig. 24 shows also the ΔE_U and ΔE_1 values for the oxide UO_2. It can be seen that the formation of a chemical bond in uranium compounds is accompanied by a substantial relative shift of the upper $2a_{2u}$ IVMO towards lower binding energies (by more than 7.0 eV). This value is 1.5 orders of magnitude higher than the experimental error and can serve as a reliable and convincing proof for the effective formation of IVMO in uranium compounds. The dependence presented in Fig. 24 *a* has the form

$$\Delta E_1 = 356.07 + 0.55(R_{U-O})^{-1.75}, \quad (9)$$

hence,

$$R_{U-O} = \frac{0.55}{(\Delta E_1 - 356.07)^{0.571}}, \quad (10)$$

where ΔE_1 is expressed in eV, and R_{U-O}, in nm. Equations (9) and (10) have been used to determine the ΔE_1 values and bond lengths in the uranyl groups of some compounds (see Table 8).

When constructing the experimental dependence of the relative $U6p_{3/2}$ binding energy in the high energy spectral range on the R_{U-L} bond length for uranyl compounds, several points are to be borne in mind (see Fig. 24 *b*). First, the structure of the local environment of the uranium atom in these compounds should be described by the same cluster, specifically, $[UO_2L_6]^{10-}$ (D_{6h} group of symmetry). Second, the ligands should be identical. In this particular case, an oxygen atom acts as the ligand L and the influence of substituents is neglected.

For such compounds, the relative electron energy (ΔE_2) obeys the following dependence on the bond length R_{U-L}

$$\Delta E_2 = 343.84(R_{U-L})^{-0.039}; \quad (11)$$

this can be transformed into the expression

$$R_{U-L} = \left(\frac{383.84}{\Delta E_2}\right)^{25.71}, \quad (12)$$

which allows one to determine the average distance from the uranium atom to the equatorial oxygen atoms based on the ΔE_2 value. For comparison, Fig. 24 *b* shows the data for uranyl compounds with oxygen-free ligands in the equatorial plane (L = Cl, F). As was to be expected, some of the points markedly deviate from the basic curve (see Fig. 24 *b*). Figure 25 shows a more comprehensive dependence[96, 97, 109] of the ΔE_i values on R_{U-O} in the UO_2^{2+} group, which reflects the variation of the IVMO energies and agrees qualitatively with the results of theoretical calculations.[26, 102] Relations have been proposed[95] for determining the distances from the uranium ion to the nearest

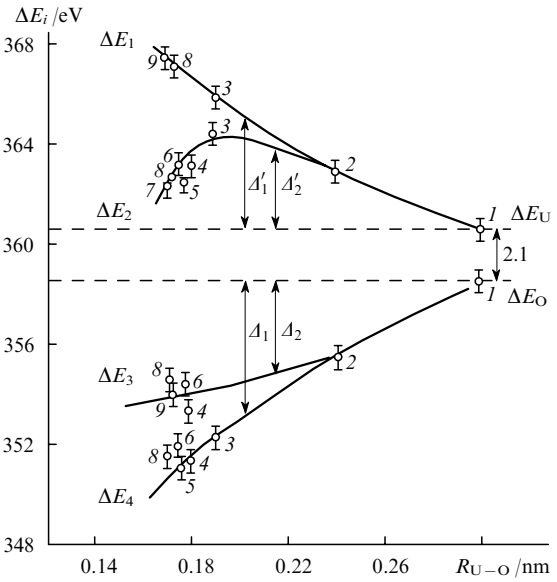


Figure 25. Experimental dependence of binding energy differences between the core and valence electrons corresponding to $\Delta E_1(2a_{2u})$, $\Delta E_2(2e_{1u})$, $\Delta E_3(1e_{1u})$ and $\Delta E_4(1a_{2u})$ for the $[UO_2O_6]^{10-}$ cluster (D_{6h} symmetry).[109] The designations of ΔE_i are given in Fig. 23.

ligand ion in the axial and equatorial positions in the uranyl compounds on the basis of U6p$_{3/2}$ line splitting ΔE:

$$R_{U-O} = b_1 \ln\left(\frac{a_1}{c_1 + \Delta E}\right), \quad (13)$$

$$R_{U-L} = b_2 \ln\left(\frac{a_2}{c_2 - \Delta E}\right), \quad (14)$$

where $a_1 = 157$ eV, $a_2 = 348$ eV, $b_1 = b_2 = 0.069$ nm, $c_1 = 8.57$ eV, $c_2 = 15.0$ eV.

Note that for uranyl difluoride (UO_2F_2), the formation of IVMO was confirmed by X-ray $O_{4,5}$(U) emission spectroscopy.[246–248]

c. XPS spectra of the core electrons

The XPS spectra of the core electrons of uranyl compounds resemble in many respects the corresponding spectra of uranium trioxide. The above considerations concerning the nature of the fine structure in the spectra of uranium oxides are largely valid for the spectral structure observed for uranyl compounds in the energy range of core electrons.

The U4f$_{7/2}$ line is used most often to determine the uranium oxidation state in compounds. The difference between the U4f$_{7/2}$ binding energies for the UO_2 and γ-UO_3 oxides equals 1.5 eV. Thus, the binding energies of the core electrons can, in principle, be used to draw conclusions about the oxidation state of uranium in a particular compound; however, this determination of the oxidation state is not always legitimate. For example, for $K_4UO_2(CO)_3 \cdot 5H_2O$ containing U^{6+}, the U4f$_{7/2}$ binding energy is lower than this value for the fluoride UF_4 in which the formal oxidation state of uranium is four (see Table 7). This indicates that for determining the oxidation state of uranium in compounds, one should resort to the whole set of data on the binding energies of the valence and core electrons and the relevant fine spectral structure.

As noted for oxides, the oxidation state of uranium can be derived from the structure of shake up satellites. The structure related to many-body perturbation is most pronounced in the U4f and U5d spectra.[47] It should be noted that in the spectra of uranyl compounds, the low-energy shake up satellites occur on the higher energy side (by $\sim$3–4 eV) of the basic lines of the U4f doublet and have a $\sim$20% intensity (see Table 7). The spin–orbit splitting of the U4f level is virtually constant for different uranyl compounds being equal on average to 10.9 eV [for uranium metal, ΔE_{sl}(U4f) = 10.8 eV].[57] The spectra of compounds containing U^{4+} ions display satellites at a distance of $\sim$7 eV from the basic lines.

Unlike the spectrum of UO_2, in the spectra of uranyl compounds, the U5d lines are sharp. This is probably due to the fact that the spectra of the UO_2 oxide, which contains U5f electrons, exhibit multiplet splitting in the U5d binding energy range. The average spin–orbit splitting of the U5d level found from the spectra of uranyl compounds [$\overline{\Delta E_{sl}}$(U5d) = 8.6 eV] is in good agreement with the corresponding value for uranium metal (8.6 eV).[57] The shake up satellites that arise in the U5d range complicate somewhat the spectra of these compounds but barely influence the spin–orbit splitting.

The U5p spectra exhibit a complex fine structure, which markedly suppresses the intensity of the U5p$_{1/2}$ component.[47] In the case of uranium oxides, the formation of this fine structure has been attributed[47,55,56] to the dynamic effect manifested in this range, which gives rise to final states of the type $U5p^55d^{10}(6s^26p^6)5f^0 \rightleftharpoons U5p^65d^8(6s^26p^6)5f^1$. The data obtained for uranyl compounds do not contradict this assumption.

The first detailed study of the U4p$_{3/2}$ spectra of uranyl compounds has been reported.[47] In all cases, the spectral structure was similar to the structure of the U5p spectra. These data are consistent with the assumption, based on the spectra of uranium oxides, stating that the structure in the U4p$_{3/2}$ spectra is due to the dynamic effect, resulting in the final states of the type $U4p^54d^{10}4f^{14}5s^2(5p^65d^{10}6s^26p^6)5f^0 \rightleftharpoons U4p^64d^94f^{14}5s^1(5p^65d^{10}.6s^26p^6)5f^0np^1$.

The U4d binding energy range also contains a fine structure, which is characteristic of particular compounds.[55] The doublet lines in the spectra are sharper than in the case of tetravalent uranium. The average spin–orbital splitting [$\overline{\Delta E_{sl}}$(U4d)] determined from the spectra of uranyl compounds is 42.4 eV, which is somewhat greater than the value of 42.1 eV found for uranium metal.[57]

On the basis of the U6s spectra of oxides, it was concluded that the final states described by the configurations $U6s^16p^65f^06d^0$ and $U6s^26p^45f^06d^1$ can arise with comparable probabilities upon photoemission of the U6s electrons from uranium compounds.[56] This gives rise to a spectral structure extending for $\sim$40 eV. The U6s spectral structure is characteristic of uranyl compounds and can be used for identification.

The experimental results on the binding energies of core and valence electrons and fine structure parameters of the XPS spectra altogether allow one to determine unambiguously the uranium oxidation states in compounds and to draw conclusions concerning the structure of the local environment of the central uranium atom and the nature of the chemical bond between this ion and the neighbouring ligand atoms. Procedure for quantitative elemental and ionic analysis of uranium compounds and for determination of the oxidation states of other ions involved on the basis of fine structure parameters of the XPS spectra of core and valence electrons has been elaborated.[47,53,55,94]

3. Natural uranium oxides

Determination of the relative contents of uranium ions in different oxidation states and the structural and phase compositions of natural uranium oxides (pichblendes) is very important for studying the conditions of formation of uranium deposits and for the exploration and development of the deposits.[208] Therefore, the possibility of using XPS studies for solving these problems has been evaluated.[65,66] The oxygen coefficients of the natural UO_x oxides were determined according to the standard procedure;[6] the specimens of minerals were taken from the collection of the researchers.[66]

The structure of the low binding energy XPS spectra of the natural oxides UO_x has much in common with the corresponding structure of complex synthetic oxides.[66] The spectra of all natural

oxide samples exhibit a relatively sharp line around a zero binding energy, which is assigned to the U5f electrons not involved directly in the chemical bond. The U6p and O2s spectral range exhibits a structure partially attributed to the IVMO electrons in natural uranium oxides. This spectral range can exhibit lines for the lead oxide PbO ($Pb5d_{5/2}$ and $Pb_{3/2}$ electrons, 19.5 and 21.8 eV, respectively; Pb6s electrons, 9.5 eV).[55] The possible occurrence of lead impurities in natural uranium oxides and complication of the structure caused by the Pb lines is taken into account in the identification of spectral peaks. The O2s energy range can also exhibit additional lines from oxygen atoms of the concomitant oxides and water molecules adsorbed on the oxide surface. Despite this possible complication of the spectra of natural uranium oxides, the most information-rich spectral ranges (0–4 and 10–20 eV) are almost free from impurity-related lines.

The line of the unbound U5f electrons in the spectra of natural uranium oxides is rather narrow and can be easily distinguished from the overall spectrum. The relative intensity of this line changes with an increase in the oxygen coefficient x in the range of $2.13 \leqslant x \leqslant 2.24$, as in the case of synthetic oxides (see Fig. 10). Then the intensity jumps up, and in the $2.47 \leqslant x \leqslant 2.68$ range, it decreases according to the same law as observed for UO_2 and γ-UO_3 mixtures (see Fig. 10).

The dependences of the lines for the U5f electrons not involved in the chemical bond on the x value established for synthetic oxides allow one to determine the ionic composition of the pitchblende studied (Table 9). This is done assuming that the natural oxides can contain three types of ions, U^{4+}, U^{5+} and U^{6+}. The results obtained in this approximation lead to the conclusion that an increase in the oxygen coefficient x in the range $2.13 \leqslant x \leqslant 2.24$ entails a sharp decrease in the U^{4+} content in the pitchblende. On further increase in x in the range $2.47 \leqslant x \leqslant 2.68$, the concentration of U^{4+} ions increases and the concentration of the U^{6+} ions decreases. No U^{5+} ions are present in the natural oxides in this x range.

The IVMO spectral range corresponding to the U6p and O2s AO (binding energy range 10–20 eV) exhibits a series of peaks. On the basis of binding energy differences between the core and inner valence electrons, one can distinguish lines corresponding to the IVMO of the U^{4+}, U^{5+} and U^{6+} ions. With allowance for relations (9) and (10), these data permit one to estimate the R_{U-O} bond lengths in natural oxides (see Table 9).

Analysis of the spectral structure of natural uranium oxides in the U6p–O2s binding energy range and the intensity of the line for the U5f unbound electrons shows that natural uranium oxides are composed of several structural phases containing U^{4+}, U^{5+} and U^{6+} ions (see Table 9). The same conclusion can be drawn on the basis of the data on the core electron spectra.[66] For example, it follows from the U4f spectral structure that natural uranium oxides contain uranium ions in different oxidation states. This can be seen from both the shapes of the U4f lines and the structure of shake up satellites, which cannot be described as a superposition of individual U4f satellites due to U^{4+} and U^{6+}, but is more complicated.

The decomposition of the $U4f_{7/2}$ line into components has made it possible to determine the relative concentrations of uranium ions in different oxidation states. The results were similar to those derived from the line intensities of unbound U5f electrons (see Fig. 10, Table 9). The $U4f_{7/2}$ binding energies presented in this Table were found as weight-average values for the electrons of the components, which characterise the uranium ions in different oxidation states. As expected, these values grow upon an increase in the U^{6+} concentration in the samples. The substantial broadening of the $U4f_{7/2}$ line compared to the narrower lines observed for individual UO_2 and γ-UO_3 oxides is itself an important

Table 9. Binding energies (E_b / eV), binding energy differences (ΔE_i / eV), line widths at half maximum (Γ / eV), relative contents of uranium ions [k (%)] and bond lengths [R_{U-O}, $R_{U-O(L)}$ / nm] in natural uranium oxides.[66]

Parameter	$UO_{2.13}$	$UO_{2.23}$	$UO_{2.24}$	$UO_{2.47}$ (see [a])	$UO_{2.47}$ (see [a])	$UO_{2.60}$	$UO_{2.63}$	$UO_{2.68}$
E_b(U5f)	2.0	2.0	2.0	1.9	2.0	2.0	2.0	1.9
E_b(OVMO)	6.2	6.3	6.2	6.1	6.2	6.1	6.2	6.1
$E_b(U6p_{3/2})$	–	–	–	14.0,	14.0,	–	14.1,	14.0,
	15.4,	15.5,	14.4,	15.7,	16.0,	14.7,	16.0,	16.1,
	17.3,	17.5,	18.0,	18.2,	18.2,	17.7,	18.0,	17.9,
	19.0	19.5	19.6	20.5	20.6	19.8	19.5	19.9
$\Delta E_i(U6p_{3/2})$	3.6	4.0	5.2	4.8	4.6	5.1	3.5	3.8
$E_b(U6p_{1/2})$	28.6,	28.7,	28.7,	28.3,	28.5,	28.8,	28.9,	28.7,
	30.1	31.2	30.7	30.5	30.2	30.6	30.9	30.1
E_b(O2s)	22.8,	22.8,	22.9,	23.0,	23.5,	22.9,	23.0,	23.0,
	25.4	25.1	25.6	25.0	26.0	25.9	25.6	25.5
ΔE_i(O2s)	2.6	2.3	2.7	2.0	2.5	3.0	2.6	2.5
E_b(O1s)	530.5,	530.8,	–	–	530.5,	530.5,	–	–
	531.7	532.1	532.0	531.7	532.0	532.0	532.1	531.3
ΔE_i(O1s)	1.2	1.3	–	–	1.5	1.5	–	–
$E_b(U4f_{7/2})$	381.4	381.6	381.7	381.9	381.5	381.9	381.7	381.8
$\Gamma(U4f_{7/2})$	2.9	2.7	2.6	2.7	2.0	2.7	2.5	2.9
$k(U^{4+})$ [b]	33	12	2	60	60	49	37	32
$k(U^{5+})$ [b]	54	65	74	–	–	–	–	–
$k(U^{6+})$ [b]	13	23	24	40	40	51	63	68
$R_{U-O}(U^{6+})$ [c]	–	–	–	0.168,	0.168,	–	0.169,	0.170,
	0.180	0.181	0.172	0.183	0.186	0.174	0.186	0.187
$R_{U-O}(U^{4+})$ [c]	0.223	0.227	0.236	0.240	0.240	0.230	0.236	0.234
$R_{U-O(L)}(U^{6+})$ [c]	0.241	0.250	0.252	0.268	0.270	0.255	0.250	0.257

[a] The samples were obtained from different deposits. [b] The error of measurement of k is ±10%. [c] The error of measurement of $R_{U-O}(U^{n+})$ ($n = 4, 6$) is ±0.002 nm, that for $R_{U-O(L)}(U^{6+})$ is ±0.004 nm.

indication of the fact that pitchblende contains uranium ions in different oxidation states.

The lines of the U5d and U4d doublets of natural oxides are broader than the corresponding lines in the spectra of synthetic uranium oxides. As the content of U^{6+} ions in the samples increases, the U5d and U4d binding energies measured as the weight average values for different states of ions increase by about 1.0 eV. A more complicated structure than that observed in the spectra of synthetic uranium oxides is also found in the $U4p_{3/2}$, U5p and U6s spectra of natural oxides. These data confirm that natural uranium oxides do not show complete similarity to either complex synthetic oxides or mixtures of simple uranium oxides but represent complex structural phases. It follows from the obtained results that at $2.13 \leqslant x \leqslant 2.24$, the natural oxides UO_x are closer in properties to berthollides, while at $2.47 \leqslant x \leqslant 2.68$, they are closer to daltonides.[5]

The XPS data obtained for a broad range of technologically important uranium compounds show that the fine structure parameters of their spectra reflect the properties of these compounds, the nature of the chemical bond in them and the secondary electronic processes which accompany the electron photoemission.

IV. Neptunium compounds

In recent years, studies of physicochemical properties of neptunium compounds have attracted considerable attention.[1, 3, 239, 249, 250] Neptunium dioxide NpO_2,[41, 79] single crystals of $Cs_3NpO_2Cl_4$ and $Cs_2NpO_2Cl_4$,[51, 53, 80] the compounds $Cs_2NpO_2(OAc)_3$, $NaNpO_2(OAc)_3$ and $RbNpO_2(NO_3)_2 \cdot 2\,H_2O$ [55] have been studied by XPS. A number of studies have been devoted to elucidation of correlations between the fine structure parameters of the XPS spectra of outer and core electrons and the neptunium oxidation states in compounds,[44, 80, 81] magnetic properties,[44, 89, 90] the nature of the chemical bond (Refs 36, 41, 51 – 53, 55, 81, 87 – 90, 115) and the secondary electronic processes.[55, 56] Non-relativistic X_α-SW calculations have been carried out for the electronic structure of the NpO_2^{2+} cluster ($D_{\infty h}$ group of symmetry) with $R_{Np-O} = 0.171$ nm,[115] while calculations for the $[NpO_2Cl_4]^{2-}$ cluster (D_{4h} group of symmetry) with $R_{Np-O} = 0.171$ nm and $R_{Np-L} = 0.262$ nm were carried out in the relativistic X_α-DV approximation.[36]

In a number of studies,[51, 53, 55, 56, 80, 114, 115] the XPS spectra of several neptunyl compounds (Table 10) have been analysed in order to establish the relationships of the spectral structure with the properties and structures of the compounds and the nature of the chemical bond in them. A key goal was to confirm the assumed formation of IVMO in neptunium compounds, which has been established for thorium and uranium compounds on the basis of the XPS spectral structure.

1. The low binding energy range of the spectra

The structure of the low binding energy XPS spectra of neptunyl compounds is fairly similar to that of the corresponding spectra of uranyl compounds. Since these compounds contain other elements apart from neptunium, the low binding energy range of the spectra exhibits an additional structure caused by electrons of these elements, which markedly complicates interpretation of the fine structure of the spectra of neptunium compounds. Thus the neptunium lines in this binding energy range in the spectra of the $Cs_3NpO_2Cl_4$ and $Cs_2NpO_2Cl_4$ single crystals are overlapped by caesium and chlorine lines and their satellites, which occur on the higher-energy side of the basic lines (Fig. 26). The spectra of other neptunium compounds also exhibit additional lines (Fig. 27). For comparison, Fig. 27 shows the spectra of NaOAc and $Ni(NO_3)_2$.

a. The spectra of the Np5f electrons

The spectra of the studied neptunium compounds exhibit a sharp line near a zero binding energy (the Fermi level for metals), like the spectra of U^{4+} (see Figs 26, 27). As the oxidation number of

Table 10. Binding energies (E_b) [55] and photoionisation cross-sections (σ) of neptunium compounds.[203]

Orbital Np, L (nl_j)	E_b /eV							σ (see [d, e])
	$NaNpO_2(OAc)_3$ (see [a])	$Cs_2NpO_2Cl_4$ (see [a])	$RbNpO_2(NO_3)_2$ (see [b])	$Cs_2NpO_2(OAc)_3$ (see [b])	$Cs_3NpO_2Cl_4$ (see [b])	NpO_2 (see [c]) [79]	Np_{theor} (see [d]) [178]	
Np5f	3.4	3.3	2.9	2.3	2.5	–	7.4	0.52
OVMO (see [f])	5.9	5.3	5.4	4.3	4.9	–		–
$Np6p_{3/2}$	15.7,	15.5,	–	–	15.7,	–	–	–
	20.2	20.0	19.3	18.9	18.6	17.5	24.6	0.39
$Np6p_{1/2}$	–	30.6	–	30.4	30.0	29.3	36.2	0.14
Np6s	50.5	50.2	49.8	49.7	48.7	–	57.2	0.17
$Np5d_{5/2}$	102.7	102.4	101.5	100.8	101.1	100.9	107.1	3.62
$Np5d_{3/2}$	112.2	112.1	–	109.9	110.0	–	120.4	2.46
$Np5p_{3/2}$ (see [f])	207.6	208.7	205.5	206.9	207.3	206.3	220.8	2.31
$Np5p_{1/2}$	–	–	–	–	–	–	280.7	0.68
Np5s (see [g])	–	338.7	335.4, 344.1	335.1, 344.2	335.2, 343.9	–	349.3	0.75
$Np4f_{7/2}$	405.2	404.6	403.6	403.0	403.4	402.5	408.4	29.18
$Np4f_{5/2}$	417.0	416.4	415.3	414.6	415.2	414.3	420.9	22.91
$Np4d_{5/2}$	771.8	771.4	770.7	769.6	770.3	771.2	779.6	17.44
$Np4d_{3/2}$	816.7	816.0	815.8	814.8	815.4	816.1	824.9	11.44
$Np4p_{3/2}$	1087.5	1087.4	1086.9	1086.0	1086.1	–	1096.6	7.83
O2s	24.2,	–	–	–	–	23.8		0.14
	26.0	25.8	27.0	27.2	26.2			
O1s	532.0	531.9	531.5, 533.1	531.5	532.3	529.7		2.93
C1s	288.8			288.3		284.5		1.00
N1s			407.1					1.80

[a] The state of neptunium is described as Np^{6+}. [b] The state of neptunium is described as Np^{5+}. [c] Np^{4+}. [d] For atomic neptunium. [e] The s values were obtained at 1487 eV and are expressed in 13.6 b per atom shell. [f] Weight average E_b values for fine structure components. [g] The E_b values corresponding to the most intense peaks in the fine structure of the corresponding binding energy range.

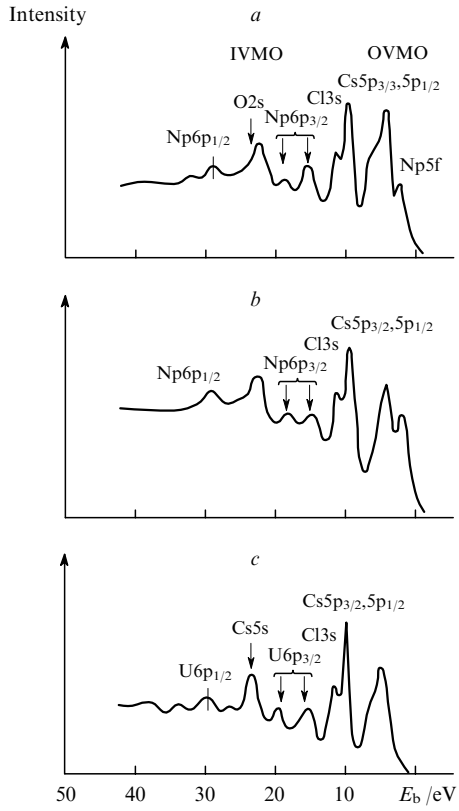


Figure 26. XPS spectra of the single crystals of $Cs_2NpO_2Cl_4$ (*a*), $Cs_3NpO_2Cl_4$ (*b*), $Cs_2UO_2Cl_4$ (*c*), containing the NpO_2^{2+}, NpO_2^{+} and UO_2^{2+} groups, respectively, in the low binding energy range.[53, 80]

Table 11. Relative intensity of the Np5f line [$I_{5f}^{exp} = I(Np5f)/I(Np4f_{7/2}) \times 10^2$] in the spectra of Np^{n+} compounds, effective magnetic moment (μ_{eff}/μ_B) and Weiss temperatures (θ / K).[55]

Compound	Np^{n+}	I_{5f}^{exp}	μ_{eff} (see [251])	θ (see [251])
NpO_2	Np^{4+}	5.9 ± 0.6	3.3 ± 0.2	181
$Cs_3NpO_2Cl_4$	Np^{5+}	4.6 ± 0.5	3.2 ± 0.2	249
$Cs_2NpO_2Cl_4$	Np^{6+}	2.6 ± 0.3	2.3 ± 0.1	216
$NaNpO_2(OAc)_3$	Np^{6+}	1.8 ± 0.2	2.2 ± 0.1	51.5

neptunium increases, the intensity of this line diminishes (Table 11). Hence, it has been suggested that this relatively narrow line near a zero binding energy is due to the Np5f electrons not involved in the chemical bond.[55, 80] As the neptunium oxidation state increases, the number of unbound Np5f electrons decreases, so does the effective magnetic moment μ_{eff} (see Table 11).

It follows from the XPS spectra [55, 79] and calculation results [137] that on passing from uranium compounds to neptunium compounds, the binding energy difference between the OVMO and An5f electrons decreases. This imposes some limitations on the accuracy of determination of the relative intensity of the Np5f line in neptunium compounds containing unbound Np5f electrons. Nevertheless, the intensity of this line can serve as not only a qualitative but also a quantitative measure of the neptunium oxidation state in compounds.

b. The spectra of the Np6p and O2s electrons

As noted above, the low binding energy range of the XPS spectra of the neptunium compounds studied contains, in addition to the

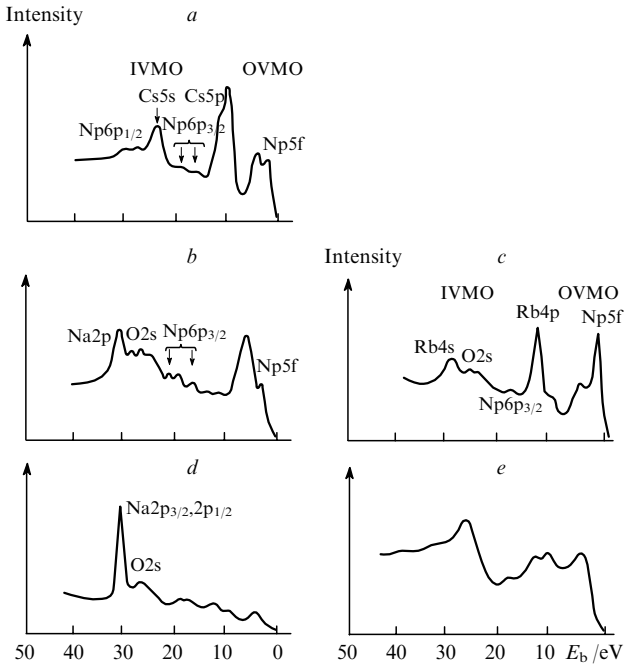


Figure 27. XPS spectra of neptunium compounds in the low binding energy range (for comparison, XPS spectra of sodium acetate and nickel nitrate are given).[55]
(*a*) $Cs_2NpO_2(OAc)_3$, (*b*) $NaNpO_2(OAc)_3$, (*c*) $RbNpO_2(NO_3)_2 \cdot 2H_2O$, (*d*) NaOAc, (*e*) $Ni(NO_3)_2$.

Np6p and O2s lines, some lines due to ligand electrons (Table 12, see Figs 26, 27), which complicate the spectrum. For example, the OVMO and IVMO spectra of the NO_3^- and AcO^- ligands exhibit a complex structure covering a range of approximately 35 eV. This structure [55] has been studied both experimentally and theoretically (for NO_3^-, it is shown in Figs 5 and 27 *e*).

Despite the complexity of the low binding energy XPS spectra of neptunium compounds containing an NpO_2^{n+} group, the structure of the $Np6p_{3/2}$ spectrum is similar to that observed in the $U6p_{3/2}$ spectra of uranyl compounds (see Fig. 26). In all cases, two components appear instead of the single $An6p_{3/2}$ line. The lower binding energy component is partially superimposed onto the Cl3s line.

The R_{An-O} bond lengths in the AnO_2^{n+} groups have been estimated using relation (8) with the assumption that the effect of the difference between the charges of the Np and U nuclei can be neglected.[80] This gave the following values: $R_{U-O} = 0.174$ nm, $R_{Np-O} = 0.180$ nm and $R_{Np-O} = 0.174$ nm for the UO_2^{2+}, NpO_2^{+} and NpO_2^{2+} groups in the compounds $Cs_2UO_2Cl_4$, $Cs_3NpO_2Cl_4$ and $Cs_2NpO_2Cl_4$, respectively. The appearance of two components in the $Np6p_{3/2}$ spectral range for neptunium compounds confirms the assumption that the XPS spectra of compounds containing AnO_2^{n+} groups should exhibit the structure typical of the IVMO.

The participation of low-energy occupied Np6p and L*n*s AO in the IVMO formation can be established on the basis of the binding energy difference between the core AO and valence MO. The researchers cited [80] could not carry out this comparison due to the lack of data for neptunium metal. However, comparison of these values for neptunium compounds shows that they are different. A reason for this discrepancy may be dissimilar participation of the Np6p and L*n*s AO in the IVMO formation in different compounds (Table 13).

Table 12. Binding energies (E_b /eV) of electrons of the ligands contained in neptunium compounds.[55]

Orbital	NaL^1	Na_2CO_3	NiL_2^2	Orbital	CsCl	Orbital	$RbYL_2^2 \cdot 2H_2O$	Orbital	$Cs_2YL_3^1$	Cs_3YCl_4	Cs_2YCl_4	Orbital	$NaYL_3^1$
MO	4.6,	3.1,	4.3,	MO	4.4	Rb4p	14.3	Cs5p	10.8	10.5	10.4,	Na2p	30.5
	9.8,	5.3,	11.8,	$Cs5p_{3/2}$	10.1	Rb4s	29.9				11.9	Na2s	63.3
	12.1,	9.6,	14.5,	$Cs5p_{1/2}$	11.7	Rb3d	110.9	Cl3s		15.8	16.0	Na1s	1071.5
	13.8,	11.7	18.2	Cl3s	15.0 (30.6,	Rb3p	238.4	Cs5s	23.4	23.7	23.6		
	17.8,				34.5, 38.4) [a]	Rb3s	321.8	$Cs4d_{5/2}$	75.5	75.5	75.4		
	19.5			Cs4d	75.3 (87.1,			$Cs4d_{3/2}$	77.6	77.7	77.7		
O2s	25.2,	23.2,	26.9,		98.9, 122.1) [a]			Cs4s	229.9	229.9	229.8		
	26.9	24.7	32.4	Cs4p	158.8			$Cs3p_{3/2}$	1065.2	1065.0	1065.2		
Na2p	30.2	30.2		Cs4s	229.5			Cl2p		198.9	199.0		
Na2s	63.0	62.8		$Cs3d_{5/2}$	724.5 (733.8) [a]								
C1s	285.0,	–		$Cs3d_{3/2}$	728.5 (747.9,								
	288.5	289.3			761.9)								
O1s	531.5	531.3	533.1	Cl2p	197.6, 199.3								
					(208.5, 216.6) [a]								

Note. The following designations are used: Y = NpO_2, L^1 = OAc, L^2 = NO_3. [a] The binding energies for the electrons responsible for the appearance of satellites are given in parentheses.

Table 13. Binding energy differences (ΔE_i) between various neptunium and oxygen shells.[55]

Compound, element	$\Delta E_i = E_k - E_l$ /eV				
	$6p_{3/2} - 6p_{1/2}$	$6p_{3/2} - 4f_{7/2}$	$5d_{5/2} - 4f_{7/2}$	$4f_{7/2} - 4d_{5/2}$	O2s – O1s
$NaNpO_2(OAc)_3$	–	389.5, 385.0	302.5	366.6	506.0, 507.8
$Cs_2NpO_2Cl_4$	–	389.1, 384.6	302.2	366.8	506.1, 508.3
$Cs_3NpO_2Cl_4$	–	387.7, 384.8	302.3	366.9	505.4, 508.1
$RbNpO_2(NO_3)_2 \cdot 2H_2O$	–	384.3	302.1	367.1	504.5
$Cs_2NpO_2(OAc)_3$		384.1	302.2	366.7	504.3
NpO_2 (see [79])	11.8	385.0	301.6	368.7	505.9
Np_{theor} (see [178])	11.6	383.8	301.3	371.2	

2. The spectra of the core electrons

In the binding energy range of core electrons, XPS spectra of neptunium compounds exhibit a complex fine structure (Figs 28 – 31).[55, 56, 79, 80] The binding energies for the most intense lines are listed in Table 10. The most intense lines correspond to the Np4f electrons (see Fig. 28). The basic lines of these spectra are least distorted due to the additional structure; therefore, the Np4f spectrum is most suitable for quantitative elemental and ionic analyses and determination of the neptunium oxidation state. For compounds containing neptunium ions in only one formal oxidation state, the Np4f binding energy varies within a range of 0.6 eV (see Table 10).[55] The greatest change in the $Np4f_{7/2}$ binding energy on passing from compounds with formally pentavalent neptunium to hexavalent neptunium compounds equals 2.2 eV, while the smallest change is 1.0 eV. Hence, the chemical shifts can be used to draw conclusions concerning the formal oxidation state of neptunium and the relative ionic – covalent natures of the bond in compounds.

In caesium- and chlorine-containing neptunium compounds, the binding energies formed by these elements are somewhat greater than the corresponding binding energies in CsCl (see Table 12). This is due to the increase in the caesium and chlorine oxidation states upon their incorporation in the compounds considered. Thus, it can be concluded that the bonds between Cl and the AnO_2^{n+} group are more covalent than the Cs–Cl bond, while the bond between the caesium and chlorine atoms in a neptunium compound is more ionic than that in CsCl.

a. The spectra of Np4f electrons

The basic lines of the Np4f doublet related to the spin – orbit splitting [ΔE_{sl}(Np4f) = 11.8 eV [80]] are relatively narrow (see Fig. 28). In this binding energy range, satellites caused by many-body perturbation appear with the highest probability. The maxima corresponding to these satellites can also be seen in the spectra of other core electron levels. However, the Np4f range exhibits most characteristic shake up satellites. For example, for Np^{4+} (NpO_2),[79] Np^{5+} ($Cs_3NpO_2Cl_4$) and Np^{6+} ($Cs_2NpO_2Cl_4$), the ΔE_{Sat} values equal ~7.0, 9.4 and 3.5 eV, and the intensities of low-energy satellites are ~17%, 12% and 20%, respectively.[80] These values are correlated satisfactorily with corresponding values for U^{4+} (UO_2) and U^{6+} ($Cs_2UO_2Cl_4$): 6.9 and 3.8 eV, 25% and 20%, respectively. This indicates that the electronic structures of isostructural neptunium and uranium compounds have much in common, which also agrees with the results of theoretical calculations.[115, 137] It is noteworthy that the structure of the Np4f spectrum related to many-body perturbation can serve as a reliable characteristic of the neptunium formal oxidation state.

b. Spectra of the Np5d and Np4d electrons

In the Np5d binding energy range, the intensity of the $Np5d_{3/2}$ line is essentially suppressed and the line is broadened (see Fig. 29). This results in a seeming substantial change in the spin – orbit splitting. Thus the average value is given by $\Delta\bar{E}_{sl}$(Np5d) = 9.2 eV and the difference between these values for the studied neptunium compounds does not exceed 0.8 eV.

The change in the spin – orbit splitting is due to the formation of the complex structure of the Np5d spectral lines. This structure may arise due to the multiplet splitting caused by the presence of unpaired Np5f electrons. In addition, the Np5d spectra may exhibit a structure related to the dynamic effect, which gives rise to the final electronic states like $Np5d^96s^26p^65f^n np^0 \rightleftharpoons Np5d^{10}6s^06p^65f^n np^1$, because the relation E_b(Np5d) ≈ $2E_b$(Np6s) holds. However, this process is relatively unlikely ($\Delta n = 1$, $\Delta l = 2$). The value ΔE_{sl}(Np5d) = 9.7 eV should be considered to be most realistic.

The Np4d spectral structure is also complicated due to superposition of lines related to the many-body effects involving ligand atoms (see Fig. 29). The other observed maxima cannot be explained in this way. Presumably,[55] this structure is a consequence of the dynamic effect, resulting in final states like $Np4d^94f^{14}(5s^25p^65d^{10}6s^26p^6)5f^n \rightleftharpoons Np4d^{10}4f^{12}(5s^25p^65d^{10}6s^2.6p^6)5f^n6d^1$. This is one of the possible mechanisms for the formation of the fine structure in the Np4d spectra.

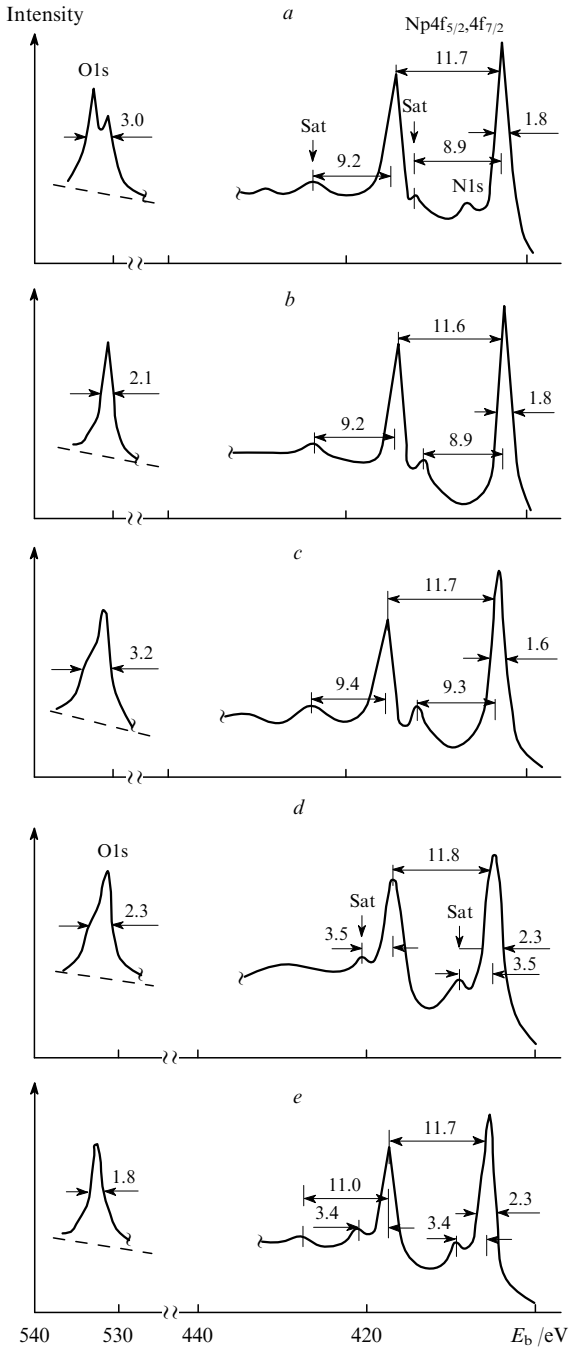


Figure 28. XPS spectra of neptunium compounds containing the NpO_2^+ (*a*–*c*) and NpO_2^{2+} (*d*, *e*) groups in the Np4f and O1s binding energy ranges.[55]
(*a*) $RbNpO_2(NO_3)_2 \cdot 2H_2O$, (*b*) $Cs_2NpO_2(OAc)_3$, (*c*) $Cs_3NpO_2Cl_4$, (*d*) $Cs_2NpO_2Cl_4$, (*e*) $NaNpO_2(OAc)_3$. The dashed lines show the background.

The appearance of the complicated fine structure in the Np4d spectra leads to a seeming change in the spin–orbit splitting on passing from one compound to another. The average value $\Delta\bar{E}_{sl}$(Np4d) is equal to 45.0 eV. This does not allow any accurate measurements of the binding energies on the basis of the Np4d spectra.

c. Spectra of the Np5p and Np4p$_{3/2}$ electrons

The Np5p binding energy range of the XPS spectra of neptunium compounds exhibits lines for the core electrons of the ligand atoms (see Fig. 30).[56] The structure of the Np5p$_{1/2}$ spectra cannot be observed, as the ΔE_{sl}(Np5p) value equals 77 eV; the binding

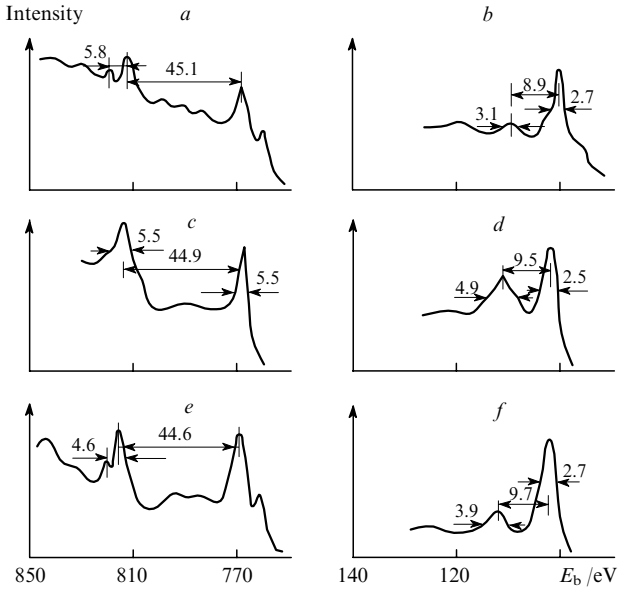


Figure 29. XPS spectra of neptunium compounds in the Np4d (*a*, *c*, *e*) and Np5d (*b*, *d*, *f*) binding energy ranges.[55, 80]
(*a*, *b*) $Cs_3NpO_2Cl_4$; (*c*, *d*) $NaNpO_2(OAc)_3$; (*e*, *f*) $Cs_2NpO_2Cl_4$.

energy of these electrons [E_b(Np5p$_{1/2}$] is approximately 283.0 eV,[20] their spectrum being superimposed onto the intense C1s lines of the AcO groups or the residual oil vapour molecules adsorbed on the sample surface. However, for some compounds, individual spectra of the Np5p$_{3/2}$ electrons can be observed (see Fig. 30).[56]

The reported[20] values for the neptunium binding energy E_b(Np5p$_{3/2}$) = 206 eV and E_b(Np5d$_{5/2}$) = 101 eV roughly satisfy the condition E_b(Np5p$_{3/2}$) $\approx 2\,E_b$(Np5d$_{5/2}$). This suggests[56] that the structure observed in the Np5p$_{3/2}$ spectra is largely caused by the dynamic effect, resulting in final states of the type $Np5p^5 5d^{10}(6s^2 6p^6)5f^n \rightleftharpoons Np5p^6 5d^8(6s^2 6p^6)5f^{n+1}$. Apparently, additional broadening of these lines can be due to multiplet

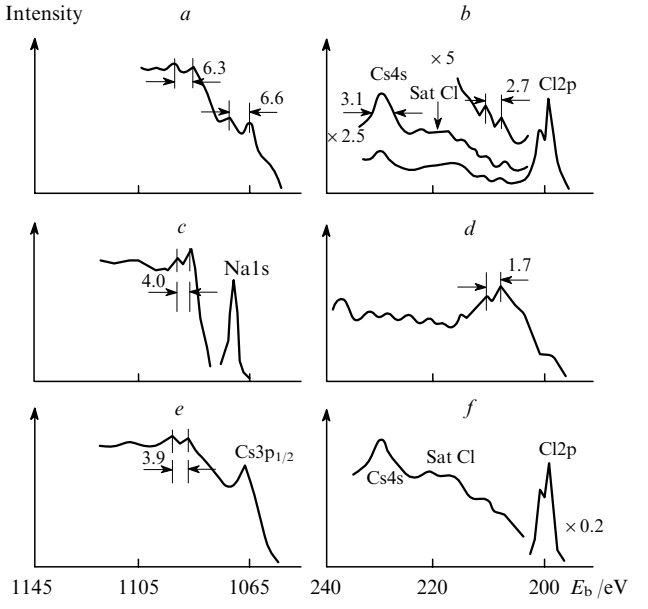


Figure 30. XPS spectra of neptunium compounds in the Np4p$_{3/2}$ (*a*, *c*, *e*) and Np5p (*b*, *d*, *f*) binding energy ranges.[56] (*a*, *b*) $Cs_3NpO_2Cl_4$; (*c*, *d*) $NaNpO_2(OAc)_3$; (*e*, *f*) $Cs_2NpO_2Cl_4$.

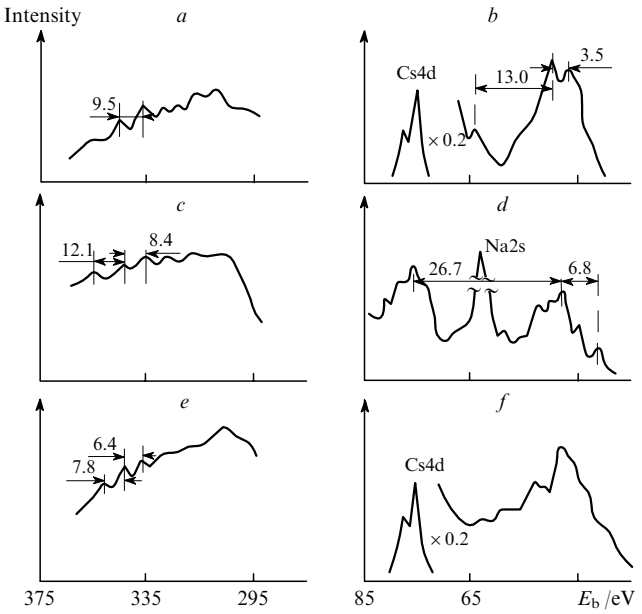


Figure 31. XPS spectra of neptunium compounds in the Np5s (*a*, *c*, *e*) and Np6s (*b*, *d*, *f*) binding energy ranges.[56] (*a*, *b*) $Cs_3NpO_2Cl_4$; (*c*, *d*) $NaNpO_2(OAc)_3$; (*e*, *f*) $Cs_2NpO_2Cl_4$.

splitting, because all the neptunium compounds considered contain unbound Np5f electrons. Some of the peaks can be attributed to shake up satellites (see Fig. 30).

The spectra of the $Np4p_{3/2}$ electrons of caesium-containing neptunium compounds are overlapped by satellites of the $Cs3p_{1/2}$ structure (see Fig. 30). The spectrum of the $Np4p_{3/2}$ electrons of $RbNpO_2(NO_3)_2 \cdot 2\,H_2O$ contains no ligand-related lines over a broad binding energy range; nevertheless, this range also displays fine structure. The binding energies of neptunium electrons reported in a study,[20] $E_b(Np4p_{3/2}) = 1087$ eV, $E_b(Np4d_{3/2}) = 773$ eV and $E_b(Np5s) = 338$ eV, roughly satisfy the relation $E_b(Np4p_{3/2}) \approx E_b(Np4d_{5/2}) + E_b(Np5s)$. Hence, one may suggest that the $Np4p_{3/2}$ spectral structure is due to the dynamic effect, resulting in final states of the type $Np4p^54d^{10}4f^{14}5s^26p^65f^n np^m \rightleftharpoons Np4p^64d^94f^{14}5s^16p^65f^n np^{m+1}$.

d. Structure of the Np6s and Np5s spectra

It is known that the Np6s electrons have a relatively small photoionisation cross-section [203] and their spectra exhibit a relatively complex fine structure. Nevertheless, the sample preparation and experimental procedures allowed researchers [55, 56] to measure the spectra of these electrons (see Fig. 31).[56] The fine structure of the Np6s spectrum extends over a binding energy range of ~40 eV. The electron binding energies found as the weight average values for electrons around the most intense band are listed in Table 10. The spectra of $RbNpO_2(NO_3)_2 \cdot 2\,H_2O$ and $NaNpO_2(OAc)_3$ exhibit a rather intense spectral structure in addition to the relatively broad bands at ~50 and ~75 eV. The spectra of these compounds reflect most fully the Np6s spectral structure over the whole binding energy range considered (see Fig. 31).

Presumably, the formation of the Np6s fine structure over this broad binding energy range may be due to the dynamic effect, resulting in final electronic states like: $Np6s^16p^65f^n6d^0 \rightleftharpoons Np6s^26p^45f^n6d^1$. The presence of unbound Np5f electrons in all of the studied neptunium compounds may give rise to an additional structure caused by multiplet splitting. Finally, shake up satellites should also be manifested in these spectra.[55, 56]

It should be noted that, without thorough theoretical analysis of the spectral structure in the Np6s binding energy range and without identification of individual lines, it is difficult to draw any qualitative conclusions concerning the involvement of the Np6s shell in the IVMO formation in neptunium compounds.

Attempted study of the Np5 spectral structure has been reported.[55, 56] In this energy range, against the relatively intense background of the broad C1s satellite band due to the OAc group or the residual vacuum oil, the spectrum exhibits an additional structure missing from the C1s spectrum of graphite (see Fig. 31). This structure always consists of two lines that cannot result from the multiplet splitting, because the corresponding binding energy difference does not exceed 2–3 eV. Therefore, it is assumed that the structure manifested in the Np5s spectra is due to the dynamic effect, which results in final states of the type $Np5s^15p^65d^{10}6s^26p^65f^n np^m \rightleftharpoons Np5s^25p^55d^{10}6s^16p^65f^n np^{m+1}$.

Thus, it can be concluded that parameters of the fine structure manifested in the spectra of neptunium compounds provide information on their magnetic properties, neptunium oxidation states and the degree of participation of the Np6p and L*n*s AO in the formation of the IVMO whose structure is determined by the local environment of the neptunium ion. The fine structure observed in the spectra of core electrons, which arises due to different mechanisms, is characteristic of particular neptunium compounds and can be used for identification.

V. Plutonium compounds

Plutonium oxides on the metal surface,[41, 64, 79, 83–86, 116, 121, 126] $Pu(NO_3)_4 \cdot n\,H_2O$,[29, 55] and the single crystal of $Cs_2PuO_2Cl_4$ [55, 82] have been studied by XPS. The correlations of fine structure parameters of the spectra of inner and outer electrons with plutonium oxidation states in compounds,[29, 64, 79, 81–86] the structures of compounds,[29, 55, 82] the types of chemical bond,[29, 37, 41, 44, 51–53, 55, 81, 82, 87–91, 115, 116] and secondary electronic processes that accompany photoemission of electrons [29, 55, 79, 82, 121] have been studied. The relativistic electronic structure parameters of plutonium were evaluated;[33, 35] nonrelativistic X_α-SW calculations were carried out for the electronic structure of the PuO_2^{2+} cluster ($D_{\infty h}$ group of symmetry) with $R_{Pu-O} = 0.171$ nm [115] and relativistic X_α-DV calculations were performed for the $PuO_2Cl_4^{2-}$ cluster (D_{4h} group of symmetry) with $R_{Pu-O} = 0.171$ nm and $R_{Pu-L} = 0.262$ nm.[36] On the basis of the XPS spectrum of outer valence electrons, the mechanism of formation of a PuO_2 film on the surface has been studied;[64] the dependence of valence and core level spectral parameters for metallic plutonium on the number of monolayers on the substrate has been analysed.[85]

For the single crystal of $Cs_2PuO_2Cl_4$ containing the PuO_2^{2+} group, the XPS spectra of various electron shells in the binding energy range from 0 to ~1250 eV have been studied [82] in order to determine the relationship between the fine spectral structure parameters and the structure of the local environment of the plutonium ion, plutonium oxidation state and the nature of the chemical bond in the compound. The spectral lines were identified using the spectra of plutonium metal [83, 116, 127] and plutonium dioxide,[41, 79, 84] the results of calculations for individual atoms [178] and model clusters,[36, 115] photoionisation cross-sections [203] and the XPS spectra of thorium, uranium and neptunium compounds and CsCl.[55] The procedure used for sample preparation and for recording made it possible to obtain the first spectra of the core and valence electrons for a bulky sample, which was a $Cs_2PuO_2Cl_4$ single crystal. This double salt contains a plutonium ion formally as Pu^{6+} with the electronic configuration $\{Rn\}5f^2$. Therefore, the fine spectral structure of the core and valence levels can be discussed conveniently using this compound as an example.

1. The spectra of valence electrons

The low binding energy XPS spectrum of $Cs_2PuO_2Cl_4$ largely resembles the spectra of isostructural uranium and neptunium compounds (see Figs 26, 31).

a. The spectrum of the Pu5f electrons

Comparison of the An5f spectra of uranium,[47] neptunium,[80] plutonium,[82] the oxides NpO_2 (see Refs 41 and 79) and PuO_2 (see Refs 41, 79 and 84) shows that on passing from uranium to plutonium, the difference between the weight-average An5f binding energy and the OVMO binding energy substantially decreases. This results in a significant overlap of the corresponding lines in the spectra of plutonium compounds (Fig. 32); this increases the error of determination of the relative intensity of the Pu5f lines.

It follows from the spectra of PuO_2 [41, 79, 84] and $Cs_2PuO_2Cl_4$ [82] that an increase in the plutonium oxidation state in compounds entails a decrease in the intensity of the Pu5f line. The magnetic properties of plutonium compounds have not been adequately studied, hence, they cannot be quantitatively correlated with the intensity of the Pu5f lines in the spectra; nevertheless, there exists some qualitative correlation. Thus on passing from the tetravalent plutonium in PuO_2 to hexavalent plutonium in the fluoride PuF_6, the specific molar susceptibility (χ) decreases from 536×10^{-6} to 170×10^{-6} mol^{-1} (see Ref. 251). This is in line with the fact that a decrease in the number of the unbound Pu5f electrons in the molecule induces both a decrease in the intensity of the Pu5f lines and a decrease in the paramagnetic term in the specific magnetic susceptibility of the compound. However, as follows from the data on the An5f line intensity and the published data on the magnetic behaviour of actinide compounds, no direct correlation can be followed between the magnetic moment and the number of unpaired An5f electrons for $n_f > 2$.[252–254]

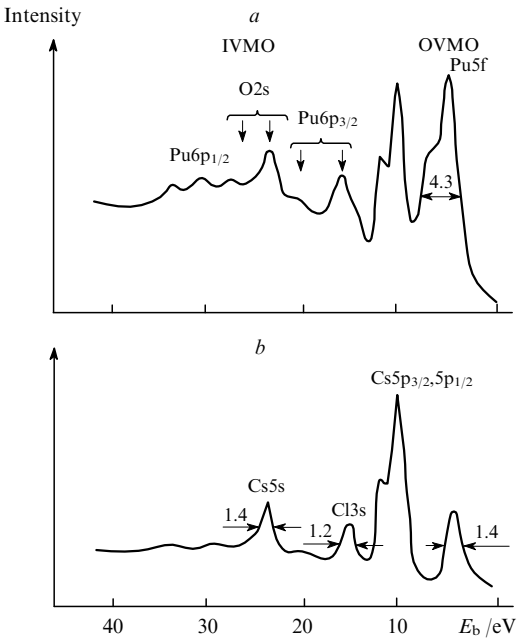


Figure 32. Low energy range of the XPS spectrum of the single crystal of $Cs_2PuO_2Cl_4$ (*a*).[82] For comparison, the XPS spectrum of caesium chloride is given (*b*).

b. The spectra of the Pu6p and O2s electrons

The $Pu6p_{3/2}$ spectrum of $Cs_2PuO_2Cl_4$, like the $An6p_{3/2}$ spectra of $Cs_2AnO_2Cl_4$ (An = U, Np), consists of two lines (see Figs 26, 32). The line characterised by the lower binding energy partially overlaps with the Cl3s line. In the spectrum of the O2s and $Pu6p_{1/2}$ binding energy range, a complex fine structure typical of compounds containing the actinyl group AnO_2^{n+} can be observed, in addition to the Cs5s peak.

Table 14. Binding energy differences (ΔE_i) between various plutonium and oxygen shells.

Compound, element	$E_i = E_k - E_l$ /eV				
	$6p_{3/2} - 6p_{1/2}$	$6p_{3/2} - 4f_{7/2}$	$5d_{5/2} - 4f_{7/2}$	$4f_{7/2} - 4d_{5/2}$	O2s – O1s
$Cs_2PuO_2Cl_4$ (see [82])	–	412.5, 408.2	321.1	374.8	506.5, 508.8
PuO_2 (see [79])	12.2	408.2	321.6	375.2	507.5
Pu_{metal} (see [83])	12.0	403.9	319.8	377.0	
Pu_{theor} (see [178])	11.9	403.8	319.3	379.8	

Comparison of the binding energy differences between the valence and core levels ΔE_i ($Pu6p_{3/2} - Pu4f_{7/2}$) for plutonium and its compounds (Table 14) shows that IVMO are formed effectively from the Pu6p and O2s AO not only in the case of $Cs_2PuO_2Cl_4$, containing the PuO_2^{2+} group, but also for the oxide PuO_2, which has a more symmetric structure. Indeed, the difference between the $Pu4f_{7/2}$ and $Pu6p_{3/2}$ binding energies for plutonium metal equals 403.9 eV. For PuO_2, this value is greater by 4.3 eV, and for the $Cs_2PuO_2Cl_4$ single crystals, these values are greater by 8.6 and 4.3 eV for the two components arising due to IVMO formation in these compounds (see, for example, Figs 4, 23).

These data also provide the conclusion concerning the nature (either bonding or antibonding) of some IVMO. The contribution of the IVMO electrons in the PuO_2^{2+} cluster to the covalent component of chemical bonding estimated on the basis of determination of the orbital forces (f^{α}_{Pu-O} /au) [53] amounts to 22% of the total contribution of the electrons of all MO.[115]

2. The spectra of core electrons of plutonium

The XPS spectra of $Cs_2PuO_2Cl_4$ for all core electron levels in the energy range from ~40 to ~1250 eV exhibit fine structure which is also typical of other plutonium compounds (Figs 33–37). The corresponding binding energies are given in Table 15. In those cases where a complex fine structure is present, instead of the expected single lines, the Table gives the weight average values for the binding energies corresponding to the most intense lines.

On passing from plutonium metal to PuO_2 or $Cs_2PuO_2Cl_4$, the core electron binding energies regularly increase (see Table 15). It can be seen that the core electron energies are correlated with the Pu oxidation states in the compound.

a. The spectrum of Pu4f electrons

The Pu4f spectrum consists of a spin doublet of sharp intense peaks accompanied by satellites on the higher binding energy side (see Fig. 33).

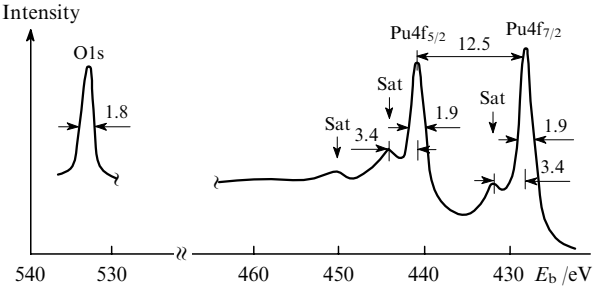


Figure 33. XPS spectra of the single crystal of $Cs_2PuO_2Cl_4$ containing the PuO_2^{2+} group in the Pu4f and O1s binding energy range.[82]

Table 15. Binding energies (E_b) and photoionisation cross-sections (σ) for plutonium compounds.

Orbital Pu, L (nl_j)	E_b /eV					σ [a]
	$Cs_2PuO_2Cl_4$ (see [82])	PuO_2 (see [79])	$Pu(NO_3)_4 \cdot n H_2O$ (see [29])	Pu_{metal} (see [83])	Pu_{theor} (see [178])	
Pu5f	5.0	–	4.1	–	4.7	0.81
OVMO	6.0	–	–			–
$Pu6p_{3/2}$	16.2, 20.5	– 18.4	19.5, 21.3	– 17.2	– 22.7	– 0.38
$Pu6p_{1/2}$	30.4, 33.3	30.6	31.4, 33.9	29.2, 32.0	34.6	0.13
Pu6s	49.0, 54.5	–	–	45.2, 52.7	55.8	0.17
$Pu5d_{5/2}$	107.6	105.0	106.0,	101.3	107.2	3.76
$Pu5d_{3/2}$	117.7	–	112.0, 118.3	113.7	123.0	2.56
$Pu5p_{3/2}$	218.0	216.2	217.4	211.1,	224.6,	2.38,
$Pu5p_{1/2}$	–	–	–	284.2	289.5	0.68
Pu5s	359.2	–	–	353.1, 365.1	359.7	0.76
$Pu4f_{7/2}$	428.7	426.6	427.1	422.1	426.5	31.03
$Pu4f_{5/2}$	441.2	439.8	439.3	435.1	440.3	24.36
$Pu4d_{5/2}$	803.5	801.8	803.9	798.1	806.3	17.81
$Pu4d_{3/2}$	851.7	849.8	852.2	844.8	854.4	11.60
$Pu4p_{3/2}$	1128.9	–	–	1122.6	1131.8	7.95
O2s	24.0, 26.3	22.8	25.8, 27.1			0.14
O1s	532.8	530.3	533.0			2.93
$Cs5p_{3/2}$	10.4 (10.1) [b]					0.33
Cs5s	23.7 (23.4) [b]					0.18
Cl3s	16.1 (15.0) [b]					0.19

[a] Obtained at 1487 eV and expressed in 13.6 b per atomic shell.[203] [b] The electron binding energies for CsCl are given in parentheses.

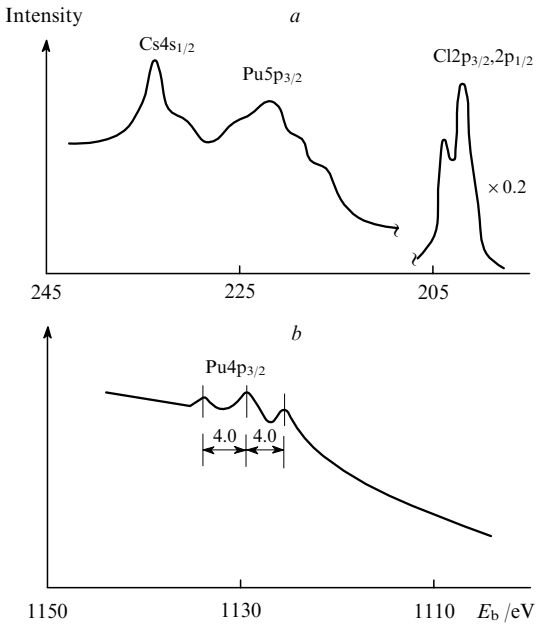


Figure 35. XPS spectra of $Cs_2PuO_2Cl_4$ in the $Pu5p_{3/2}$ (*a*) and $Pu4p_{3/2}$ (*b*) binding energy ranges.[55]

Comparison of the Pu4f lines in the spectra of $Cs_2PuO_2Cl_4$,[82] containing Pu^{6+}, and the dioxide PuO_2,[79] containing Pu^{4+}, shows that the binding energy distance from the basic lines of the doublet to the satellites (ΔE_{Sat}) can characterise, as in the case of uranium and neptunium compounds, the plutonium oxidation state. In the spectra of $Cs_2AnO_2Cl_4$ with An = Pu^{6+}, Np^{6+} and U^{6+}, the ΔE_{Sat} values equal 3.4, 3.5 and 3.8 eV, and the intensities I_{Sat} are 20, 20 and 20%, respectively. In the spectra of AnO_2 for An = Pu^{4+}, Np^{4+} and U^{4+}, the ΔE_{Sat} values amount to ~7,

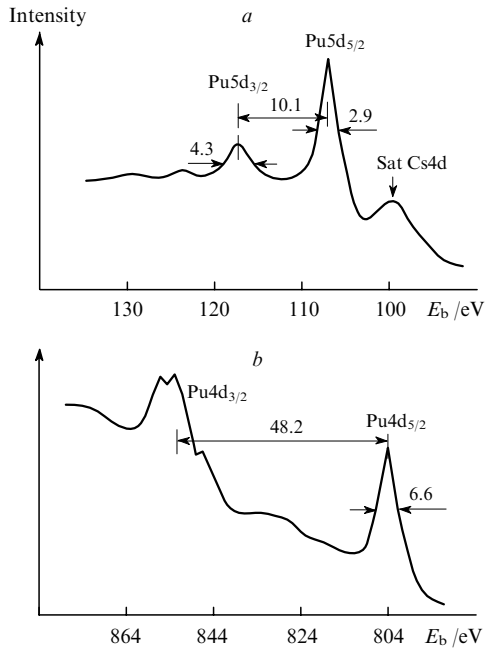


Figure 34. XPS spectra of $Cs_2PuO_2Cl_4$ in the Pu5d (*a*) and Pu4d (*b*) binding energy ranges.[82] A satellite arising on the higher binding energy side of the basic Cs4d line is shown.

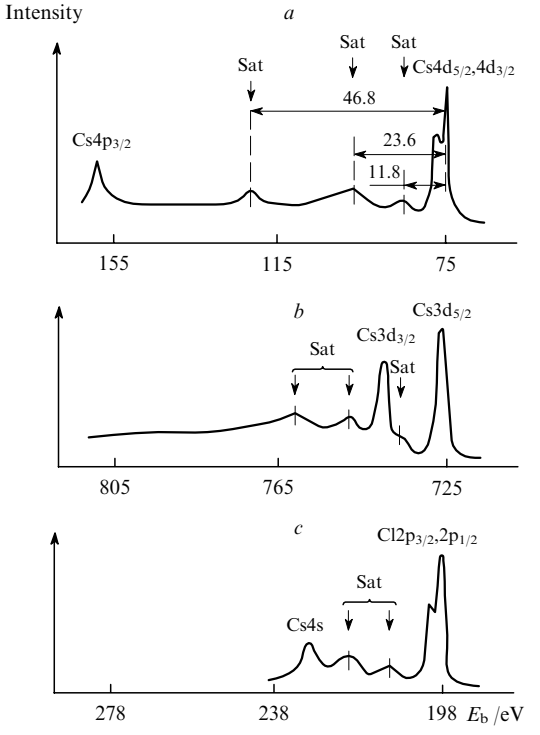


Figure 36. XPS spectra of caesium chloride in the binding energy range of core electrons.[55]
(*a*) $Cs4p_{3/2}$ and Cs4d electrons; (*b*) Cs3d-electrons, (*c*) Cs4s electrons.

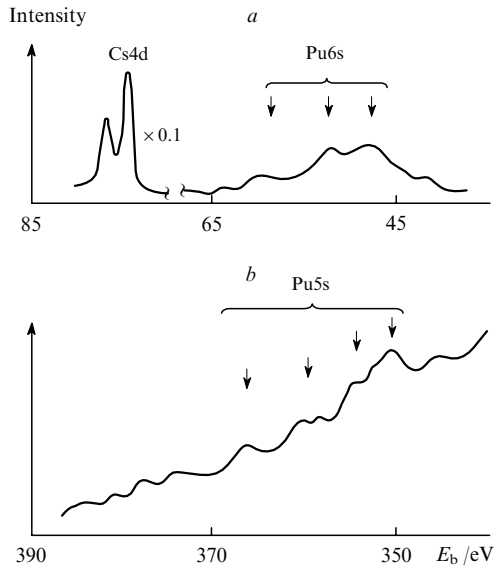


Figure 37. XPS spectra of $Cs_2PuO_2Cl_4$ in the Pu6s (*a*) and Pu5s binding energy ranges (*b*).[55]

~7 and 6.9 eV, while I_{Sat} are ~20, ~17 and 25%, respectively. The spin–orbit splitting ΔE_{sl}(Pu4f) values found by different researchers are 13.0, 12.7 and 12.5 eV for plutonium metal,[83] PuO_2 oxide[79] and $Cs_2PuO_2Cl_4$,[82] respectively. The observed differences in the ΔE_{sl}(Pu4f) values are related to the error of determination (see Table 15).

b. The spectra of Pu5d and Pu4d electrons

In the Pu5d binding energy range (see Fig. 34), an intense band with $E_b \approx 100$ eV due to the satellite of the Cs4d line is observed on the lower binding energy side of the basic $Pu5d_{5/2}$ line. The intensity of the $Pu5d_{3/2}$ component is largely suppressed, and it is broad compared to the basic $Pu5d_{5/2}$ line.

Despite the complicated spectral structure, the $Pu5d_{5/2}$ line can be used to determine the Pu oxidation state in compounds. Thus on passing from plutonium metal to the Pu^{6+} ion, the binding energy of these electrons decreases by $\Delta E_b(Pu5d_{5/2}) = 6.3$ eV (see Table 15). When the plutonium oxidation state changes from Pu^{4+} to Pu^{6+}, the corresponding energy difference is 2.6 eV. For individual compounds, these differences can be easily measured experimentally. The fine structure of the Pu5d spectra can also characterise the plutonium oxidation states in compounds. However, the exact energy of the spin–orbit splitting of the Pu5d line [ΔE_{sl}(Pu5d) = 11 eV][20] is difficult to determine due to the complex shape of this line (see Table 15).

The $Pu4d_{5/2}$ line for $Cs_2PuO_2Cl_4$ (see Fig. 34) is relatively broad ($\Gamma = 6.6$ eV) and symmetric. In the $Pu4d_{3/2}$ binding energy range, fine structure is observed. A structured band, possibly associated with Auger transition electrons, occurs at these energies. Against the background of this structure, a peak attributable to the $Pu4d_{3/2}$ electrons is observed. The spin–orbit splitting ΔE_{sl}(Pu4d) found from this spectrum is 48.2 eV. This coincides with the value $\Delta E'_{sl}$(Pu4d) = 48.2 eV obtained from the PuO_2 spectra,[79] but differs from the value $\Delta E''_{sl}$(Pu4d) = 46.7 eV, found from the spectrum of plutonium metal in the Pu4d binding energy range, by 1.5 eV.[83]

c. The spectra of $Pu5p_{3/2}$ and $Pu4p_{3/2}$ electrons

The Pu5p binding energy range of the XPS spectrum of $Cs_2PuO_2Cl_4$ contains several rather intensive peaks attributed to ligands and carbon atoms of the residual organic substances adsorbed on the surface in vacuum (see Fig. 35). For example, the $Pu5p_{1/2}$ line is superimposed by the C1s spectrum, which precludes drawing conclusions concerning its structure.

The spectra of various ligands have been analysed.[55] In particular, the spectrum of CsCl has been thoroughly studied (see Table 12, Fig. 36). This allowed researchers to identify the structure due to the $Pu5p_{3/2}$ electrons upon comparison of the spectra of $Cs_2PuO_2Cl_4$ and CsCl in the Cl2p and Cs4s binding energy ranges (see Fig. 35).

Comparison of the $Pu5p_{3/2}$ spectral structure for the studied compounds with the An5p spectra of other actinides shows that this structure can be attributed to the dynamic effect resulting in final states of the type $Pu5p^5 5d^{10}(6s^2 6p^6)5f^n \rightleftharpoons Pu5p^6 5d^8.(6s^2 6p^6)5f^{n+1}$. Indeed, the ratio of the Pu5p and Pu5d binding energies does not contradict this assumption. Thus for $Cs_2PuO_2Cl_4$, $E_b(Pu5p_{3/2}) = 218$ eV and $E_b(Pu5d_{5/2}) = 107.6$ eV (see Table 15), which approximately satisfies the condition $E_b(Pu5p_{3/2}) \approx 2\,E_b(Pu5d_{5/2})$.

The structure observed in the $Pu4p_{3/2}$ spectrum largely resembles that observed in the $Pu5p_{3/2}$ spectrum. The binding energies $E_b(Pu4p_{3/2}) = 1128.9$ eV, $E_b(Pu4d_{3/2}) = 851.7$ eV and $E_b(Pu5s) = 359.2$ eV approximately satisfy the condition $E_b(Pu4p) \approx E_b(Pu4d) + E_b(Pu5s)$. This suggests that, as for thorium, uranium and neptunium compounds, in this case, too, the structure observed in the spectrum of $Cs_2PuO_2Cl_4$ in the $Pu4p_{3/2}$ binding energy range may be due to a large extent to the dynamic effect, resulting in the formation of final states of the type $Pu4p^5 4d^{10}(4f^{14})5s^2(5p^6 5d^{10}6s^2 6p^6)5f^n np^m \rightleftharpoons Pu4p^6 4d^9(4f^{14})5s^1.(5p^6 5d^{10}6s^2 6p^6)5f^n np^{m+1}$.

d. The spectra of Pu6s and Pu5s electrons

Instead of the expected single peak for Pu6s electrons, the spectrum exhibits a complicated fine structure in an energy span covering ~30 eV.[55] A number of averaged peaks at 49.0, 54.5, 59.5 and 67.3 eV can be noted. The weight-average binding energy for these electrons E_b – (Pu6s) amounts to 51.2 eV (see Fig. 37).

Probably, the structure of the Pu6s spectrum is mainly due to the dynamic effect giving final states like $Pu6s^1 6p^6 5f^n 6d^m \rightleftharpoons 6s^2 6p^4 5f^n 6d^{m+1}$. Indeed, the values $\overline{E}_b$ (Pu6s) = 51.2 eV, $E_b(Pu6p_{3/2}) = 20.5$ eV and $E_b(Pu6p_{1/2}) = 30.4$ eV obey satisfactorily the condition $\overline{E}_b$ (Pu6s) $\approx 2\,E_b$(Pu6p), which is not at variance with the assumption concerning the dynamic effect. The spectral structure parameters can hardly allow a conclusion about the possible participation of the Pu6s shell in the OVMO and IVMO formation.

The Pu5s spectrum is expected to exhibit a fine structure in the region where the intensity of the C1s satellite corresponding to the carbon atoms of the adsorbed oil declines (see Fig. 37). Indeed, this range in the spectrum of $Cs_2PuO_2Cl_4$ contains peaks at 351.2, 354.9, 358.2 and 365.8 eV (see Fig. 37) for which the weight average binding energy is given by $\overline{E}_b$ (Pu5s) = 359.2 eV (see Table 15).

In the Pu5s binding energy range equal to ~35 eV, the XPS spectrum of Pu metal exhibits two peaks with the width $\Gamma \approx 10$ eV having a fine structure.[83] Hence, it can be suggested that the structure at 351.2 and 354.9 eV ($\Delta E_b = 3.7$ eV) (see Fig. 37) is partially due to the multiplet splitting. It is evident that the pronounced broadening (to ~35 eV) of the Pu5s binding energy range containing fine structure in the spectrum of $Cs_2PuO_2Cl_4$ cannot be attributed to the multiplet splitting alone.

For $Cs_2PuO_2Cl_4$, the binding energies $\overline{E}_b$ (Pu5s) = 359.2 eV, $E_b(Pu5p_{3/2}) = 218.0$ eV and $E_b(Pu5d_{5/2}) = 107.6$ eV satisfy the condition $\overline{E}_b$ (Pu5s) $\approx E_b$(Pu5p) + E_b(Pu5d). Thus, it can be suggested that the structure observed in the Pu5s binding energy range can also be attributed to the dynamic effect with the final states like $Pu5s^1 5p^6 5d^{10}(6s^2 6p^6)5f^n \rightleftharpoons Pu5s^2 5p^5 5d^9(6s^2 6p^6)5f^{n+1}$. The same conclusions have been drawn by other researchers,[83] who analysed the XPS spectral structure for plutonium metal.

It should be noted that, as for compounds of other actinides, this XPS spectral structure can be used to identify particular plutonium compounds.

VI. General rules of the formation of fine structure in the XPS spectra of actinide compounds

The fine structures of the XPS spectra of light actinide compounds have much in common. As noted above, this is due to the fact that actinides form a row of transition elements in which the An5f shell is gradually occupied by electrons with the increase in the atomic number. A complex fine structure is manifested to one or another extent in the XPS spectra of all electronic levels in the binding energy range of 0 – 1250 eV. On the one hand, the reasons for fine structure formation in the spectra of various electron shells of actinide compounds are largely similar, but on the other hand, parameters of the fine spectral structure are characteristic of particular compounds. Thus, the XPS spectral structure of the core and outer electron shells can be used to elucidate the physicochemical properties of actinide compounds. A typical feature of the An6p$_{3/2}$ and An5f valence electrons of actinides is relatively weak dependence of the binding energies (E_b) on the atomic number (Z) compared to analogous dependences for core electrons (Fig. 38). In the series of actinide dioxides, the binding energy for the valence An5f electrons increases by 3.1 eV, that of the An6p$_{3/2}$ electron, by 2.7 eV, and the core An5d$_{5/2}$ binding energy increases by 38.0 eV as the atomic number increases in the range of $90 \leqslant Z \leqslant 98$. The substantial increase in the An6p$_{1/2}$ binding energy is due to enhancement of the spin – orbit splitting ΔE_{sl}(An6p). Indeed, as noted above, the peaks in the An6p$_{3/2}$ and An6p$_{1/2}$ binding energy ranges observed in the spectra of actinide dioxides reflect the inner valence molecular orbitals rather than atomic levels. As a result, the An6p electrons are delocalised and shielded from the core charge, their energy depending only slightly on the atomic number Z. As was to be expected, the An5d, An4f and An4d binding energies of the core levels of actinides (Th, U, Np, Pu, Am, Cm, Bk, Cf), for example, in oxides,[79] increase appreciably with an increase in the atomic number (Table 16).

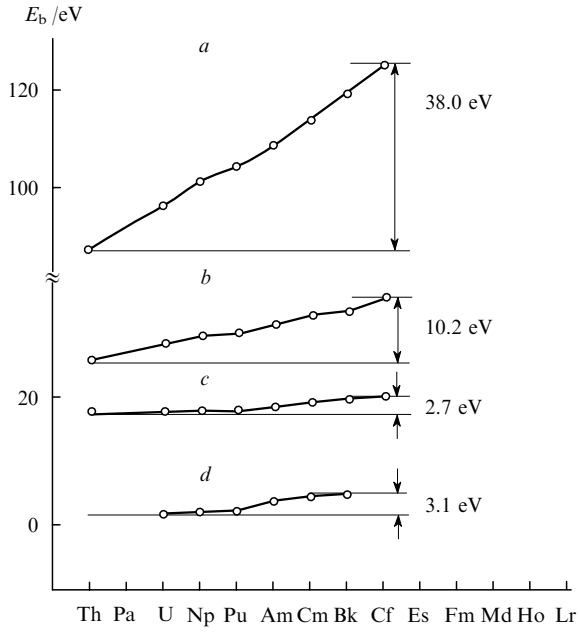


Figure 38. Variation in the binding energies (E_b) of valence and inner electrons in actinide dioxides in the series Th – Lr.[79]
(*a*) An5d$_{5/2}$ electrons; (*b*) An6p$_{1/2}$ electrons; (*c*) An6p$_{3/2}$ electrons; (*d*) An5f electrons.

1. Spectra of the An5f electrons

The An5f electrons not involved in the chemical bond largely determine the magnetic properties of actinide compounds.[143, 255–257] The XPS spectra of compounds containing the An5f electrons exhibit a relatively narrow line around a zero binding energy (Fig. 39). The assumption that this line is due to free An5f electrons based on experimental data [38–40, 67, 68, 87, 127, 197, 252, 253] is consistent with the results of theoretical calculations.[93, 129, 137, 180] In particular, the correlation between the core An4f binding energy and the An5f line intensity observed for uranium and neptunium compounds confirms the assignment of the lines near a zero binding energy in the XPS spectra to the An5f electrons.[81, 88] Indeed, a decrease in the intensity of the line for the An5f electrons not involved in the chemical bond (*i.e.*, a decrease in the relative density of the An5f electrons on the actinide ions) brings about an increase in the actinide oxidation state and, hence, an increase in the core electron binding energies (Fig. 40).

It follows from the above results that the An5f electrons not involved in the chemical bond are largely accumulated on the actinide ions in compounds, and the corresponding orbitals are quasi-atomic (see Fig. 39).

Figure 41 shows that the slopes of the straight lines that reflect the dependence of the relative intensity of the An5f lines on the actinide oxidation state (Table 17) are equal to within the experimental error.[55] This allowed a group of researchers [81, 88–90] to find a general mathematical expression for the dependence of the relative intensity I_{5f}^{exp} on the number n_{5f} of free An5f electrons (Fig. 42).

It can be seen from Figs 41 and 42 that the An5f line intensity in the XPS spectra of the studied actinide compounds in the range of $0 \leqslant n_f \leqslant 7$ is proportional to the number of electrons not involved in the chemical bond. Within the framework of the approximations used, it can be inferred that the oxidation state of actinides changes discretely and that the An^{n+} ions have the electron configuration $\{Rn\}5f^n$.

Table 16. Binding energies (E_b) for core electrons in actinide oxides.[79]

Oxide	E_b /eV										
	6p$_{3/2}$	6p$_{1/2}$	5d$_{5/2}$	5p$_{3/2}$ (see [a])	4f$_{7/2}$	4f$_{5/2}$	4d$_{5/2}$	4d$_{3/2}$	O2s	O1s	C1s
ThO_2	17.2	25.2	87.0	178.9	334.6	343.9	675.7	713.0	22.9	530.5	285.4
UO_2	17.2	28.1	96.0	197.2	379.6	390.5	737.7	780.1	22.5	529.7	284.6
NpO_2	17.5	29.3	100.9	206.3	402.5	414.3	771.2	816.1	23.8	529.7	284.5
PuO_2	18.4	30.6	105.0	216.2	426.6	439.3	801.8	849.8	22.8	530.3	285.3
AmO_2	18.1	31.1	108.4	–	448.2	462.5	832.0	883.1	23.1	529.0	284.4
CmO_2	18.4	32.1	113.2	231.7	472.7	487.4	865.2	918.7	22.7	530.1	284.0
BkO_2	18.3	34.0	120.1	245.8	498.5	514.4	901.4	957.7	23.4	529.5	285.3
Cf_2O_3	19.4	34.9	124.5 [b]	–	523.3	541.1	933.1	993.7	24.7	530.3	283.9
AnO_x									23.2 [c]	529.9 [c]	284.7 [c]

[a] High energy component of the doublet. [b] The highest peak. [c] Average values.

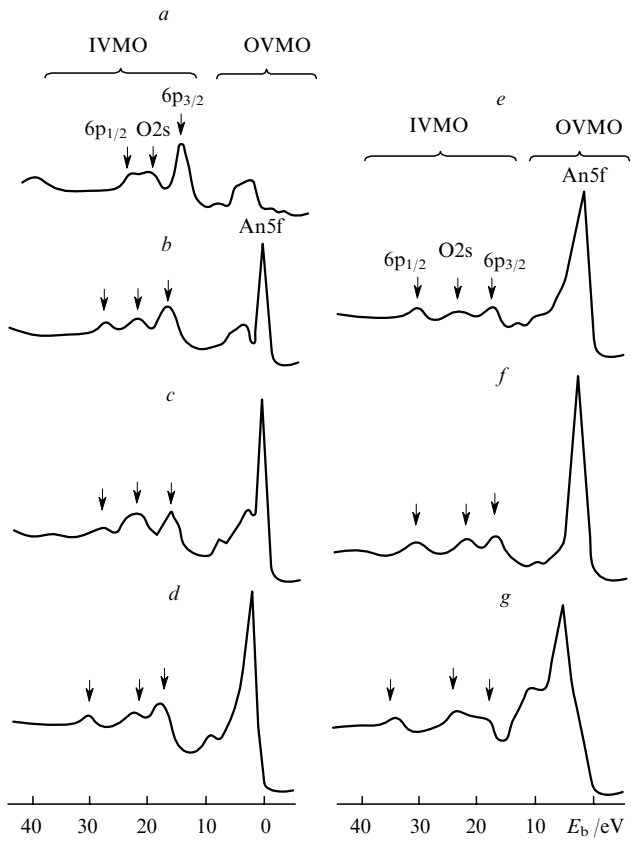


Figure 39. XPS spectra of actinide dioxides (AnO_2) in the low binding energy range.[79]
(*a*) ThO_2, (*b*) UO_2, (*c*) NpO_2, (*d*) PuO_2, (*e*) AmO_2, (*f*) CmO_2, (*g*) BkO_2.

The relative intensity of the An5f line was measured as the ratio of the area confined by the An5f line to the area confined by the $An4f_{7/2}$ line, $I_{5f}^{exp} = I(An5f)/I(An4f_{7/2})$. The satellite lines caused by the shake up process which accompanies the photo-

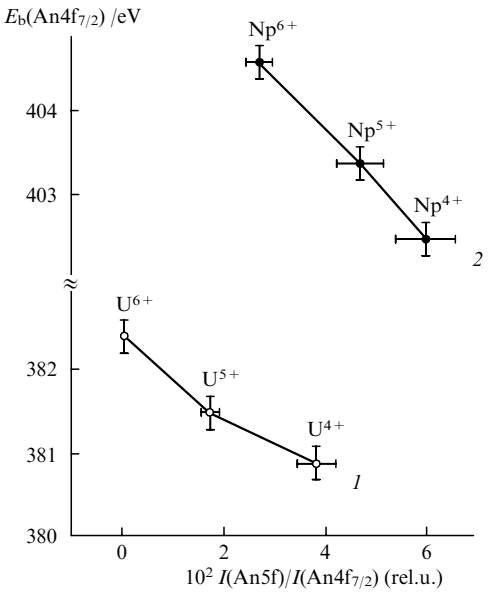


Figure 40. Correlation of the $An4f_{7/2}$ binding energy [$E_b(An4f_{7/2})$] with the relative intensity of the An5f lines [$I(An5f)/I(An4f_{7/2})$] in the XPS spectrum of uranium (*1*) and neptunium compounds (*2*).[81, 88] The dots are experimental data.

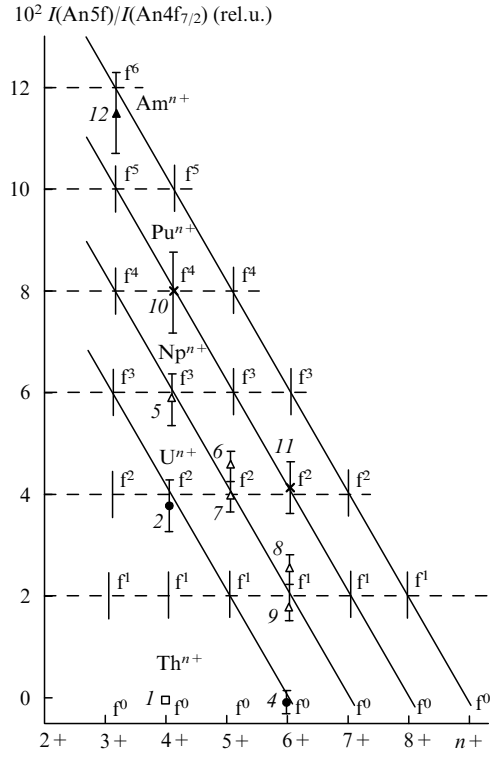


Figure 41. Relative intensity of the An5f lines [$I(An5f)/I(An4f_{7/2})$] in the XPS spectra of actinides (An = Th, U, Np, Pu, Am) *vs*. their oxidation state (n^+) in oxygen-containing compounds of thorium (square), uranium (dark circles), neptunium (light triangles), plutonium (crosses), and americium (dark triangle).[90, 253]
The dots show the experimental data; their numerals correspond to the numbers of compounds in Table 17.

Table 17. Binding energy differences between the An5f levels and OVMO (ΔE_i), relative intensities (I_{5f}^{exp}) of the lines for the An5f electrons not involved in the chemical bond for actinide ions in various oxidation states (An^{n+}).[81]

Compound	ΔE_i[a] /eV	$10^2\, I_{5f}^{exp}$ (red.u.)			n_{5f} (see [b])
		An^{4+}	An^{5+}	An^{6+}	
ThO_2 (**1**)	–	0			0
UO_2 (**2**)	4.2	3.8			2
UO_2 (**3**)[c]	–	3.8			2
γ-UO_3 (**4**)	–			0	0
NpO_2 (**5**)[c]	2.0	5.9			3
$Cs_3NpO_2Cl_4$ (**6**)	2.4		4.6		2
$RbNpO_2(NO_3)_2 \cdot 2H_2O$ (**7**)	2.5		4.0		2
$Cs_2NpO_2Cl_4$ (**8**)	2.0			2.6	1
$NaNpO_2(OAc)_3$ (**9**)	2.5			1.8	1
PuO_2 (**10**)[c]	1.0	8.0			4
$Cs_2PuO_2Cl_4$ (**11**)	1.0			4.2	2
$Am(NO_3)_3 \cdot n\,H_2O$ (**12**)[d]	–				6
AmO_2 (**13**)[c]	0.5	11.6			5
CmO_2 (**14**)[c]	–	12.2			6
BkO_2 (**15**)[c]	–	13.9			7
$Pu(NO_3)_4 \cdot n\,H_2O$ (**16**)	–	8.3			4

[a] Binding energy differences found from the maxima of the An5f lines and OVMO (energy gap). [b] The number of weakly bound An5f electrons. [c] The I_{5f}^{exp} values were found by renormalisation of published data[41, 79] with allowance for the I_{5f}^{exp} value for UO_2 and are expressed in units used in Ref. 81. [d] For An^{3+}, the I_{5f}^{exp} value is 11.5×10^{-2} red.u.

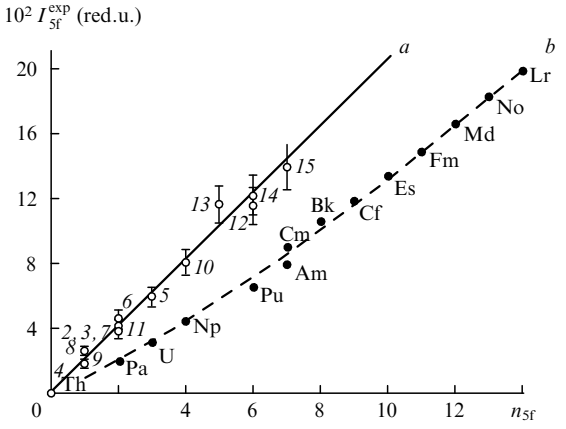


Figure 42. Relative intensity of the An5f lines [$I_{5f}^{exp} = I(An5f)/I(An4f_{7/2})$] in the XPS spectra of actinides and their compounds *vs*. the number of 5f electrons (n_{5f}).[88]
(*a*) Experimental values for actinide compounds (the numerals correspond to the numbers of compounds in Table 17); (*b*) calculated values for actinide atoms.

emission of the An4f electron were not taken into account.[81, 88–90] The area confined by the lines for such satellites can reach 20% of the area corresponding to the basic lines.[90] For example, the OVMO band in the spectra of actinide oxides located in the binding energy range from 0 to ~15 eV is mainly formed by the An5f, An6d and An7s electrons of the actinide and the O2p electrons of oxygen. For the X-ray excitation energy normally used in XPS studies (1486.6 eV), the photoionisation cross-sections (σ) for the O2s and $O2p_{3/2}$ electrons are equal to 0.00191 and 0.000263 Mb, respectively,[258] which is substantially lower than the value $\sigma \approx 0.02$ Mb for the An5f electrons. In addition, the photoionisation cross-sections for the An5f electrons of all actinides are much greater than the corresponding σ value for the $An6d_{3/2}$ (~0.0020 Mb) and An7s electrons (~0.00018 Mb).[258] Therefore, the intensity of the low binding energy XPS spectrum is mainly due to the An5f electrons.

The experimental data for the dependence of the relative intensity of the An5f line on the number of weakly bound electrons reported in several publications [81, 88–90] (see Table 17, Fig. 42) are described satisfactorily by the following equation:[90]

$$I_{5f}^{exp} = 0.0217\, n_{5f}. \qquad (15)$$

Equation (15) was derived with the assumption that the oxidation states of actinides in compounds are integers and the photoionisation cross-section barely depends on the atomic number (Z). This approximation is most adequate for light actinides since the energy gap between the E_b values for weakly bound An5f electrons and OVMO electrons determined from the XPS spectra of these actinides is rather narrow (see Table 17). Physically, this means that the An5f electron involved in chemical bonding passes from the localised state corresponding to a relatively narrow low binding energy XPS line to the delocalised state corresponding to the OVMO band. Despite the roughness of this approximation, the experimental dependence considered (see Fig. 42) can be effectively used for determination of actinide oxidation states in compounds.[90] For example, for AmO_2 (see Table 17, Fig. 42), this dependence suggests that either the oxide Am_2O_3 or another Am^{3+} compound is formed on the sample surface.

In the MO LCAO approximation, during the MO formation in actinide compounds, the An5f electrons can either directly participate in a chemical bond with retention of their nature ($l = 3$, where l is the orbital quantum number) [137] or be first excited, for example, to the An6d level, and participate in the chemical bond having the new d nature ($l = 2$). The relative intensity of the X-ray photoelectron lines of the OVMO electrons (I_{OVMO}^{theor}) in actinide oxides,[81] equal to the ratio of the intensities of the lines due to the OVMO (including An5f) and IVMO (including An6p and O2s orbitals) electrons, was estimated theoretically taking into account the corresponding photoionisation cross-sections [258] according to the equation

$$I_{OVMO}^{theor} = \frac{n_{5f}\sigma_{5f} + n_{6d}\sigma_{6d} + n_{7s}\sigma_{7s} + \nu n_{O2p}\sigma_{O2p}}{n_{6p}\sigma_{6p} + \nu n_{O2s}\sigma_{O2s}}, \qquad (16)$$

where n_{nl} and σ_{nl} are the numbers of electrons and the corresponding photoionisation cross-sections, and ν is the number of oxygen atoms ($\nu = 2$ for AnO_2 and 3 for AnO_3). Since all the considered lines fall in a binding energy range of ~35 eV, no corrections taking into account the binding energy differences between the electrons of different levels were introduced in relation (16).

The I_{OVMO}^{theor} values obtained in this approximation can be compared with the corresponding experimental data for actinide oxides (Table 18). The experimental values of I_{OVMO}^{exp} are presented in Table 18 for the electronic configurations acquired by the actinide ions in those cases where the An5f electrons involved in the chemical bond lose their f nature upon the formation of the bond. Although the error in the measurement of I_{OVMO}^{exp} can reach 20% and An5f and other valence electrons become delocalised upon chemical bonding and their photoionisation cross-sections should decrease, a number of qualitative conclusions have been reported.[81, 87, 88] Indeed, the fact that the I_{OVMO}^{exp} values (0.35 for ThO_2 and 0.72 for γ-UO_3) are substantially greater than the I_{OVMO}^{theor} values (0.20 and 0.30, respectively) can be related to the involvement of the An5f AO in the OVMO formation. As a result, An5f states occupied by electrons are present in the valence band of the oxides, ThO_2 and γ-UO_3; these states are missing, for example, for the thorium atom. This experimental result, although qualitative, is very important and agrees with the data of calculations of the electronic structures of these oxides.[137] It follows from the foregoing that upon the formation of chemical bond in actinide oxides, the An5f electrons can lose the f nature only partially.

In order to evaluate the validity of the assumption of localisation of weakly bound An5f electrons in actinide compounds made on the basis of experimental data, [35, 81, 87, 88] the experimental intensities of the An5f lines were compared with the corre-

Table 18. Theoretical [I_{OVMO}^{theor} (rel.u.)] and experimental [I_{OVMO}^{exp} (rel.u.)] relative intensities of the OVMO line in the XPS spectra for various occupancies of the shells (n_{nl}).[81]

Oxide	n_{5f}	n_{6d}	n_{7s}	I_{OVMO}^{theor}	I_{OVMO}^{exp}
ThO_2	0	2	2	0.20	0.35
UO_2	3	1	2	1.15	–
	2	2	2	0.87	1.03
γ-UO_3	3	1	2	1.01	–
	2	2	2	0.77	–
	1	3	2	0.52	–
	0	4	2	0.30	0.72
NpO_2	4	1	2	1.63	–
	3	2	2	1.30	1.38
	2	3	2	0.99	–
PuO_2	6	0	2	2.39	–
	5	1	2	2.06	–
	4	2	2	1.73	1.73
AmO_2	7	0	2	3.05	–
	6	1	2	2.71	–
	5	2	2	2.33	2.34
CmO_2	7	1	2	3.41	–
	6	2	2	3.03	2.45
BkO_2	9	0	2	4.57	–
	8	1	2	4.14	–
	7	2	2	3.72	2.75

sponding theoretical values determined from the photoionisation cross-sections of these electrons with allowance for the influence of spectroscopic and other factors on the An5f line intensity (see Fig. 42). The question of why the experimental dependence [see Fig. 42, Eqn (15)] is approximately linear was considered.

The dependences of the photoionisation cross-section $\sigma(An4f_{7/2})$ and $\sigma(An5f)$ on the number of An5f electrons n_{5f} (see Refs 53, 81) are shown in Fig. 43. It can be seen that these dependences are not linear. However, the variation of the $\sigma(An5f)/\sigma(An4f_{7/2})$ ratio as a function of n_{5f} is described by a smoother curve and, to a certain approximation, it can be regarded as linear. This explains qualitatively the course of the corresponding experimental dependence (see Fig. 42). However, the calculated $\sigma(An5f)/\sigma(An4f_{7/2})$ values are much smaller than the experimental values derived from the intensities of spectral lines.

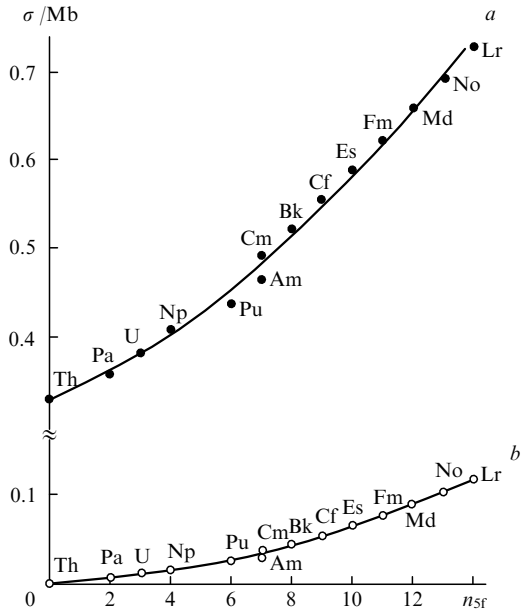


Figure 43. Photoionisation cross-sections (σ) for $An4f_{7/2}$ (*a*) and An5f shells (*b*) of actinide atoms *vs.* the number of An5f electrons (n_{5f}). The calculations were carried out in the Dirac – Fock approximation with precise calculation of the exchange integral.[35,81]

The theoretical values of the relative intensity I_{5f}^{theor} calculated using full photoionisation cross-sections and spectroscopic and other factors[81,88] for the basic configurations of actinide atoms are given in Fig. 42 in comparison with the corresponding experimental data. This comparison is qualitative, because the theoretical dependence was constructed without taking into account the participation of actinide atoms in the chemical bond. Nevertheless, it follows from Fig. 42 that the overall pattern of the theoretical curve following the increase in the number of An5f electrons is in qualitative agreement with experimental data.

The experimental relative intensity $I_{5f}^{exp} = I(An5f)/I(An4f_{7/2})$ of the An5f line was used[35] to estimate the non-formal number of these electrons (n_{5f}) in actinide ions. This was done according to the equation

$$n_{5f} = I_{5f}^{exp}\frac{f_{4f}n_{4f}\sigma'_{4f}\lambda_{4f}[1-\beta_{4f}(0.75\cos^2\theta-0.25)]F_{4f}}{f_{5f}\sigma'_{5f}\lambda_{5f}[1-\beta_{5f}(0.75\cos^2\theta-0.25)]F_{5f}}, \qquad (17)$$

where f is the spectroscopic factor, σ'_{nf} is the photoionisation cross-section per electron, λ is the electron free path, β is the asymmetry parameter, θ is the angle between the non-polarised radiation and the photoelectron escape (in this case, $\theta = 90°$), F is the transmittance of the analyser. Only the $An4f_{7/2}$ shell was considered, therefore the subscript 7/2 is omitted. The spectroscopic factor (the fraction of the basic peak without inclusion of satellites) has been calculated.[35]

It was shown[35] that for a neptunium oxidation state of 4+ the number of the Np5f electrons, equal to 4.25, differs little from the number of these electrons for the free atom. For pentavalent neptunium, the number of Np5f electrons is approximately 3, while for hexavalent neptunium, it is between 1 and 2. For UO_2, these data are consistent with the results presented in Table 18. Indeed, the value $I_{OVMO}^{exp} = 1.03$ for UO_2 corresponds to an n_{5f} value ranging from 2 to 3 (see Table 18). The data for other oxides indicate that the An5f orbitals take a significant part in chemical bonding.

Thus, for analysis of the electronic structure and quantitative ionic composition of actinides and for determination of actinide oxidation states in compounds, important information can be gained from the XPS spectral parameters for the An5f binding range. The quantitative correlation found between the relative intensity of the line for the weakly bound An5f electrons and the actinide oxidation state (U, Np, Pu, Am, Cm, Bk) in compounds is used to determine the ionic composition of actinides. The fact that the An5f electrons can directly participate in chemical bond formation is in line with the data of resonance X-ray $O_{4,5}$(U) emission spectra of uranium oxides measured using synchrotron radiation.[259–261] On the basis of chemical shifts of the X-ray $L_{\alpha1}$, $L_{\beta2,4}$, $L_{\beta1,5}$ and $L_{\gamma1}$ emission spectra, the conclusion about the existence of bound Th5f states in thorium oxide and halides has also been drawn.[262]

Despite the scantiness of the information on the magnetic behaviour of actinide compounds, a number of conclusions have been reached[44,89,90] from comparison of the data on their magnetic moments and magnetic susceptibilities with XPS data. During filling of the An5f shell in uranium and neptunium compounds, no direct proportionality between the effective magnetic moment (μ_{eff}) and the An5f line intensity can be followed (Fig. 44). The curve shown in the Figure is in good agreement with the dependence of molar magnetic susceptibility on the number of the Np5f electrons obtained previously.[254] The magnetic susceptibility data for the Pu^{4+} and Pu^{3+} ions also indicate that further filling of the An5f shell ($n_{5f} = 4, 5$) should entail a decrease in the

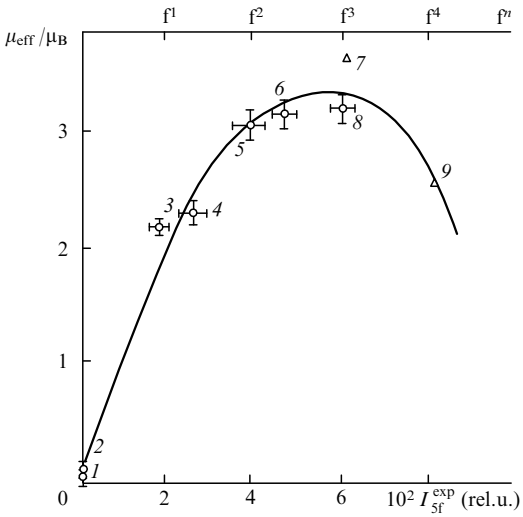


Figure 44. Relationship between the effective magnetic moments (μ_{eff}) of actinide compounds and relative intensity (I_{5f}^{exp}) of the XPS line for unbound An5f electrons.[89,90,253]
The μ_{eff} values were taken from Refs 211 and 251 (light circles) and from Ref. 263 (triangles). (*1*) ThO_2, (*2*) γ-UO_3, (*3*) $NaNpO_2(OAc)_3$, (*4*) $Cs_2NpO_2Cl_4$, (*5*) UO_2, (*6*) $Cs_3NpO_2Cl_4$, (*7*) $U(HCO_2)_3$, (*8*) NpO_2, (*9*) $Np(HCO_2)_3$. For $U(HCO_2)_3$ and $Np(HCO_2)_3$, the I_{5f}^{exp} values were not measured.

magnetic moment.[98, 254, 263] These results attest to a complex pattern of the influence of unbound An5f electrons on the magnetic properties of actinide compounds. Many problems are still to be solved in this field.

2. The spectra of the An6p and O2s, L*n*s electrons

Th comparison of binding energy differences between the core and valence electron levels of metals and compounds used in a number of studies [53–55] allowed the researchers to elucidate legitimately the MO structure, to construct the MO diagrams and to estimate the degree of participation of the low-energy occupied An6p and O2s L*n*s AO of the neighbouring atoms in the formation of the IVMO in actinide compounds. This approach provides the possibility of estimating the effect of IVMO formation not only in asymmetric actinide compounds containing AnO_2^{n+} actinyl groups, but also in highly symmetric compounds like AnO_2 (AnO_8^{12-}, O_h group of symmetry), whose XPS spectra exhibit less pronounced IVMO structure in the low energy XPS range. For example, the splitting between bonding and antibonding IVMO in uranium compounds can reach 15 eV,[109] which is comparable with the energy difference between IVMO in the nitrogen molecule (18.7 eV).[19] The method of 'differences' can also be used to evaluate the nature (bonding, antibonding or non-bonding) of individual IVMO, which is important for comparison with the results of calculations of the contribution of IVMO electrons to chemical binding. The use of this method, with allowance for the data of theoretical calculations of the electron structure, allows one to identify the IVMO structure based on the low binding energy XPS spectra and to correlate the parameters of this structure with the structure of the local environment of the actinide ion in the compound. The distances from the actinide to the nearest ligand atoms can often be estimated experimentally. For amorphous compounds, these data can hardly be obtained by X-ray diffraction.

Theoretical estimates have shown [52, 102, 115, 226] that the contribution of the IVMO electrons to the energy of chemical bonds in the AnO_2^{2+} clusters (An = U, Np, Pu) is approximately 25% of the contribution of the electrons from all MO. The experimental data on the natures of various IVMO do not contradict qualitatively these results. The XPS data on the OVMO and IVMO structures in actinide compounds are qualitatively in line with the results of non-relativistic X_α-DV calculation of the electronic structure of the $[UO_2F_5]^{3-}$ cluster (D_{5h} group of symmetry) [264] and relativistic X_α-DV calculation for the UF_6, NpF_6, PuF_6,[265] UF_6 [266–268] and $UO_2(NO_3)_2 \cdot 2H_2O$ [204, 269] molecules as well as with the data of X-ray emission,[100, 182, 185, 186, 188, 234, 246, 247, 259] Auger,[235, 236] X-ray absorption,[189, 191, 270] conversion electron spectroscopy,[218–221] *etc*.

3. The role of the An6p and An5f electrons in the formation of chemical bond

Since the XPS spectra of actinide compounds together with the ionisation cross-sections reflect the total valence electron density in a binding energy range of 0–50 eV, additional information for determination of the partial density, for example, of the An6p and An5f states, can be derived from other X-ray spectral methods.

While examining the XPS spectra of actinides, it has been noted [53, 55, 103, 104] that the lines observed in the low binding energy range (E_b = 0–50 eV) are usually several electron-volt wide, being often wider than the lines for deeper core electrons.[53, 55] For example, in the case of UO_2, the FWHM (Γ) of the O1s line (E_b = 531.4 eV) amounts to 1.6 eV, whereas the width of the O2s line ($E_b \sim 23.3$ eV) exceeds 4 eV, and this line is structured.[66] In conformity with the uncertainty principle $\Delta E \Delta\tau \sim h/2\pi$ (h is Planck's constant), the natural width (ΔE) of the level from which the photoelectron has been removed is inversely proportional to the hole lifetime ($\Delta\tau$) of the ion formed. Since the hole lifetime decreases as the absolute binding energy increases, the width of the XPS lines for some atoms is expected to decrease rather than increase, as is really the case in experiments (see, for example, Figs 8, 19). This served as the main reason for the thorough investigation of the spectral structure for actinide compounds in this energy range.[53, 55, 103, 104] It was found that, among other reasons, line broadening in the low energy range (0–50 eV) of the XPS spectra is due to the formation of OVMO and IVMO in actinide compounds (see, for example, the studies [51–55]). These spectra reflect the band structure and are observed as several electron-volt wide lines. In particular, in uranium compounds, the IVMO arise due to the significant overlap of the U6p and L(O,F,Cl)*n*s shells of neighbouring atoms and ligands.

Yet another important aspect vigorously studied in recent years is efficient participation of the An5f shell in the OVMO formation. Previously, it has been traditionally assumed that prior to chemical bonding, the An5f electrons are excited to, for example, the An6d AO. However, the calculation results show that the An5f shells can be directly involved in the formation of MO in actinide compounds.[129, 228] This basically important fact requires experimental corroboration.[81, 88] The commensurability of experimental and theoretical values for the partial density of the An5f and An6p electrons of actinide compounds can serve as a criterion for the consistency of calculations.

As an example of the information on the An6p and An5f electronic states of actinides that can be gained from X-ray spectral and theoretical data, we shall consider the results obtained for uranium trioxide. In particular, the fine structure of the low binding energy range of the XPS spectrum of uranium trioxide has been analysed taking into account the results of calculations of the electronic structure of the $[UO_2O_4]^{6-}$ cluster (D_{4h} group of symmetry) reflecting the local environment of the uranium atom in γ-UO_3 (first carried out in the relativistic X_α-DV approximation).[110, 123, 271] The fine structure of the X-ray $O_{4,5}$(U) emission spectrum of γ-UO_3, reflecting the partial densities of the U6p and U5f electronic states in the valence band, has been studied for the first time.[185, 234]

As noted above, the low energy range (0–40 eV) of the XPS spectrum of uranium trioxide can be divided conventionally into two parts (Fig. 45). The first part (0–13 eV) exhibits a structure caused by the OVMO, which are mainly formed from partially occupied outer valence U5f, U6d, U7s and O2p AO of neighbouring atoms. The fine structure observed in the second part of the spectrum (13–40 eV) is due to the IVMO, which mainly arise due to the substantial interaction of the electrons from completely occupied valence U6p and O2s AO of the neighbouring atoms. The OVMO spectral structure has three characteristic features and can be divided into three components. Eight clear-cut peaks can be observed in the IVMO range, and eight components can be distnguished (see Fig. 45). Despite the formalism of such subdivision, it allows one to perform qualitative and quantitative comparison of parameters of the XPS spectrum with the corresponding parameters of the X-ray O4,5(U) emission, Auger and other spectra and with the results of relativistic calculations for the electronic structure of the $[UO_2O4]^{6-}$ cluster (D_{4h} symmetry group).

The intensity of the OVMO band was found to contain a contribution of the outer valence U5f, U6d and O2p AO and a substantial contribution of the inner valence U6p AO of neighbouring atoms. Experimental evidence for the direct participation of the U5f electrons in the chemical bonding with partial loss of their f nature has been obtained. Indeed, the experimental intensity ratio of the OVMO and IVMO bands is 0.70,[81] which is comparable with the theoretical value (0.93).[123] Since the U5f AO almost does not participate in the formation of the IVMO, the difference between these values may be due to the decrease in the photoionisation cross-section of the U5f electrons involved in chemical bonding. However, if the intensity of the OVMO band in uranium trioxide is assumed to be formed only by the $U6d^47s^2$ and $3O^2p^4$ electrons, and the IVMO intensity, by $U6p^6$ and $3O2s^2$ electrons, the corresponding theoretical value would have been 0.30 (see Table 18), which is significantly smaller than the

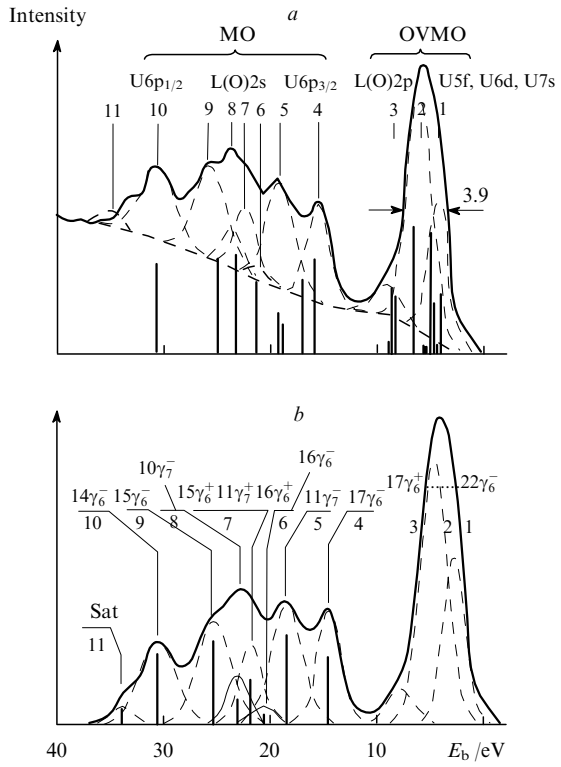


Figure 45. X-Ray photoelectron spectrum of γ-UO_3 with (*a*) and without (*b*) the background. The dashed lines show the spectral pattern of the subtracted background and thin lines show the conventional decomposition of the spectrum into components. The vertical segments in Fig. 45 *a* are the results of relativistic X_α-DV calculation for the $[UO_2O_4]^{6-}$ cluster (D_{4h} symmetry);[123] the vertical segments in Fig. 45 *b* show the expected correct spectrum simulated with allowance for calculations and experimental data;[110] $n\gamma_i^+$ and $n\gamma_i^-$ are designations of molecular orbitals; the digits are the numbers of peaks.

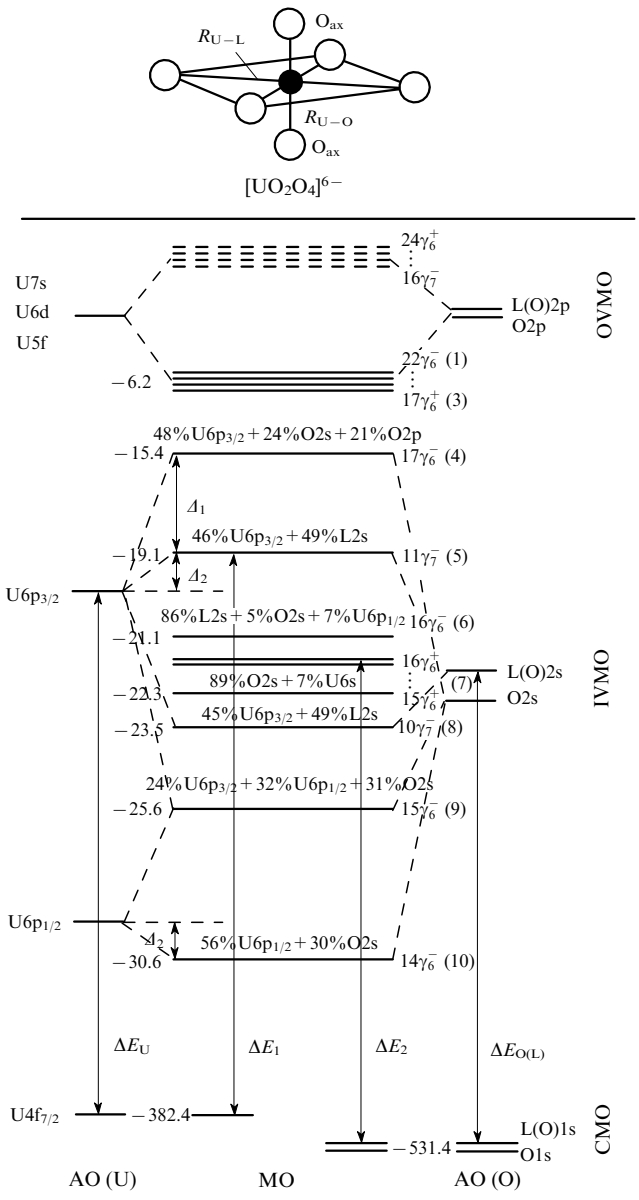


Figure 46. Diagram of MO energy levels in the $[UO_2O_4]^{6-}$ cluster (D_{4h} symmetry) constructed with allowance for calculations and experimental data.[271]
The chemical shifts of the energy levels upon the formation of the cluster from single atoms are not shown. The arrows show the energy differences that can be measured experimentally. The digits on the left are experimental E_b values, eV (the energy scale is not maintained).

experimental value.[81] This contradicts the traditional view that, before being involved in chemical bonding, the U5f electrons are excited to the U6d shell. Thus, the results of the relativistic calculation reflect rather reliably the partial electron density of the U5f states (see Fig. 45). This means that about two U5f electrons participate directly in the chemical bond, while the vacant U5f states are located in an energy range of 6 eV near the absorption edge.[123] This is in qualitative agreement with the X-ray $O_{4,5}$(U) emission spectroscopy [185] and X-ray near-edge $O_{4,5}$(U) absorption spectroscopy data for uranium trioxide.[189, 270]

In the IVMO binding energy range, the best agreement has been obtained for the $17\gamma_6^-$, $15\gamma_6^-$ and $14\gamma_6^-$ orbitals characterising the width of the spectrum of these electrons. Since the theoretical and experimental total relative intensities are comparable, the calculated energies of the $11\gamma_7^-$ – $10\gamma_7^-$ IVMO (see Fig. 45) may differ appreciably from the corresponding experimental values.

Using the data of relativistic calculations for the $[UO_2O_4]^{6-}$ cluster (D_{4h} group of symmetry) and experimental binding energy differences between the core and outer electron levels of uranium [57] and for uranium trioxide (see, for example, the studies [55, 109]), an MO diagram has been constructed in the MO LCAO approximation (Fig. 46).[123] This diagram provides understanding of the real XPS structure of uranium trioxide. In this approximation, one can distinguish conventionally the $17\gamma_6^-$ (4), $15\gamma_6^-$ (9) and $14\gamma_6^-$ (10) IVMO, which characterise the U – O bond length in the UO_2^{2+}; the $11\gamma_7^-$ (5) and $10\gamma_7^-$ (8) IVMO which characterise the U – L bond and its length in the equatorial plane of the cluster and the quasiatomic $16\gamma_6^-$ (6), $16\gamma_6^+$ (7), $11\gamma_7^+$ (7) and $15\gamma_6^+$ (7) orbitals formed from the O(L)2s AO of two types of oxygen atoms (O and L). Note that this separation of the IVMO has been experimentally substantiated.[55, 109] It follows from the experimental data that the energies of the quasi-atomic $16\gamma_6^-$ (6) – $15\gamma_6^+$ (7) IVMO should be similar to each other. Indeed, it follows from the parameters of the XPS spectrum of γ-UO_3 in the O1s binding energy range that the difference between the E_b values for these orbitals should not exceed 0.9 eV, as this line is asymmetric and its FWHM (Γ) equals 2.2 eV. The binding energy should be approximately 23.4 eV, because $\Delta E_{L,O}$ = 508 eV and the O1s binding energy for γ-UO_3 is 531.4 eV (see Fig. 46). In view of the fact that ΔE_U = 360.6 eV and ΔE_1 = 363.0 eV, one can find Δ_2 = 2.4 eV and Δ_1 = 3.7 eV.[55] Since the binding energy difference between the $14\gamma_6^-$ (10) and $17\gamma_6^-$ (4) IVMO equals 15.2 eV and the U6p spin – orbit splitting in the atom is given by ΔE_{sl}(U6p) = 10.0 eV,[57] it is possible to estimate the perturbation Δ_3 = 2.6 eV (*i.e.*, it is comparable with the value Δ_2 = 2.4 eV). These data led to the conclusion [123] that the contribution of U6p to the $11\gamma_7^-$ (5) and

$14\gamma_6^-$ (10) IVMO should be markedly higher, while that to the $10\gamma_7^-$(8) IVMO should be much lower than its contribution to the$17\gamma_6^-$ (4) IVMO. As expected, the width of lines corresponding to quasi-atomic orbitals, $16\gamma_6^-$ (6) – $15\gamma_6^+$ (7) is smaller than the corresponding values for other IVMO. The observed relative reduction of the $17\gamma_6^-$ (4) IVMO line width can be attributed to the partial loss of the antibonding nature of this MO resulting from a significant admixture of O2p AO (21%).[53]

It is noteworthy that a stricter comparison of the theoretical and experimental electron binding energies requires resorting to values calculated [272] for the transition state.

For qualitative and quantitative comparative analysis of the experimental and theoretical intensities of spectral lines, the spectra were decomposed into components with allowance for the data given in Fig. 46. The electron binding energies were derived from experiments, while the theoretical intensities were calculated. The results of identification of the XPS spectral structure are shown in Fig. 45. However, experimental IVMO intensities often differ significantly from the corresponding theoretical values. The closest agreement is observed for the electrons of the $17\gamma_6^-$ (4), $16\gamma_6^-$ (6) and $14\gamma_6^-$ (10) IVMO. It has been found[123] that $\sim$1.3 U6p electrons (mainly, the U6p$_{3/2}$ electrons) are involved in the formation of the OVMO. This is comparable with the theoretical value, equal to 1.0 e. Similar agreement is observed in some cases for the IVMO energy range. For example, the antibonding $17\gamma_6^-$ (4) IVMO contains 0.8 U6p$_{3/2}$ electrons, which does not differ much from the calculated value equal to 0.98 e. Similar agreement is observed for the bonding $14\gamma_6^-$ (10) IVMO. For the antibonding $11\gamma_7^-$ (5) and the corresponding bonding $10\gamma_7^-$ (8) IVMO, the calculated overlap of the U6p and O2s AO is approximately twice as great as the experimental value.

Since the pattern of variation of line intensities in the XPS spectra upon the change in the MO energy levels is known from quantum mechanics, it is possible to discuss whether the experimental and theoretical results agree with each other. As has been shown previously,[53, 55] the greater the participation (bonding or antibonding) of AO in the MO formation, the wider the MO lines. The sharpest lines are those corresponding to non-bonding or quasi-atomic MO. Therefore, the relatively small width of the $17\gamma_6^-$ (4) IVMO line can be attributed, as noted above, to the substantial content of the O2p AO in this MO, which also results in a significant decrease in its intensity and the loss of the antibonding nature (see Fig. 46). The observed discrepancy in the intensities of the $11\gamma_7^-$ (5) IVMO lines confirms the assumption that the degree of participation of the U6p AO in this MO is about twice as high as that in the $17\gamma_6^-$ (4) IVMO. The degree of participation of the U6p state in the corresponding bonding $10\gamma_7^-$ (8) IVMO is approximately the same. Unfortunately, it is difficult to determine reliably the line width corresponding to the $10\gamma_7^-$ (8) IVMO electrons.

The energy region of the $16\gamma_6^-$ (6) – $10\gamma_7^-$ (8) IVMO is most ambiguous for interpretation. As can be seen, the structure of this spectral range is mainly due to the O(L)2s electrons, which agrees with the results of calculations. However, the overlap of the uranium U6p AO with the oxygen L2s MO, which occurs in the equatorial plane upon the formation of the $11\gamma_7^-$ (5) and $10\gamma_7^-$ (8) IVMO, was apparently overestimated in the calculations; this resulted in a wrong order of the $16\gamma_6^-$ (6) – $10\gamma_7^-$ (8) IVMO. This may be due to the fact that the distances between the uranium and oxygen atoms in the equatorial plane used in the calculation of the $[UO_2O_4]^{6-}$ cluster were understated compared to the real values. In view of the foregoing, this spectral range has been decomposed.[123] The correct order of the IVMO is especially important for elucidation of their contribution to the covalent component of the chemical bond in uranium trioxide. The peak (11) observed in the spectrum (see Fig. 45) is apparently due to the shake up process which accompanies the emission of electrons from the sample. The expected theoretical spectrum is shown in Fig. 45 *b* by vertical segments.

In conclusion, we would like to note that, despite a number of approximations used in the calculation of the electronic structure of the $[UO_2O_4]^{6-}$ cluster, which models the nearest environment of uranium in γ-UO_3, the results obtained agree qualitatively with experimental data. This allowed the first reliable identification of a series of lines, at least, the upper and lower IVMO lines. These data can be used, in particular, to determine the structures and bond lengths in uranyl compounds [55, 109] and to interpret the structures of other X-ray spectra of uranium compounds. Since the electronic structures of actinide compounds are fairly similar, the results can be used for qualitative discussions of the electronic structures of compounds of not only uranium but also other actinides.

4. Parameters of the fine spectral structure of core electrons

Analysis of the fine XPS structure of the core electron shells of actinide compounds ($\sim$40 – 1250 eV) has shown that there exist general regularities of the formation of such structure and that its parameters depend on the physicochemical properties of compounds. For some actinide compounds, the fine structure parameters are characteristic and can be used for identification. For example, within the error of measurement, the spin – orbit splitting (ΔE_{sl}) of lines corresponding to the core electron levels of actinides does not change on passing from one compound to another. The observed apparent differences between the ΔE_{sl} values for actinides contained in various compounds are related, most often, to multiplet splitting and dynamic effect.

It was found that shake up satellites arise in the spectra of all electronic levels accessible for measurements, their intensity decreasing with a decrease in the electron binding energy. The parameters of these satellites were found to be correlated with the actinide oxidation state and the ionic – covalent nature of the bond.

For all actinide compounds studied, the structure of the An4f spectra is very sensitive to changes in the stoichiometric composition, the structure parameters being correlated with the oxidation state of the central actinide ion. Thus, the distance (along the energy scale) from the basic lines of the An4f doublet to the satellites related to many-body perturbation (ΔE_{Sat}) for An^{6+} lies in the range of 3 – 4 eV, while that for An^{4+} is 7 eV.

The An5d spectra of actinide compounds containing unpaired An5f electrons exhibit multiplet splitting, resulting in a substantial broadening of the An5d$_{3/2}$ line relative to the An5d$_{5/2}$ component of the doublet.

The XPS fine structure caused by the dynamic effect is most clear-cut for electrons whose binding energies are in a certain ratio to the binding energies of electrons less involved in the bonding, so that the energy conservation law and the selection rules hold. In particular, the dynamic effect results in substantial spreading of the An5s and An6s spectral lines; as a consequence, the An6s spectral structure covers a range of $\sim$40 eV. The intensity of the high binding energy component related to the An5p$_{1/2}$ electrons is strongly suppressed, and the An5p$_{3/2}$ component exhibits a complex fine structure. In all cases, fine structure is present in the An4p$_{3/2}$ spectra. It was shown experimentally that the structure in the XPS spectra of actinide compounds in the An4p, An5s, An5p and An6s binding energy range is mainly due to interaction of final state configurations of the type $An4p^54d^{10}(4f^{14})5s^2(5p^65d^{10}6s^26p^6)\ 5f^np^m \rightleftharpoons An4p^64d^9(4f^{14})5s^1.(5p^65d^{10}6s^26p^6)5f^np^{m+1}$; $An5s^15p^65d^{10}(6s^26p^6)5f^n \rightleftharpoons An5s^25p^5.5d^9(6s^26p^6)5f^{n+1}$; $An5p^55d^{10}(6s^26p^6)5f^n \rightleftharpoons An5p^65d^8(6s^26p^6).5f^{n+1}$; and $An6s^16p^65f^n \rightleftharpoons An6s^26p^45f^n6d^1$, respectively.

X-Ray photoelectron studies of the properties of actinide compounds and the nature of the chemical bond in them have provided a number of interesting results. It should also be noted that in recent years, X-ray photoelectron spectroscopy has been used more and more extensively for ecological studies to determine the physical and chemical state of radionuclides in the environment (see, for example, a series of studies [262, 273 – 276]).

VII. Conclusion

Thus, we have shown that knowledge of the parameters of fine XPS structure, together with the traditional information (line intensities and chemical shifts) significantly extends the potential of the XPS method for diverse studies in solid state physics and theoretical and physical chemistry, in particular, studies of the electronic structure and properties of actinide compounds and the nature of the chemical bond in them. The mechanisms of formation of this fine structure have been analysed using compounds with well-known properties. The understanding of the nature of the fine structure provides new information on the physicochemical properties of actinide compounds and the ions they contain. The three questions stated in the Introduction can be answered in the following way.

1. The XPS spectra of compounds of light actinides (Th, U, Np, Pu, Am, Cm, Bk, Cf) exhibit a complex fine structure for almost all electron shells in the energy range of 0 – 1250 eV. This structure may be due to many reasons, in particular, the formation of inner and outer valence molecular orbitals; multiplet splitting; spin – orbit splitting; splitting due to the induced charge; dynamic effect; many-body perturbation; overlap with the Auger spectral lines; the presence of actinide ions in different oxidation states and so on. General regularities of the formation of the fine spectral structure can be followed for particular electron shells.

2. It was found experimentally that particular mechanisms of fine structure formation are manifested in the spectra of different electron shells with different probabilities. This made it possible to establish qualitative and quantitative correlations of structure parameters with the physical and chemical properties of actinide compounds. For example, the line intensity around a zero binding energy is proportional to the number of An5f electrons not involved in the chemical bond. The structure of the low binding energy spectral range (0 – 50 eV) reflects the degree of participation of the An6p and An5f shells in the formation of outer and inner valence molecular orbitals, the nature and the sequence of these orbitals and the structure of the local environment of the actinide ion. The multiplet splitting of the core levels characterises the number of unpaired electrons in the compound. The spectral structures caused by the dynamic effect and many-body perturbation reflect the secondary many-body processes that accompany electron photoemission and the configuration of the final states of the electronic system.

3. The fine structure parameters of the spectra of actinide compounds can be used to determine the degree of delocalisation of the An5f electrons; the degree of their participation in the chemical bond; the electron configuration and oxidation state of the metal atom in these compounds; the density of unpaired electrons on paramagnetic ions; the degree of participation of the low-energy occupied An6p and L*n*s shells of neighbouring actinide atoms and ligand atoms in the formation of outer and inner valence molecular orbitals; the structure and the nature of these orbitals; and the structure of the local environment, in particular, uranium ions in amorphous substances. These data cannot be obtained directly by other methods.

Despite the substantial advances in the understanding of the electronic and crystal structures of actinide compounds and extension and deepening of the knowledge on the nature of the chemical bond in them, some points still remain obscure. For example, the structures of the IVMO spectra for compounds of most actinides still cannot be completely interpreted, due to the lack of results of proper relativistic calculations. The role of the IVMO electrons in the formation of the chemical bonds in compounds has not been ultimately clarified, because procedures for experimental and theoretical estimation of the contributions of particular orbitals to the binding energy have not been adequately developed.

The greatest success in solving the problems mentioned above can be attained by performing X-ray photoelectron spectral studies for diatomic gaseous molecules such as thorium and uranium monoxides using synchrotron radiation for excitation. In this case, relativistic calculations of the electronic structures can be done most easily as, for example, for the UF_6 molecule. No ultimate opinion on the role of IVMO in the formation and structures of actinide compounds has been formed as yet. However, there already exist a number of examples that imply that the concept of efficient IVMO formation allows one to interpret some experimental results, for example, the formation of the complex fine structure in the XPS spectra of actinide compounds in the $\sim 15-50$ eV binding energy range; the relationship between fine XPS structure characteristics in this region and the structure of the nearest environment and distances from the metal atoms to the closest ligand atoms in the compounds; the appearance of peaks and fine structure in the binding energy range of $\sim 15-50$ eV in the emission spectra of thorium oxide and fluoride and uranium oxides, Auger spectra of uranium oxide and conversion spectra of uranium oxides and fluorides. The formation of IVMO might also be a reason for the appearance of stable actinyl groups AnO_2^{n+}. In conclusion, it should be noted that the experimental and theoretical studies of the electronic structure of compounds and solids and the nature of the chemical bond carried out in recent years deal, most often, with the binding energy range of 0 – 50 eV rather than 0 – 15 eV studied traditionally. This is a recent and important achievement in chemistry, biology and solid-state physics.

This review was written with the financial support of the International Science and Engineering Centre (Grant No. 1358), the Russian Foundation for Basic Research (Project Nos 02-03-32693 and 04-03-32892), and the State Program for the Support of Leading Scientific Schools (Project No. 1763).

References

1. J J Katz, G T Seaborg, L R Morss *The Chemistry of the Actinide Elements* Vols 1-3 (London, New York: Chapman and Hall, 1986)
2. D Brown *Halides of the Transition Elements. Halides of the Lanthanides and Actinides* (London, New York, Sydney: Wiley-Interscience, 1968)
3. M P Mefod'eva, N N Krot *Soedineniya Transuranovykh Elementov* (Compounds of Transuranium Elements) (Moscow: Nauka, 1987)
4. G I Ionova, V G Pershina, V I Spitsyn *Elektronnoe Stroenie Aktinidov* (Electronic Structure of Actinides) (Moscow: Nauka, 1986)
5. Yu M Dymkov *Priroda Uranovoi Smolyanoi Rudy* (The Nature of Pitchblende) (Moscow: Atomizdat, 1973)
6. A K Lisitsin *Gidrogeokhimiya Rudoobrazovaniya* (Hydrogeochemistry of Ore Formation) (Moscow: Nauka, 1975)
7. G A Sidorenko *Kristallokhimiya Mineralov Urana* (Crystal Chemistry of Uranium Minerals) (Moscow: Atomizdat, 1978)
8. A S Baev, A S Bogatov, E I Bykhovskaya, E I Lebedeva, E A Obukhova, Yu A Teterin *Preprint IAE-5484/14* (Moscow: I V Kurchatov Institute of Nuclear Energy, 1992)
9. A S Baev, Yu A Teterin, S K Lisin, in *Voprosy Atomnoi Nauki i Tekhniki (Ser. Obshchaya i Yadernaya Fizika)* [Problems of Nuclear Science and Engineering (General and Nuclear Chemistry Series)] (Moscow: Russian Research Centre 'Kurchatov Institute' 1992) Vol. 3, p. 55
10. Yu A Teterin, A S Baev, S A Bogatov *J. Electron Spectrosc. Relat. Phenom.* **68** 685 (1994)
11. V I Nefedov, Yu A Teterin, A M Lebedev, A Yu Teterin, A P Dementiev, M Bubner, T Reich, S Pompe, K Heise, H Nitsche *Inorg. Chim. Acta* **273** 234 (1998)
12. Yu A Teterin, K E Ivanov, A S Baev, V I Nefedov, G Gaipel, T Reich, H Nische *Surf. Inv.* **13** 613 (1998)
13. Yu A Teterin, C Ronneau, R M Polevoi, V F Shikalov, P Froment, J Cara, I O Utkin, A S Nikitin, K E Ivanov *Poverkhnost'* **3** 54 (2001)
14. Yu A Teterin, V I Nefedov, C Ronneau, A S Nikitin, P Froment, J Cara, I O Utkin, A P Dementiev, A Yu Teterin, K E Ivanov *Radiokhimiya* **43** 537 (2001) [a]

15. Yu A Teterin, V I Nefedov, A S Nikitin, C Ronneau, J Vanbegin, J Cara, A P Dementiev, I O Utkin, A Yu Teterin, K E Ivanov, V G Yarjemsky *J. Nucl. Sci. Technol.* (Suppl. 3) 477 (2002)
16. R J Silva, H Nitshe *Radiochim. Acta* **70/71** 377 (1995)
17. V G Pershina *Chem. Rev.* **96** 1977 (1996)
18. G V Ionova *Usp. Khim.* **71** 461 (2002) [*Russ. Chem. Rev.* **71** 401 (2002)]
19. K Siegbahn, C Nordling, G Johansson, J Hedman, P F Heden, K Hamrin, U Gelius, T Bergmark, L O Weme, Y Baer *ESCA Applied to Free Molecules* (Amsterdam: North-Holland, 1969)
20. K Siegbahn, C Nordling, A Fahlman, R Nordberg, K Hamrin, J Hedman, C Johansson, T Bergmark, S E Karlsson, I Lindgren, B Lindberg *ESCA: Atomic, Molecular, and Solid State Structure Studied by Means of Electron Spectroscopy* (Uppsala: Almqvist and Wiksells, 1967)
21. V I Nefedov, in *Stroenie Molekul i Khimicheskaya Svyaz' (Itogi Nauki i Tekhniki)* [The Structure of Molecules and Chemical Bond (Advances in Science and Engineering Series)] (Moscow: Izd-vo VINITI, 1973) Vol. 1, p. 1
22. V V Nemoshkalenko, V G Aleshin *Elektronnaya Spektroskopiya Kristallov* (Electronic Spectroscopy of Crystals) (Kiev: Naukova Dumka, 1978)
23. V I Nefedov *Rentgenoelektronnaya Spektroskopiya Khimicheskikh Soedinenii* (X-Ray Photoelectron Spectroscopy of Chemical Compounds) (Moscow: Khimiya, 1984)
24. D E Ellis, A Rosen, P F Walch *J. Quant. Chem. Symp.* **9** 351 (1975)
25. P F Walch, D E Ellis *J. Chem. Phys.* **65** 2387 (1976)
26. A L Gubskii, A P Kovtun, Yu A Teterin, A S Baev *Preprint IAE-4053/12* (Moscow: I V Kurchatov Institute of Nuclear Energy, 1984)
27. V A Gubanov, E Z Kurmaev, A L Ivanovskii *Kvantovaya Khimiya Tverdogo Tela* (Quantum Chemistry of Solid) (Moscow: Nauka, 1984)
28. V A Gubanov, A L Ivanovskii, M V Ryzhkov *Kvantovaya Khimiya v Materialovedenii* (Quantum Chemistry in Material Science) (Moscow: Nauka, 1987)
29. Yu A Teterin, A S Baev, N G Yakovlev, in *Voprosy Atomnoi Nauki i Tekhniki (Ser. Yaderno-Fizicheskie Issledovaniya)* [Problems of Nuclear Science and Engineering (Nuclear Physical Investigations Series)] (Moscow: TsNIIatominform, 1992) Vol. 3, p. 58
30. M Ya Amus'ya *Atomnyi Fotoeffekt* (Nuclear Photoeffect) (Moscow: Nauka, 1987)
31. P Pyykko, L L Lohr *Inorg. Chem.* **20** 1950 (1981)
32. V L Sukhorukov, S A Yavna, V F Demekhin *Fiz. Tv. Tela* **24** 1856 (1982) [b]
33. P Pyykko, L Laaksonen *J. Phys. Chem.* **88** 4892 (1984)
34. V I Nefedov, V G Yarjemsky, M M Gofman, in *Khimicheskaya Svyaz' i Stroenie Molekul* (The Chemical Bond and Molecular Structure) (Moscow: Nauka, 1984) p. 108
35. V G Yarjemsky, V I Nefedov, N M Band, M B Trzhaskovskaya, Yu A Teterin, A Yu Teterin *Dokl. Akad. Nauk* **364** 653 (1999) [c]
36. M V Ryzhkov, V A Gubanov, Yu A Teterin, A S Baev *Radiokhimiya* **34** 81 (1992) [a]
37. Yu A Teterin, in *Proceedings of the 9th Congress of Physicists of Yugoslavia, Petrovats na Moru* (Montenegro: Society of Mathematicists and Physicists, 1995) p. 793
38. J Verbist, J Riga, J J Pireaux, R Caudano *J. Electron Spectrosc. Relat. Phenom.* **5** 193 (1974)
39. B W Veal, D J Lam *Phys. Rev. B* **10** 4902 (1974)
40. B V Veal, D J Lam *Phys. Lett. A* **49** 466 (1974)
41. B W Veal, D J Lam, H Diamond *Physica B* **86–88** 1193 (1977)
42. M V Ryzhkov, V A Gubanov, Yu A Teterin, A S Baev *Radiokhimiya* **33** 22 (1991) [a]
43. Yu A Teterin, A S Baev, L G Mashirov, D N Suglobov, in *Voprosy Atomnoi Nauki i Tekhniki (Ser. Yaderno-Fizicheskie Issledovaniya)* [Problems of Nuclear Science and Engineering (Nuclear Physical Investigations Series)] (Moscow: TsNIIatominform, 1986) Vol. 3 (36), p. 60
44. Yu A Teterin, A S Baev, in *Voprosy Atomnoi Nauki i Tekhniki (Ser. Yaderno-Fizicheskie Issledovaniya)* [Problems of Nuclear Science and Engineering (Nuclear Physical Investigations Series)] (Moscow: TsNIIatominform, 1986) Vol. 3 (36), p. 63
45. B W Veal, D J Lam, W T Carnall, H R Hoekatra *Phys. Rev. B* **12** 5651 (1975)
46. Yu A Teterin, in *Voprosy Atomnoi Nauki i Tekhniki (Ser. Yaderno-Fizicheskie Issledovaniya)* [Problems of Nuclear Science and Engineering (Nuclear Physical Investigations Series)] (Moscow: TsNIIatominform, 1985) Vol. 4 (33), p. 54
47. A S Baev, Yu A Teterin, L G Mashirov, D N Suglobov *Radiokhimiya* **28** 460 (1986) [a]
48. A S Baev, Yu A Teterin, in *Voprosy Atomnoi Nauki i Tekhniki (Ser. Yaderno-Fizicheskie Issledovaniya)* [Problems of Nuclear Science and Engineering (Nuclear Physical Investigations Series)] (Moscow: TsNIIatominform, 1986) Vol. 3 (36), p. 61
49. V M Kulakov, Yu A Teterin *Priroda* **2** 78 (1977)
50. V I Nefedov, V I Vovna *Elektronnaya Struktura Khimicheskikh Soedinenii* (Electronic Structure of Chemical Compounds) (Moscow: Nauka, 1987)
51. Yu A Teterin, in *Rentgenovskie, Elektronnye Spektry i Khimicheskaya Svyaz'* (X-Ray and Electron Spectra and Chemical Bond) (Vladivostok: Far Eastern University, 1986) p. 165
52. Yu A Teterin, S G Gagarin *Vnutrennie Valentnye Molekulyarnye Orbitali i Vliyanie ikh Elektronov na Kharakter Khimicheskoi Svyazi Soedinenii* (Inner Valence Molecular Orbitals and The Effect of their Electrons on the Nature of Chemical Bond in Compounds) (Moscow: TsNIIatominform, 1985)
53. Yu A Teterin, S G Gagarin *Usp. Khim.* **65** 895 (1996) [*Russ. Chem. Rev.* **65** 825 (1996)]
54. Yu A Teterin, A Yu Teterin *Usp. Khim.* **71** 403 (2002) [*Russ. Chem. Rev.* **71** 347 (2002)]
55. Yu A Teterin, A S Baev *Rentgenovskaya Fotoelektronnaya Spektroskopiya Soedinenii Legkikh Aktinoidov* (X-Ray Photoelectron Spectroscopy of Light Actinide Compounds) (Moscow: TsNIIatominform, 1986)
56. Yu A Teterin, I O Utkin, A M Lebedev, A Yu Teterin, K E Ivanov, A S Nikitin, in *Proceedings of the Workshop on Speciation, Techniques, and Facilities for Radioactive Materials at Synchrotron Light Sources, Grenoble, France, 1998* (Paris: Nuclear Energy Agency, OECD, 1999) p. 297
57. J C Fuggle, A F Burr, W Lang, L M Watson, D Y Fabian *J. Phys. F: Met. Phys.* **4** 335 (1974)
58. Yu A Teterin, A S Baev, S G Gagarin, V D Klimov *Radiokhimiya* **27** 3 (1985) [a]
59. V D Klimov, V A Legasov, A V Lebedev, S S Khoroshev, Yu A Teterin, A S Baev, N S Tolmacheva *Radiokhimiya* **27** 415 (1985) [a]
60. E Thibant, J J Pireaux, J Riga, C Tenret-Nokl, R Caudano, E G Deronane, J Verbist, in *Proceedings of the 2nd International Conference on Electronic Strict. Actinides, Wroclaw, Poland, 1976* p. 139
61. A S Baev, Yu A Teterin, in *Voprosy Atomnoi Nauki i Tekhniki (Ser. Yaderno-Fizicheskie Issledovaniya)* [Problems of Nuclear Science and Engineering (Nuclear Physical Investigations Series)] (Moscow: TsNIIatominform, 1990) Vol. 5 (13), p. 82
62. Yu A Teterin, I O Utkin, I V Melnikov, A Yu Teterin, A M Lebedev, K E Ivanov, L Vuckchevich, A S Nikitin, in *Proceedings of the Workshop on Speciation, Techniques, and Facilities for Radioactive Materials at Synchrotron Light Sources, Grenoble, France, 1998* (Paris: Nuclear Energy Agency, OECD, 1999) p. 287
63. Yu A Teterin, I O Utkin, I V Mel'nikov, A M Lebedev, A Yu Teterin, K E Ivanov, A S Nikitin, L Vukchevich *Zh. Strukt. Khim.* **41** 1167 (2000) [d]
64. T Gouder, L Havela, F Miserque, F Wastin, J Rebizant, in *Extended Abstracts of 31emes Journees des Actinides, Saint-Malo, France, 2001* p. O29
65. Yu A Teterin, V M Kulakov, A S Baev, A G Zelenkov, N B Nevzorov, I V Mel'nikov, V A Strel'tsov, L G Mashirov, D N Suglobov *Dokl. Akad. Nauk SSSR* **255** 434 (1980) [c]
66. Yu A Teterin, V M Kulakov, A S Baev, N B Nevzorov, I V Melnikov, V A Streltsov, L G Mashirov, D N Suglobov, A G Zelenkov *Phys. Chem. Miner.* **7** 151 (1981)
67. S Evans *J. Chem. Soc., Faraday Trans. 2* **73** 1341 (1977)
68. N Beatham, A P Orchard, G Thornton *J. Electron Spectrosc. Relat. Phenom.* **19** 205 (1980)

69. E Thibaut, J-P Boutique, J J Verbist, J-C Level, H Nokl *J. Am. Chem. Soc.* **104** 5266 (1982)
70. J J Pireaux, N Martensson, R Didriksson, K Siegbahn, J Riga, J Verbist *Chem. Phys. Lett.* **46** 213 (1977)
71. G C Allen, A J Griffiths, B J Lee *Transition Met. Chem.* **3** 229 (1978)
72. A H Al Rayyes, C Ronneau *Radiochim. Acta* **54** 189 (1991)
73. P Benard, D Louer, N Dacheux, V Brandel, M Genet *Chem. Mater.* **6** 1049 (1994)
74. G C Allen, N R Holmes *Can. J. Appl. Spectrosc.* **38** 124 (1993)
75. C Miyake, M Kanamaru, S Imoto, K Taniguchi *Nuclear Mater.* **138** 36 (1986)
76. G S Allen, N R Holmes *J. Chem. Soc., Dalton Trans.* 3009 (1987)
77. T Gouder, C Colmenares, J R Naegele, J Verbist *Surf. Sci.* **235** 280 (1989)
78. E Talik, M Kulpa, W Suski, R Tros, in *Extended Abstracts of 32emes Journees des Actinides, Ein-Gedi, Israel, 2002* p. P3
79. B W Veal, D J Lam, H Diamond, H R Hoekstra *Phys. Rev. B* **15** 2929 (1977)
80. Yu A Teterin, A S Baev, L G Mashirov, D N Suglobov *Dokl. Akad. Nauk SSSR* **276** 154 (1984) [c]
81. Yu A Teterin *Kondens. Sredy i Mezhfaz. Granitsy* **2** 60 (2000)
82. Yu A Teterin, A S Baev, L G Mashirov, D N Suglobov *Dokl. Akad. Nauk SSSR* **277** 131 (1984) [c]
83. R Baptist, D Courteix, J Chayrouse, L Heintz *J. Phys. F: Met. Phys.* **12** 2103 (1982)
84. D Courteix, J Chayrouse, L Heintz, R Baptist *Solid State Commun.* **39** 209 (1981)
85. T Gouder, L Havela, F Wastin, J Rebizant, in *Extended Abstracts of 31emes Journees des Actinides, Saint-Malo, France, 2001* p. O36
86. A J Arko, J J Joyce, L Morales, J Wills, J Lashley, F Wastin, J Rebizant *Phys. Rev. B* **62** 1773 (2000)
87. Yu A Teterin, K E Ivanov, A Yu Teterin, I O Utkin, A S Nikitin, in *Proceedings of the 3rd International Yugoslav Nuclear Society Conference* (*YUNSC-2000*) (Belgrade: VINCA Institute of Nuclear Sciences, 2001) p. 396
88. Yu A Teterin, A Yu Teterin, K E Ivanov, I O Utkin *J. Nucl. Technol.* (Suppl. 3) 140 (2002)
89. Yu A Teterin, A S Baev, A Yu Teterin, K E Ivanov, L Vukchevich, in *Proceedings of Yugoslav Nuclear Society Conference (YUNSC'96)* (Belgrade: VINCA Institute of Nuclear Sciences, 1997) p. 453
90. Yu A Teterin, A S Baev, A Yu Teterin, K E Ivanov *Dokl. Akad. Nauk* **348** 213 (1996) [c]
91. Yu A Teterin, V M Kulakov, K E Ivanov, in *NATO ASI-Series. Microbial Degradation Processes in Radioactive Waste Repository and in Nuclear Fuel Storage Areas. Ser. 1. Disarmament Technologies* (Ed. J H Wolfram) (Dordrecht: Kluwer Academic, 1997) p. 233
92. Yu A Teterin, A S Baev, R V Vedrinskii, A L Gubskii, A G Zelenkov, A P Kovtun, V M Kulakov, V P Sachenko, in *Fizicheskie i Matematicheskie Metody v Koordinatsionnoi Khimii* (Physical and Mathematical Methods in Coordination Chemistry) (Kishinev: Shtiintsa, 1980) p. 73
93. Yu A Teterin, A S Baev, R V Vedrinskii, A L Gubskii, A G Zelenkov, A P Kovtun, V M Kulakov, V P Sachenko *Dokl. Akad. Nauk SSSR* **256** 381 (1981) [c]
94. Yu A Teterin, A S Baev, K E Ivanov, L G Mashirov, D N Suglobov *Radiokhimiya* **38** 395 (1996) [a]
95. V I Nefedov, Yu A Teterin, T Reich, H Nitshe *Dokl. Akad. Nauk* **348** 634 (1996) [c]
96. Yu A Teterin, K E Ivanov *Poverkhnost'* **4–5** 211 (1997)
97. Yu A Teterin, K E Ivanov, in *Proceedings of Yugoslav Nuclear Society Conference* (*YUNSC'96*) (Belgrade: VINCA Institute of Nuclear Sciences, 1997) p. 437
98. Yu A Teterin, A S Baev, in *Voprosy Atomnoi Nauki i Tekhniki (Ser. Yaderno-Fizicheskie Issledovaniya)* [Problems of Nuclear Science and Engineering (Nuclear Physical Investigations Series)] (Moscow: TsNIIatominform, 1985) Vol. 4, p. 53
99. Yu A Teterin, V A Terehov, M V Ryzhkov, A Yu Teterin, I O Utkin, K E Ivanov, A S Nikitin, L J Vukchevich, in *Workshop Proceedings on Speciation, Techniques, and Facilities for Radioactive Materials at Synchrotron Light Sources, Grenoble, France, 2000* (Paris:Nuclear Energy Agency, OECD, 2002) p. 325
100. Yu A Teterin, V A Terehov, M V Ryzhkov, A Yu Teterin, I O Utkin, K E Ivanov, L J Vukchevich, in *Extended Abstracts of 32emes Journees des Actinides, Ein-Gedi, Israel, 2002* p. C2
101. Yu A Teterin, M V Ryzhkov, V A Gubanov, S G Gagarin, in *Kvantovaya Khimiya Tverdogo Tela* (*Preprint UNTs Akad. Nauk SSSR*) [Quantum Chemistry of Solids (Preprint Urals Scientific Centre, Academy of Sciences of the USSR)] (Sverdlovsk: Institute of Chemistry, 1984) p. 62
102. Yu A Teterin, M V Ryzhkov, V A Gubanov, S G Gagarin *Dokl. Akad. Nauk SSSR* **264** 915 (1985) [a]
103. A S Baev, A G Zelenkov, V M Kulakov, L G Mashirov, V P Smilga, D N Suglobov, Yu A Teterin, in *Tez. Dokl. XII Vsesoyuz. Soveshchaniya po Rentgenovskoi Spektroskopii* (Abstracts of Reports of the XIIth All-Union Meeting on X-Ray Spectroscopy) (Leningrad: Leningrad State University, 1978) p. 118
104. Yu A Teterin, V M Kulakov, A S Baev, A G Zelenkov, I V Mel'nikov, N B Nevzorov, V A Strel'tsov, in *Tez. Dokl. Vsesoyuz. Soveshchaniya 'Rentgenovskie i Rentgenoelektronnye Spektry i Elektronnaya Struktura Metallov, Splavov i Khimicheskikh Soedinenii'* (Abstracts of Reports of the All-Union Meeting 'X-Ray and X-Ray Photoelectron Spectra and Electronic Structure of Metals, Alloys and Chemical Compounds) (Izhevsk: Physical and Technical Institute, 1979) p. 25
105. J J Pireaux, J Riga, E Thibaut, C Tenret-Nöl, R Caudano, J J Verbist *Chem. Phys.* **22** 113 (1977)
106. P R Norton, R L Tapping, D K Creber, W J L Buyers *Phys. Rev. B* **21** 2572 (1980)
107. A S Baev, Yu A Teterin, in *Proceedings of the 5th Seminar on Electron Spectroscopy of Socialist Countries* (Dresden: Technische Universität, 1984) p. 15
108. Yu A Teterin, A S Baev, in *X-84. International Conference on X-Ray and Inner Shell Processes in Atoms, Molecules and Solid (Abstracts of Reports), Leipzig, 1984* Pt. 2, p. 466
109. Yu A Teterin, K E Ivanov *Surf. Inv.* **13** 623 (1998)
110. Yu A Teterin, M V Ryzhkov, A Yu Teterin, A D Panov, A S Nikitin, K E Ivanov, I O Utkin *J. Nucl. Technol.* (Suppl. 3) 74 (2002)
111. L E Cox *J. Electron Spectrosc. Relat. Phenom.* **26** 167 (1982)
112. Yu A Teterin, in *Abstracts of Reports of the 5th Seminar on Electron Spectroscopy of Socialist Countries* (Dresden: Technische Universität, 1984) p. 145
113. A S Baev, V M Kulakov, Yu A Teterin, N G Gorshkov, L G Mashirov, D N Suglobov, in *Tez. Dokl. XII Mendeleevskogo S'ezda po Obshchei i Prikladnoi Khimii. Radiokhimiya* (Abstracts of Reports of the XIIth Mendeleev Congress on General and Applied Chemistry. Radiochemistry) (Moscow : Nauka, 1981) Vol. 1, p. 154
114. A S Baev, N G Gorshkov, V M Kulakov, L G Mashirov, D N Suglobov, Yu A Teterin *Radiokhimiya* **24** 576 (1982) [a]
115. Yu A Teterin, A S Baev, A D Sidorenko, S G Gagarin, in *Rentgenovskaya Spektroskopiya Tverdogo Tela* (*Preprint UNTs AN SSSR*) (X-Ray Spectroscopy of Solids (Preprint Urals Scientific Centre, Academy of Sciences of the USSR)] (Sverdlovsk: Institute of Chemistry, 1984) p. 23
116. L E Cox, J W Ward *Inorg. Nucl. Chem. Lett.* **17** 265 (1981)
117. R J Thorn *J. Phys. Chem. Solids* **43** 571 (1982)
118. G M Bancroft, T K Sham, J L Esquivel, S Larsson *Chem. Phys. Lett.* **51** 105 (1977)
119. G T Bancroft, T K Sham, S Larsson *Chem. Phys. Lett.* **46** 551 (1977)
120. T K Sham, G Wendin *Phys. Rev. Lett.* **44** 817 (1980)
121. T Novakov, J M Hollander *Phys. Rev. Lett.* **21** 1133 (1968)
122. R L Dekock, E J Baerends, P M Boerrigter, J G Snijders *Chem. Phys. Lett.* **105** 308 (1984)

123. Yu A Teterin, M V Ryzhkov, A Yu Teterin, A D Panov, A S Nikitin, K E Ivanov, I O Utkin *Radiokhimiya* **44** 206 (2002) [a]
124. M Ohno *Phys. Rev. B* **35** 5453 (1987)
125. O Gunnarson, K Schönhammer, D D Sarma, F U Hillebrecht, M Campagna *Phys. Rev. B* **32** 5499 (1985)
126. D T Larson *J. Vac. Sci. Technol.* **17** 55 (1980)
127. J R Naegele, L Manes, J C Spirlet, W Muller *Phys. Rev. Lett.* **52** 1834 (1984)
128. B Johansson *Phys. Rev. B* **30** 3533 (1984)
129. V A Gubanov, A Rosen, D E Ellis *Solid State Commun.* **22** 219 (1977)
130. M Boring, J H Wood, J M Moscowitz *J. Chem. Phys.* **63** 638 (1975)
131. D D Koelling, D E Ellis, R J Bartlett *J. Chem. Phys.* **65** 3331 (1976)
132. G L Gutsev, A A Levin *Dokl. Akad. Nauk SSSR* **246** 1366 (1979) [c]
133. S Shiokawa, H Adachi, S Imoto *J. Phys. Soc. Jpn.* **48** 327 (1980)
134. I A Topol', B I Zhilinskii *Teor. Eksp. Khim.* **20** 406 (1984) [e]
135. V I Nefedov, V G Yarjemsky, I S Nefedova, I M Band, M B Trzhaskovskaya, Yu A Teterin *Poverkhnost'* **6** 16 (2000)
136. N Kaltsoyannis, B E Bursten *Inorg. Chem.* **34** 2735 (1995)
137. V A Gubanov, A Rosen, D E Ellis *J. Phys. Chem. Solids* **40** 17 (1979)
138. F Gerken, J Schmidt-May *J. Phys. F: Met. Phys.* **13** 1571 (1983)
139. T H Gouder, C A Colmenares *Surf. Sci.* **341** 51 (1995)
140. T Gouder, J R Naegele, C A Colmenares. *Surf. Sci.* **342** 299 (1995)
141. T Gouder *J. Electron Spectrosc. Relat. Phenom.* **101 – 103** 419 (1999)
142. J W Allen, J M Peek, L E Cox *Physica B* **259 – 261** 1147 (1999)
143. B Reihl, N Martenson, D E Eastman *Phys. Rev. B* **24** 406 (1981)
144. L Black, T Gouder, F Wastin, J Rebizant, L Havela *Surf. Sci.* **504** 83 (2002)
145. Y Saito, S Suzuki, Y Onuki, N Sato, S-I Fujimori, T Komatsubara, S Sato, Y Haga, K-i Yamak *J. Electron Spectrosc. Relat. Phenom.* **88 – 91** 353 (1998)
146. J W Allen, Y-X Zhang, L H Tjeng, L E Cox, M B Maple, C-T Chen *J. Electron Spectrosc. Relat. Phenom.* **78** 57 (1996)
147. K Sato, Y Saito, S Suzuki, T Komatsubara, K Tamura, M Seki, T Okane, S-I Fujimori, N Sato, S Sato, A Tanaka, M Mizuta, Y Tezuka, S Shin, K-I Yamaki *J. Electron Spectrosc. Relat. Phenom.* **101 – 103** 439 (1999)
148. T Gouder, L Havela *Mikrochim. Acta* **138** 207 (2002)
149. A S Baev, Yu A Teterin, K E Ivanov, A Yu Teterin, S A Bogatov *Radiokhimiya* **39** 171 (1997) [a]
150. Yu A Teterin, in *Proceedings of Second International Yugoslav Nuclear Society Conference (YUNSC'98)* (Belgrade: VINCA Institute of Nuclear Sciences, 1999) p. 503
151. Yu A Teterin, A S Baev, A Yu Teterin, K E Ivanov, L G Mashirov, D N Suglobov *Radiokhimiya* **39** 177 (1997) [a]
152. Yu A Teterin, V I Nefedov, K E Ivanov, A S Baev, G Geipel, T Reich, H Nitshe *Dokl. Akad. Nauk* **344** 206 (1995) [c]
153. Yu A Teterin, V I Nefedov, K E Ivanov, A S Baev, G Geipel, T Reich, H Nitshe *Zh. Neorg. Khim.* **41** 1884 (1996) [f]
154. T Reich, G Geipel, Yu A Teterin, V I Nefedov, K E Ivanov, A S Baev, M A Denecke, G Bernhard, H Nitshe, P G Allen, J J Bucher, in *Extended Abstracts of the 4th International Conference on Nuclear and Radiochemistry (NRC4)* Vol. 1 (St Malo, France: Institute de Physique Nucleare, 1996) p. DP-11
155. Yu A Teterin, V I Nefedov, K E Ivanov, A S Baev, G Geipel, T Reich, H Nitshe *Dokl. Akad. Nauk* **350** 503 (1996) [c]
156. Yu A Teterin, K E Ivanov, A S Baev, V I Nefedov, G Geipel, T Reich, H Nitsche *Poverkhnost'* **4 – 5** 202 (1997)
157. Yu A Teterin, V I Nefedov, A Yu Teterin, A M Lebedev, K E Ivanov, A P Dementiev, G Geipel, M Bubner, T Reich, S Pompe, K-H Heise, H Nitshe, in *Sbornik Dokl. Natsional'noi Konf. po Primeneniyu Rentgenovskogo, Sinkhrotronnogo Izlucheniya Neitronov i Elektronov dlya Issledovaniya Materialov (RSNE'97)* [Collection of Reports of National Conference on Application of X-Ray and Synchroton Radiation of Neutrons and Electrons for Investigation of Materials (RSNE'97)] (Dubna: Joint Institute for Nuclear Research, 1997) Vol. 2, p. 436
158. Yu A Teterin, V I Nefedov, A Yu Teterin, A M Lebedev, A P Dementiev, I O Utkin, M Bubner, T Reich, S Pompe, K-H Heise, H Nitshe *Zh. Neorg. Khim.* **44** 593 (1999) [f]
159. Yu A Teterin, V I Nefedov, A Yu Teterin, A M Lebedev, K E Ivanov, A P Dementiev, I O Utkin, G Geipel, M Bubner, T Reich, S Pompe, K-H Heise, H Nitshe *Poverkhnost'* **2** 79 (1999)
160. Yu A Teterin, A Yu Teterin, A M Lebedev, A P Dementiev, I O Utkin, V I Nefedov, M Bubner, T Reich, S Pompe, K-H Heise, H Nitsche *J. Prakt. Chem.* **341** 773 (1999)
161. Yu A Teterin, V I Nefedov, A Yu Teterin, A M Lebedev, A P Dementiev, I O Utkin, I V Melihov, in *Proceedings of the Workshop on Speciation, Techniques, and Facilities for Radioactive Materials at Synchrotron Light Sources, Grenoble, France, 1998* (Paris: Nuclear Energy Agency, OECD, 1999) p. 307
162. Yu A Teterin, A Yu Teterin, A P Dementiev, A M Lebedev, I O Utkin, I V Melikhov, V I Nefedov, D G Berdonosova, Dj Bek-Uzarov, L Vukchevich *Zh. Strukt. Khim.* **41** 749 (2000) [d]
163. A F Francis *J. Alloys Compd.* **213/214** 226 (1994)
164. A F Francis, C J Dodje, F Lu, G P Halada, C R Clayton *Environ. Sci. Technol.* **28** 636 (1994)
165. C J Dodje, A F Francis *Environ. Sci. Technol.* **28** 1300 (1994)
166. Yu A Teterin, V I Nefedov, A S Nikitin, C Ronneau, J Vanbegin, J Cara, A P Dementiev, I O Utkin, A Yu Teterin, K E Ivanov, V G Yarzhemsky, in *Proceedings of the Workshop on Speciation, Techniques, and Facilities for Radioactive Materials at Synchrotron Light Sources, Grenoble, France, 2000* (Paris: Nuclear Energy Agency, OECD, 2002) p. 305
167. Yu A Teterin, I O Utkin, A Yu Teterin, A S Nikitin, K E Ivanov, A M Lebedev, V I Nefedov, C Ronneau, J Vanbegin, J Cara, L J Vukchevich, Dj Bek-Uzarov, in *Proceedings of the 3rd International Yugoslav Nuclear Society Conference* (*YUNSC-2000*) (Belgrade: VINCA Institute of Nuclear Sciences, 2001) p. 401
168. Yu A Teterin, V I Nefedov, C Ronneau, J Vanbegin, J Cara, I O Utkin, A Yu Teterin, A S Nikitin, K E Ivanov, L Vukchevich, Dj Bek-Uzarov *Radiokhimiya* **43** 531 (2001) [a]
169. Yu A Teterin, V I Nefedov, A S Nikitin, C Ronneau, J Vanbegin, J Cara, A P Dementiev, I O Utkin, A Yu Teterin, K E Ivanov, V G Yarjemsky *Radiokhimiya* **43** 544 (2001) [a]
170. Yu A Teterin, V I Nefedov, C Ronneau, J Vanbegin, J Cara, I O Utkin, A P Dementiev, A Yu Teterin *Kondens. Sredy Mezhfaz. Granitsy* **2** 67 (2000)
171. Yu A Teterin, V I Nefedov, C Ronneau, A S Nikitin, J Vanbegin, J Cara, I O Utkin, A P Dementiev, A Yu Teterin, K E Ivanov, L Vukchevich, Dj Bek-Uzarov *Radiokhimiya* **43** 524 (2001) [a]
172. Yu A Teterin, C Ronneau, R M Polevoi, V F Shikalov, P Froment, J Cara, I O Utkin, A S Nikitin, K E Ivanov, in *Proceedings of the Workshop on Speciation, Techniques, and Facilities for Radioactive Materials at Synchrotron Light Sources, Grenoble, France, 2000* (Paris: Nuclear Energy Agency, OECD, 2002) p. 337
173. Yu A Teterin, in *Proceedings of the 3rd International Yugoslav Nuclear Society Conference (YUNSC-2000)* (Belgrade: VINCA Institute of Nuclear Sciences, 2001) p. 391
174. Yu A Teterin, V I Nefedov, C Ronneau, J Vanbegin, J Cara, I O Utkin, A P Dementiev, A Yu Teterin, A S Nikitin, K E Ivanov *Kondens. Sredy Mezhfaz. Granitsy* **2** 75 (2000)
175. Yu A Teterin, V I Nefedov, C Ronneau, J Vanbegin, J Cara, I O Utkin, A P Dementiev, A Yu Teterin, A S Nikitin, K E Ivanov, L J Vukchevich, Dj Bek-Uzarov *Bulg. J. Phys.* **27** (2) 9 (2000)
176. Y Baer, J K Lang *Phys. Rev. B* **21** 2060 (1980)
177. S B Nornes, R G Meisenheimer *Surf. Sci.* **88** 191 (1979)
178. K N Huang, M Aouogi, M H Chen, B Grasemant, H Mark *At. Data Nucl. Data Tables* **18** 243 (1976)
179. J M Dyke, G D Josland, A Morris, P M Tucker, J W Tyler *J. Chem. Soc., Faraday Trans. 2* **77** 1273 (1981)
180. V A Gubanov, A Rosen, D E Ellis *J. Inorg. Nucl. Chem.* **41** 975 (1979)

181. V P Zhukov, V A Gubanov, V I Anisimov *Opt. Spektrosk.* **46** 85 (1979) [g]
182. Yu F Batrakov, R V Bogdanov, E V Puchkova, A S Surgeev *Radiokhimiya* **42** 112 (2000) [a]
183. Yu A Teterin, V A Terekhov, A Yu Teterin, I O Utkin, A M Lebedev, L Vukchevich *Dokl. Akad. Nauk* **358** 637 (1998) [c]
184. Yu A Teterin, V A Terekhov, A Yu Teterin, I O Utkin, A M Lebedev, L Vukchevich *Zh. Strukt. Khim.* **39** 1052 (1998) [d]
185. Yu A Teterin, V A Terekhov, A Yu Teterin, K E Ivanov, I O Utkin, A M Lebedev, L Vukchevich *J. Electron Spectrosc. Relat. Phenom.* **96** 229 (1998)
186. Yu A Teterin, V A Terekhov, A Yu Teterin, I O Utkin, A M Lebedev, L Vukchevich, in *Proceedings of Second International Yugoslav Nuclear Society Conference (YUNSC'98)* (Belgrade: VINCA Institute of Nuclear Sciences, 1999) p. 507
187. T M Zimkina, I I Lyakhovskaya, A S Shulakov *Opt. Spektrosk.* **62** 285 (1987) [g]
188. I I Lyakhovskaya, V M Ipatov, T M Zimkina *Zh. Strukt. Khim.* **18** 688 (1977) [d]
189. G Kalkowski, G Kaindl, W D Brewer, W Krone *Phys. Rev. B* **35** 2667 (1987)
190. L E Cox, W P Ellis, R D Covan, J W Allen, S-J Oh, I Lindau, B B Pate, A J Arko *Phys. Rev. B* **35** 5761 (1987)
191. J Petiau, G Calas, D Petitmaire, A Bianconi, M Benfatto, A Marcelli *Phys. Rev. B* **34** 7350 (1986)
192. Yu A Teterin, T N Bondarenko, A Yu Teterin, A M Lebedev, I O Utkin *Radiokhimiya* **40** 103 (1998) [a]
193. S A Prosandeev, Yu A Teterin, R V Vedrinskii, V M Kulakov *Preprint IAE-3206* (Moscow: I V Kurchatov Institute of Nuclear Energy, 1979)
194. M Boring, R D Cowan, R L Martin *Phys. Rev. B* **23** 445 (1981)
195. F U Hillebrecht, D D Sarma, N Martensson *Phys. Rev. B* **33** 4376 (1986)
196. J Brunner, M Erbudak, F Hulliger *Solid State Commun.* **38** 841 (1981)
197. F U Hillebrecht, D D Sarma, N Martensson *J. Magn. Magn. Mater.* **52** 129 (1985)
198. S Suga, M Yamamoto, K Soda, T Mori, S Takagi, N Nitsuma, T Suzuki, T Kasuya *J. Magn. Magn. Mater.* **52** 297 (1985)
199. D B Beach, K D Bomben, N M Edelstein, D C Eisenberg, W L Jolly, R Shinomoto, A Streitwieser *J. Inorg. Chem.* **25** 1735 (1986)
200. N Martensson, P-A Maisquiat, S Svensson, B Johansson *J. Chem. Phys.* **80** 5458 (1984)
201. N Martensson, P-A Malmquiat, S Svensson *Chem. Phys. Lett.* **100** 375 (1983)
202. J M Dyke, N K Fayad, A Morris, I R Trickle, G C Alien *J. Chem. Phys.* **72** 3822 (1980)
203. J H Scofield *J. Electron Spectrosc. Relat. Phenom.* **8** 129 (1976)
204. M Hirata, H Monjyushiro, R Sekine, J Onoe, H Nakamatsu, T Mukoyama, H Adachi, K Takeuchi *J. Electron Spectrosc. Relat. Phenom.* **83** 59 (1997)
205. T Mukoyama, H Nakamatsu, H Adachi *J. Electron Spectrosc. Relat. Phenom.* **63** 409 (1993)
206. C K Jurgensen *Chem. Phys. Lett.* **89** 455 (1982)
207. A S Vil'nyanskii, I S Glazunov *At. Tekhn. za Rubezhom* **7** 3 (1984)
208. B N Laskorin, V A Mamilov, Yu A Koreisho, D I Skorovarov, L I Vodolazov, I P Smirnov, O L Kedrovskii, V P Shchulika B V Nevskii, V N Mosinets *At. Energ.* **54** 286 (1983)
209. Y Baer, J Schoenes *Solid State Commun.* **33** 885 (1980)
210. G C Allen, J A Crofts, M T Curtis, P M Tucker, D Chadwick, P J Hampson *J. Chem. Soc., Dalton Trans.* 1296 (1974)
211. Y K Dawson, M W Lister *J. Chem. Soc.* 2181 (1950)
212. A Arrott, J E Goldman *Phys. Rev.* **108** 948 (1957)
213. R P Rafal'skii, V A Alekseev, L A Anan'eva *Geokhimiya* **11** 1601 (1979) [h]
214. S Bertram, G Kaindl, J Jove, M Pages, J Gal *Phys. Rev. Lett.* **63** 2680 (1989)
215. G C Allen, E J Baerends, P Vernooijs, J M Dyke, A M Ellis, M Feher, A Morris *J. Chem. Phys.* **89** 5363 (1988)
216. C Miyake, H Sakurai, S Imoto *Chem. Phys. Lett.* **36** 158 (1975)
217. M Boring, J H Wood, J V Moskowitz *J. Chem. Phys.* **61** 3800 (1974)
218. V I Zhudov, A G Zelenkov, V M Kulakov, B V Odinov, Yu A Teterin, in *Tez. Dokl. XXX Vsesoyuz. Soveshchaniya po Yadernoi Spektroskopii i Strukture Atomnogo Yadra* (Abstracts of Reports of the XXXth All-Union Meeting on Nuclear Spectroscopy and The Structure of Atomic Nucleus) (Leningrad: Nauka, 1980) p. 614
219. D P Grechukhin, V I Zhudov, A G Zelenkov, V M Kulakov, B V Odinov, A A Soldatov, Yu A Teterin *Pis'ma Zh. Eksp. Teor. Fiz.* **31** 627 (1980) [i]
220. A D Panov, V I Zhudov, Yu A Teterin *Zh. Strukt. Khim.* **39** 1047 (1998) [d]
221. Yu A Teterin *Zh. Strukt. Khim.* **39** 1037 (1998) [d]
222. M Boring, J H Wood *J. Chem. Phys.* **71** 32 (1979)
223. M Boring, J H Wood *J. Chem. Phys.* **71** 392 (1979)
224. P J Hay, W R Wadt, L R Kahn, R C Raffenetti, D H Phillips *J. Chem. Phys.* **71** 1767 (1979)
225. D A Case, C Y Yang *J. Chem. Phys.* **72** 3443 (1980)
226. V A Glebov *Elektronnoe Stroenie i Svoistva Uranilovykh Soedinenii* (Electronic Structure and Properties of Uranyl Compounds) (Moscow: Energoatomizdat, 1983)
227. J H Wood, M Boring, S B Woodruff *J. Chem. Phys.* **74** 5225 (1981)
228. D E Ellis, A Rosen, V A Gubanov *J. Chem. Phys.* **77** 4051 (1982)
229. G C Allen, P M Tucker, J W Tyier *J. Phys. Chem.* **86** 224 (1982)
230. N B Borkovskii, A B Kovrikov, D S Umreiko *Dokl. Akad. Nauk Bel. SSR* **27** 213 (1983)
231. V I Sergeenko, L I Ignat'eva, G L Gudev, A I Boldyrev *Zh. Strukt. Khim.* **26** 131 (1985) [d]
232. A A Soldatov *Zh. Strukt. Khim.* **26** 3 (1985) [d]
233. S G Gagarin, A A Soldatov, A D Sidorenko, Yu A Teterin, in *Tez. Dokl. XIV Vsesoyuz. Soveshch. po Rentgenovskoi i Elektronnoi Spektroskopii, Irkutsk, 1984* (Abstracts of Reports of the XIVth All-Union Meeting on X-Ray and Electronic Spectroscopy, Irkutsk, 1984) p. 91
234. Yu A Teterin, V A Terekhov, K E Ivanov *Dokl. Akad. Nauk* **345** 356 (1995) [c]
235. Yu A Teterin, K E Ivanov, A Yu Teterin, A M Lebedev, L Vukchevich, in *Proceedings of Yugoslav Nuclear Society Conference (YUNSC'96)* (Belgrade: VINCA Institute of Nuclear Sciences, 1997) p. 449
236. Yu A Teterin, K E Ivanov, A Yu Teterin, A M Lebedev, I O Utkin, L Vukchevich *J. Electron Spectrosc. Relat. Phenom.* **101–103** 401 (1999)
237. J Weber, V A Gubanov *J. Inorg. Nucl. Chem.* **41** 693 (1979)
238. L E Cox, W P Ellis, R D Cowan, J W Allen, S-J Oh *Phys. Rev. B* **31** 2467 (1985)
239. D L Clark, D E Hobart, M P Neu *Chem. Rev.* **95** 25 (1995)
240. Yu M Mikhailov *Khimiya Platinovykh i Tyazhelykh Elementov. Problemy Koordinatsionnoi Khimii* (The Chemistry of Platinum and Heavy Elements. The Problems of Coordination Chemistry) (Moscow: Nauka, 1975)
241. L V Volod'ko, A I Komyak, D S Umreiko *Uranilovye Soedineniya* (Uranyl Compounds) (Minsk: Byelorussian State University, 1981) Vol. 1
242. M E Dyatkina, Yu M Mikhailov *Kompleksnye Soedineniya Urana* (Complex Compounds of Uranium) (Ed. I I Chernyaev) (Moscow: Nauka, 1964)
243. B F Ormont *Struktura Neorganicheskikh Veshchestv* (The Structure of Inorganic Substances) (Moscow, Leningrad: Gos. Izd. Tekhn.-Teoret. Lit., 1950)
244. Yu A Teterin, A S Baev, V M Kulakov, A G Zelenkov, in *Voprosy Atomnoi Nauki i Tekhniki (Ser. Obshchaya i Yadernaya Fizika)* [Problems of Nuclear Science and Engineering (General and Nuclear Chemistry Series)] (Khar'kov: Khar'kov Physicotechnical Institute, 1982) Vol. 2 (20), p. 68
245. W R Wadt *J. Am. Chem. Soc.* **103** 6053 (1981)
246. Yu A Teterin, V A Terekhov, M V Ryzhkov, I O Utkin, A S Nikitin, E D Haritonova *Kondens. Sredy Mezhfaz. Granitsy* **2** 83 (2000)
247. Yu A Teterin, V A Terekhov, V M Ryzhkov, I O Utkin, A S Nikitin, E D Kharitonova *Poverkhnost'* **3** 44 (2001)

248. Yu A Teterin, V A Terekhov, M V Ryzhkov, I O Utkin, K E Ivanov, A S Nikitin *J. Electron Spectrosc. Relat. Phenom.* **114–116** 915 (2001)
249. N N Krot, D N Suglobov *Radiokhimiya* **6** 1 (1989) [a]
250. I A Lebedev, B F Myasoedov *Radiokhimiya* **6** 700 (1982) [a]
251. C Keller *The Chemistry of the Transuranium Elements* Vol. 3 (Ed. K H Lieser) (Weinhem: Verlag Chemie, 1971)
252. B C Frazer, G Shirane, D E Cox, C E Olsen *Phys. Rev. A.* **140** 1448 (1965)
253. Yu A Teterin, A S Baev, L G Mashirov, D N Suglobov, in *Tez. Dokl. III Vsesoyuz. Konf. po Khimii Urana* (Abstracts of Reports of the IIIth All-Union Conference on Uranium Chemistry) (Moscow: Nauka, 1985) p. 39
254. G T Seaborg, J J Kats (Eds) *The Actinide Elements* (New York: McGraw-Hill, 1954)
255. W Suski *Physica B* **86–88** 11 (1977)
256. K G Gurtovoi, R Z Levitin *Usp. Fiz. Nauk* **153** 193 (1987) [j]
257. J R Moore, S E Nave, R G Haire, P G Huray *J. Less-Common Met.* **121** 187 (1986)
258. I M Band, Yu I Kharitonov, M B Trhaskovskaya *At. Data Nucl. Data Tables* **23** 443 (1979)
259. D K Shuh, K E Ivanov, S M Butorin, J Guo, M Magnuson, E J Nordgren, in *Abstracts of Reports of the International Conference Actinides-2001, Hayama, Japan, 2001* p. 55
260. K E Ivanov, D K Shuh, Yu A Teterin, A Yu Teterin, S M Butorin, J-H Guo, M Vagnusov, J Nordgren, in *Proceedings of the 4th International Yugoslav Nuclear Society Conference (YUNSC-2002)* (Belgrade: Yugoslav Nuclear Society, 2003) p. 31
261. Yu A Teterin, V A Terekhov, K E Ivanov, in *Proceedings of the 9th Congress of Physicists of Yugoslavia, Petrovats na Moru* (Montenegro: Society of Mathematicists and Physicists, 1995) p. 797
262. L L Makarov, R I Karaziya, Yu F Batrakov, N P Chibisov, A N Masevich, Yu M Zaitsev, A I Udris, L V Shishkunova *Radiokhimiya* **1** 116 (1978) [a]
263. J Drozdzynski, K Schwochan, H-J Schenk *J. Inorg. Nucl. Chem.* **43** 1845 (1981)
264. V I Sergeev, L I Ignat'eva, G L Gutsev, A I Boldyrev *Zh. Strukt. Khim.* **26** 131 (1985) [d]
265. D E Ellis, in *Proceedings of the Actinides-1981 Conference, Pacific Grove, CA, 1982* p. 123
266. J Onoe, K Takeuchi, H Nakamatsu, T Mukoyama, R Sekine, H Adachi *J. Electron Spectrosc. Relat. Phenom.* **60** 29 (1992)
267. J Onoe, K Takeuchi, H Nakamatsu, T Mukoyama, R Sekine, Bong-Il Kim, H Adachi *J. Chem. Phys.* **99** 6810 (1993)
268. J Onoe, H Nakamatsu, R Sekine, T Mukoyama, H Adachi, K Takeuchi *J. Electron Spectrosc. Relat. Phenom.* **70** 89 (1994)
269. M V Ryzhkov, V A Gubanov *J. Radioanal. Nucl. Chem.* **143** 85 (1990)
270. K E Ivanov, D K Shuh, A Yu Teterin, S M Butorin, J-H Guo, M Magnuson, J Nordgren, in *Proceedings of the 4th International Yugoslav Nuclear Society Conference (YUNSC-2002)* (Belgrade: Yugoslav Nuclear Society, 2003) p. 431
271. Yu A Teterin, M V Ryzhkov, A Yu Teterin, A D Panov, A S Nikitin, K E Ivanov, I O Utkin *J. Nucl. Technol. Radioact. Protect.* **1–2** 3 (2002)
272. J C Slater, K H Johanson *Phys. Rev. B* **5** 844 (1972)
273. Yu A Teterin, V I Nefedov, A S Nikitin, A Yu Teterin, K E Ivanov, K I Maslakov, I O Utkin, M Bubner, T Reich, S Pompe, K H Heise, H Nitsche, in *Workshop Proceedings on Speciation, Techniques, and Facilities for Radioactive Materials at Synchrotron Light Sources, Grenoble, France, 2002* (Paris: Nuclear Energy Agency, OECD, 2002) p. 317
274. Yu A Teterin, V I Nefedov, A S Nikitin, A Yu Teterin, K E Ivanov, K I Maslakov, I O Utkin, M Bubner, T Raikh, S Pompe, K-H Heise, H Nitshe *Inzh. Fiz.* **2** 28 (2001)
275. Yu A Teterin, V I Nefedov, A S Nikitin, A Yu Teterin, K E Ivanov, K I Maslakov, I O Utkin, M Bubner, T Raikh, S Pompe, K-H Heise, H Nitshe *Zh. Neorg. Khim.* **46** 990 (2001) [f]
276. Yu A Teterin, in *Biotechnology for Waste Management and Site Restoration. Technological, Educational, Business, Political Aspects. (NATO ASI Ser. 2, Environment)* Vol. 34 (Eds C Ronneau, O Bitchaeva) (Dordrecht: Kluwer Academic, 1997) p. 135

[a] — *Radiochemistry (Engl. Transl.)*
[b] — *Phys. Solis State (Engl. Transl.)*
[c] — *Dokl. Chem. (Engl. Transl.)*
[d] — *Russ. J. Struct. Chem. (Engl. Transl.)*
[e] — *J. Theor. Exp. Chem. (Engl. Transl.)*
[f] — *Russ. J. Inorg. Chem. (Engl. Transl.)*
[g] — *Opt. Spectrosc. (Engl. Transl.)*
[h] — *Geochem. Int. (Engl. Transl.)*
[i] — *J. Exp. Theor. Phys. Lett. (Engl. Transl.)*
[j] — *Physics-Uspekhi (Engl. Transl.)*